ATTACHMENT 1-NP to LD-83-015

SYSTEM 80

CESSAR FSAR

DOCKET STN 50-470

RESPONSES TO QUESTIONS ON CESEC

FEBRUARY 1983

COMBUSTION ENGINEERING, INC.
NUCLEAR POWER SYSTEMS
WINDSOR, CONNECTICUT

8303080236 830228
PDR ADOCK 05000470
A PDR

LEGAL NOTICE

THIS REPORT WAS PREPARED AS AN ACCOUNT OF WORK SPONSORED BY COMBUSTION ENGINEERING, INC. NEITHER COMBUSTION ENGINEERING NOR ANY PERSON ACTING ON ITS BEHALF:

A. MAKES ANY WARRANTY OR REPRESENTATION, EXPRESS OR IMPLIED INCLUDING THE WARRANTIES OF FITNESS FOR A PARTICULAR PURPOSE OR MERCHANTABILITY, WITH RESPECT TO THE ACCURACY, COMPLETENESS, OR USEFULNESS OF THE INFORMATION CONTAINED IN THIS REPORT, OR THAT THE USE OF ANY INFORMATION, APPARATUS, METHOD, OR PROCESS DISCLOSED IN THIS REPORT MAY NOT INFRINGE PRIVATELY OWNED RIGHTS; OR

B. ASSUMES ANY LIABILITIES WITH RESPECT TO THE USE OF, OR FOR DAMAGES RESULTING FROM THE USE OF, ANY INFORMATION, APPARATUS, METHOD OR PROCESS DISCLOSED IN THIS REPORT.

CONFIRMATORY QUESTIONS REGARDING CESEC

Section 1.0

440.83 (440.1) Describe in detail the relationship between CESEC-SAR, CESEC-ATWS, CESEC-SLB and CESEC-III with an emphasis on the difference.

Response:

The significant differences between various CESEC versions are summarized in Section 18 of Ref. 13 in terms of CESEC-I, CESEC-II, and CESEC-III. CESEC-SAR is a generic term which refers to the version used specifically for a particular safety analysis report.

CESEC-ATWS is essentially the same as CESEC-II, but with additional detail in the steam generator and reactivity feedback models. The CESEC-ATWS steam generator includes a dynamic simulation of the effect of two-phase level on primary to secondary heat transfer during loss of feedwater events. (See Reponse to Question 440.143). The reactivity model provides explicitly for void reactivity feedback.

CESEC-SLB is essentially the same as CESEC-III. The latter version adds to CESEC-SLB certain user conveniences of CESEC-II and explicitly models all four cold legs and each reactor coolant pump. CESEC-SLB lumps the two cold legs and reactor coolant pumps in each steam generator loop into one cold leg and pump per steam generator.

440.84 (440.2) There is no discussion of DNBR calculations. If the code does compute DNBR, provide details.

Response:

CESEC-III does not calculate DNBR. Earlier CESEC versions (Ref. 1) calculated DNBR trends. However DNBR values presented in licensing analyses are never those calculated by a CESEC version.

440.85 (440.3) Describe the self-initialization procedure.

Response:

The subroutine STEADY serves as a calling subroutine which coordinates the self initialization process and input data loading in CESEC-III. The reactor system modules are called to set up their input information and to define their initial conditions at time zero. The CESEC code can be initialized at any combination of reactor power level, reactor coolant system flow rate, and steam generator power sharing. Since some of the main steam system parameters are mutually dependent on one another (i.e., PSECR, PSECL, PHEAD, etc.) an iteration process is used among subroutines SGLEQL, SGREQL, and SECEQL to find their equilibrium initial conditions. The calling sequence in STEADY is as follows:

a. Call FLOWOL to define full power symmetric coolant flow, core inlet temperature at full power, and core inlet temperature at initial power level;
b. Call COREQI to load input data and to initialize the reactor core at specified power level and to find core outlet temperature at full powe. operating conditions;
c. Call FEEDEQI to find feedwater enthalpy;
d.* Call SGREQI, SGLEQI, annd SECEQI to load their input data and evaluate design full power steam generator heat transfer parameters;
e.* Call SGLEQL, SGREQL, and SECEQL to perform power sharing between the two steam generators which equalizes,

within a specified convergence criteria, the main steam line header pressure (PHEAD);

f.* Call SGREQS, SGLEQS, and SECEQS to define their initial equilibrium conditions which are consistent with the power sharing found through iteration;

g. Call the initialization section of the rest of the reactor system modules to load input data and to define their initial equilibrium conditions. [FEEDQI, PRESQI, COOLQI, FLOWQI, WALLQI, PROTQI, BOREQI, LAMEQI]

Figure 440.85-1 details the above steps in block diagram form. The loop at the center of this diagram shows the iterative procedure used to arrive at values for power sharing. Steam line pressure loss is accounted for during this iterative procedure for solving for power sharing. The effective flow loss coefficient for the piping modaled in the header simulation equations (see Figure 15-1A of Ref. 13) is used to calculate the header pressure that would result from the pressure in each steam generator and the steam flow from that generator due to the heat transfer from primary to secondary (i.e., power) in that generator. Iteration is continued until the resultant header pressure calculated from the pressure and steam flow of one generator equals that for the other.

Design full power conditions for primary system cold leg temperature, pressure, power, flow rates in each loop, secondary pressure, and steam generator tube heat transfer area are input. Assuming saturation the secondary temperature can be found using the secondary pressure. Knowing these design values of the temperatures

of the fluids on both sides of the tubes, the heat transfer area, and heat flux, a resultant value for the overall steam generator tube heat transfer coefficient can be found. Since the primary and secondary side heat transfer coefficients are determined from heat transfer correlations, the only undetermined parameter in this overall heat transfer coefficient is the effective steam generator tube heat transfer resistance. This resistance is thus fixed by this calculation at design conditions and is then held constant and used for the particular case being analyzed with CESEC at the time.

---

*Figure 440.85-1 is a flow diagram of steps d, e, and f.

FIGURE 440.85-1

STEAM GENERATOR

INITIALIZATION

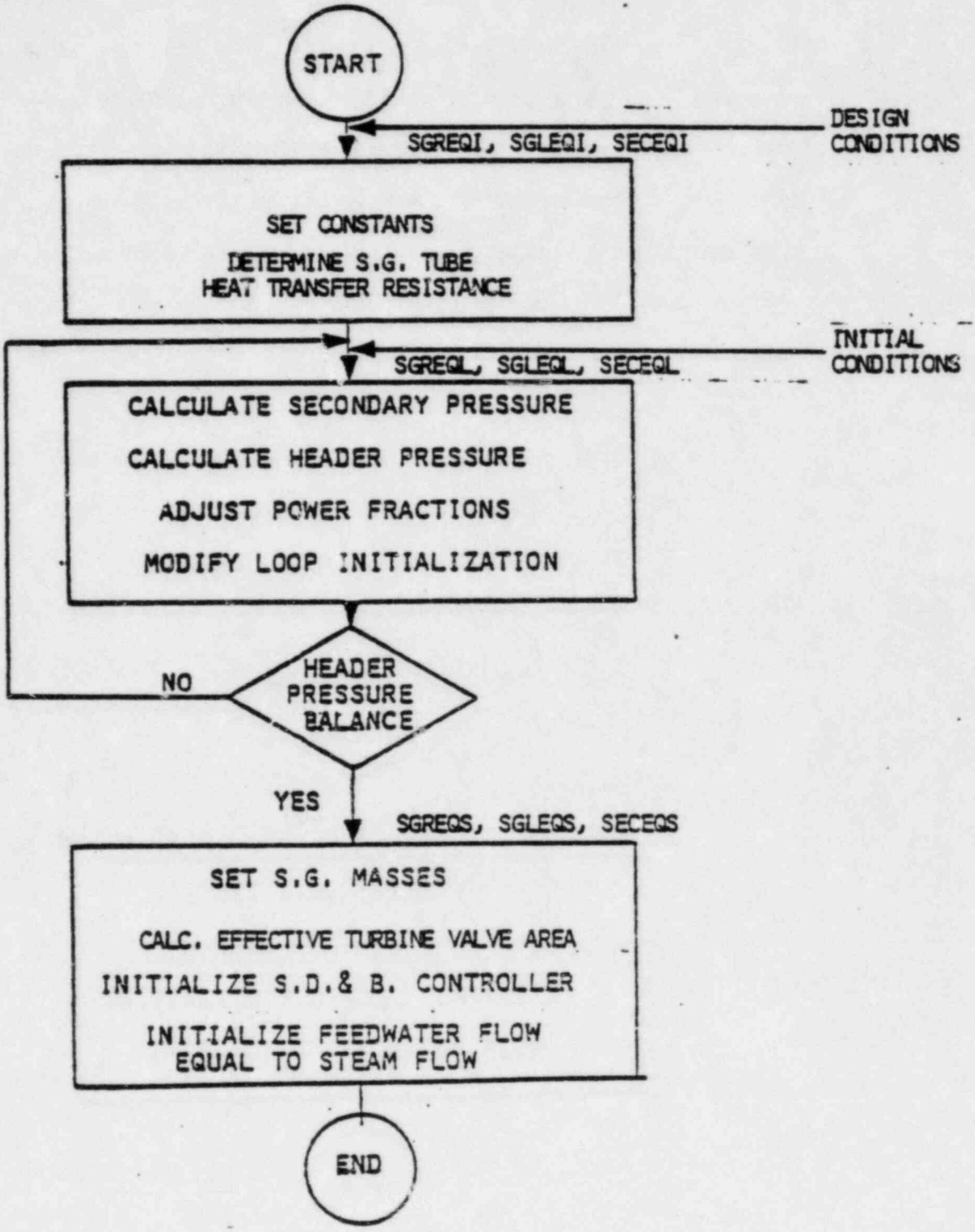

440.86 How is the closure head bubble modelled?
(440.4)

Response:

The thermal hydraulic equations for the upper head region of the reactor vessel are the same as for the other regions of the RCS excluding the pressurizer (see Section 2 and Appendix B of Ref 13). User input control of the algorithm used to calculate the enthalpy of fluid leaving this upper head node permits simulation of the degree of separation of the liquid and vapor phases in the region. For steam line break and steam generator tube rupture events phase separation and RCS pressure are maximized by causing the enthalpy of fluid leaving the node to be that of saturated liquid when two phases are present. For other transients the enthalpy of fluid leaving the node is the average enthalpy of the fluid in the node. User input control also allows the value of the fraction of flow to the upper head, F_H, to be changed once during the transient. This may be used to simulate a reduction in flow to the upper head due to reactor coolant pump coastdown or due to RCS contraction during severe increase in heat removal events.

Section 2.0

440.87 (440.5) Does assumption (1) of Appendix B, assuming pressure to be spatially uniform throughout the entire primary coolant system, imply that no differentiation is made between pressurizer pressure and system pressure in the derivation of the T/H equations, eq. (B-30) through eq. (B-78)? Where and how is each pressure used?

Response:

A distinct differentation is made between pressurizer pressure and RCS pressure. For all of the equations of the form of Eqn. (B-29), i.e., eqns. (B-30) through (B-54), the appropriate pressure is the RCS pressure, P_{RCS}. All properties and their derivatives are evaluated at P_{RCS} for these equations. The relationship $\dot{P}_{RCS} = \dot{P}_{PRZ} + \Delta\dot{P}_{ws}$, where P_{PRZ} is the pressurizer pressure and ΔP_{ws} is the surge line pressure drop which is calculated in the code, is used to transform the P of Eqns (B-30) through (B-54) from $\dot{P}_{RCS}$ to $\dot{P}_{PZR}$. As a result, ε_i of Eq. (B-29) contains the term $(-\delta_i \Delta\dot{P}_{ws})$, with $\Delta\dot{P}_{ws}$ being determined as described in chapter 7 of Ref. 13. Thus for Eqns (B-30) through (B-54)

$$\beta_i (\Sigma W_{int})_i + \alpha_i (\Sigma h W_{int})_i + \delta_i \dot{P}_{PRZ} = \varepsilon_i'$$

and

$$\varepsilon_i' = \varepsilon_i - \delta_i \Delta\dot{P}_{ws} .$$

8

(See page B-5 of Ref. 13 for definitions of parameters) For Eqns (B-55) through (B-83) $\dot{P}$ is $\dot{P}_{PRZ}$, directly, and all properties and their derivatives are evaluated at the pressurizer pressure. The only exception to the foregoing is that the average of P_{RCS} and P_{PRZ} is used in the determination of the properties of surge line fluid.

Section 3.0

440.88 (440.6) How are the crossflows, bypass flows, mixing flows, head flows and leak flows incorporated into eq. (3-1), the equation for the pump flow?

Response:

All flows mentioned, except the leak flows are directly incorporated into Eq. (3-1) of Ref. 13 according to the definition of the flow model nodal flow as being the arithmetic mean of sums of internodal flows entering the node and internodal flows leaving the node.

$$W_i = \frac{1}{2}\left[\sum_j W_{in,j} + \sum_j W_{out,j}\right]_i$$

The leak flows are not directly incorporated into Eq. (3-1), however, they are accounted for in the thermal-hydraulic (T-H) model as external flows. The solution of the T-H equation system gives the internodal flows used in determination of the flow model nodal flows as described above.

The T-H equation system assumes one dimensional flow and does not consider the effect of momentum flux in the solution. Momemtum flux terms are negligible for the transients analyzed by CESEC-III and small break LOCAs. Only large break LOCA methods consider the effect of momentum flux in the T-H solution.

440.89
(440.7) How does the inertia term in eq. (3-1) take account of the flow split for parallel pumps?

Response:

The flow model calculates the mass flow rate through each of four reactor coolant pumps using Eq. (3-1) of Ref. 13. The term "loop" in the description should be understood as four separate loops consisting the specified series of nodes following (refer to Fig. 3-1 of Ref. 13):

Pump Loop 1: nodes 1, 2, 3 through 12 — Right Hand

Pump Loop 3: nodes 13, 14, 3 through 12 — (RH) loops

Pump Loop 2: nodes 15, 16, 17 through 26 — Left Hand

Pump Loop 4: nodes 27, 28, 17 through 26 — (LH) loops

The inertia term (denominator) in Eq. (3-1) is defined as a sum of terms L_i/A_i around each of these four loops.

Section 4.0

440.90 (440.8) Justify the use of the Semiscale degraded two phase pump data to model C-E pumps.

Response:

The appropriateness of the Semiscale degraded two phase pump data for modelling of C-E pumps has been established by the NRC acceptance of the model (Section III.C.6 of Ref. 15) and of the CEFLASH-4A computer code (Section III.8.17 of Ref. 16) which utilizes the model.

Section 6.0

440.91 (440.9) Describe how the level in the pressurizer is determined and how the external heat transfer/mass flow terms are divided between the steam region and the liquid region.

Response:

Pressurizer liquid level is determined by dividing the volume of liquid in the pressurizer by the cross sectional area of the pressurizer. Complete separation of the vapor and liquid phases, or an effectively infinite bubble rise velocity, is assumed. The measured liquid level is determined as described in Section 4.3.1 of Ref. 3. The external heat transfer/mass flow terms are divided between the steam region and the liquid region as described in Sections 4.3.2 through 4.3.4 of Ref. 3.

Section 7.0

440.92 (440.10) Why does the gravity term in the surge line momentum equation, eq. (7.1) contain expressions for the pressurizer when the inertia term is written only for the surge line?

Response:

The surge line momentum equation can be written as (see Figure 440.92-1).

$$P_1 - P_2' = \frac{\left(\frac{L}{A}\right)}{144g}\frac{dW}{dt} + \frac{f(L/De)|W|W}{288\rho g A^2}\phi + \frac{Kg\,|W|W}{288\bar{\rho}\,g\,A^2} + \frac{\bar{\rho}\,(Z_a - Z_2)}{144} \quad (1)$$

The static pressure balance inside the pressurizer yields

$$P_2' - P_2 = \frac{\rho_w}{144}(Z_w - Z_a) + \frac{\rho_s}{144}(Z_p - Z_w) \quad (2)$$

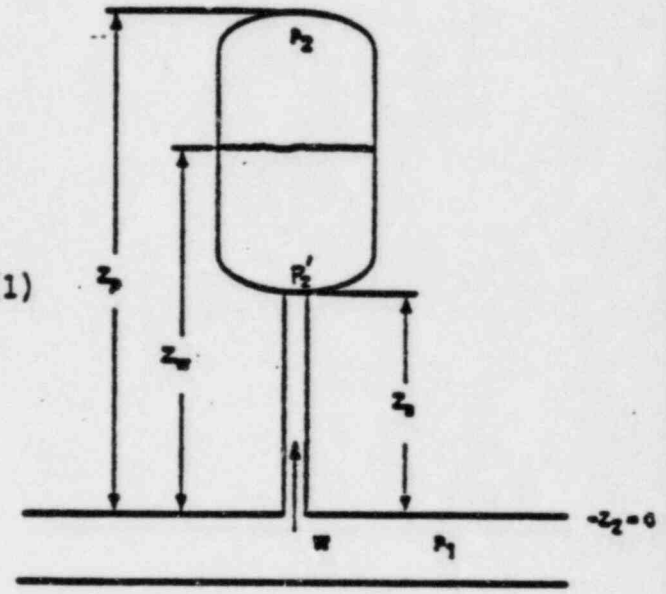

Figure 440.92-1

Therefore, substituting Equation (2) into Equation (1) for P_2' yields Equation (7.1).

The (L/A) in the inertia term is written in terms of the surge line since the L/A for the pressurizer is small compared with the L/A for the surge line.

440.93 (440.11) Show the table of f values used in eq. (7-1) when Re > 15000.

Response:

The table of f values used in eq. (7-1) when Re > 15000 is as follows:

Re / f	1.5×10^4	1.0×10^5	4.0×10^5	1.0×10^6	4.0×10^6	1.0×10^7	4.0×10^7	1.0×10^8	1.0×10^{14}
	.0275	.018	.0139	.0122	.0103	.0095	.009	.0088	.0088

See Section 4.4.5 of Ref. 3.

Section 8.0

440.94 (440.12) Why is the pressurizer pressure time derivative and not the RCS pressure time derivative used in eq. (8-1)?

Response:

Refer to the response to Question 440.87.

Section 9.0

440.95 (440.13) Are the 13 nodes referred to in the wall heat transfer model radial nodes? Provide a figure for the model to illustrate it.

Response:

The 13 nodes are referred to in the wall heat transfer model are radial nodes. Figure 440.95-1 presents the basic geometry of the wall heat model in the thermal hydraulic node.

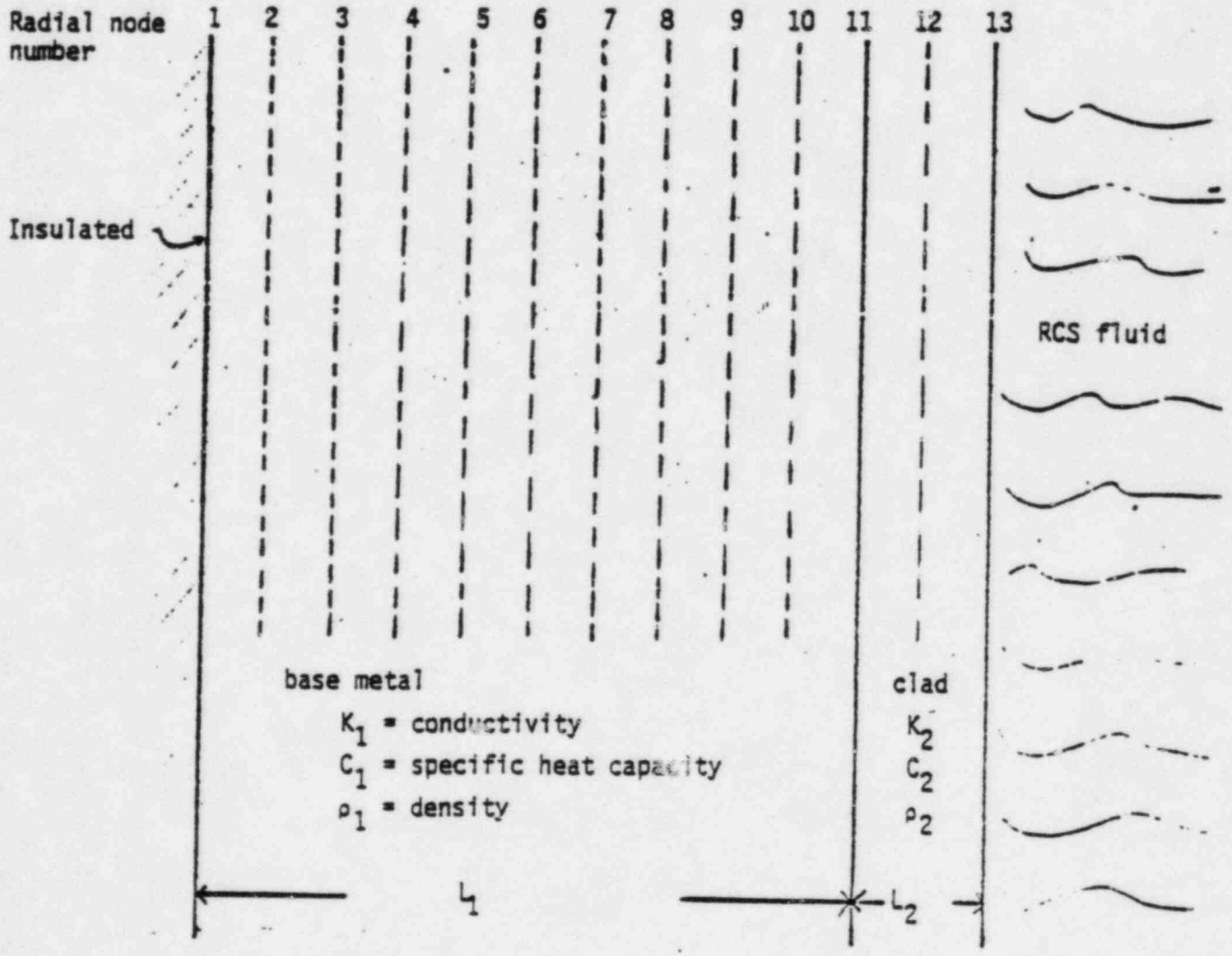

Figure 440.95-1
Basic geometry of wall heat model

440.96 (440.14) How is heat conduction through the steam generator tubes modelled?

Response:

Heat conduction through the steam generator tubes is modelled by two equations--one for conducted heat, $Q_{c,n}$, and one for stored heat, $Q_{s,n}$.

$$Q_{c,n} = U_n A_n (\overline{T_{pri}}_n - T_{sec})$$

(This is Eq. 13-1 of Ref 13; the notation is the same as defined there.)

$$Q_{s_{n,i+1}} = C_n (T_{pri_{n,i+1}} - T_{pri_{n,i}}) / \Delta t,$$

where, additionally,

C_n = heat capacity of steam generator tubes in node n (BTU/F),

i = time step number, and

Δt = time step size (sec).

This assumes that the tube walls essentially follow the temperature of the primary coolant, rather than the secondary fluid. This is consistent with the small time constant (on the order of one second) for heat transfer to the tube walls.

The source term for net heat rate into the thermal hydraulic equation, Eq. 2-1 of Ref. 13 for the steam generator tube node is then

$$Q_n = - (Q_{c,n} + Q_{s,n}).$$

440.97 (440.15) Is eq. (9-2) for the shroud heat capacity solved simultaneously with the thermal hydraulic equations of Appendix B?

Response:

Eq. (9-2) of Ref. 13 for the shroud heat capacity is not solved simultaneously with the thermal hydraulic equations of Appendix B of Ref. 13. The time constant for heat transfer to the shrouds is of the order of one second. Time step sizes are typically small fractions of a second. Therefore, no large change in heat transfer to the relatively thin walled shrouds would be expected from one time step to another.

Section 10.0

440.98 (440.16) For the Doppler and the moderator reactivity feedback calculation does the core have only one axial node? How is the split core accounted for?

Response:

Present applications of the CESEC code utilize only one axial node.

The Doppler reactivity is determined from a tabular input function of reactivity versus fuel temperature with the fuel temperature calculated as specified in the response to Question 440.100. The coolant temperature utilized in the fuel temperature calculation is the arithmetic average of the coolant temperatures associated with the core thermal-hydraulic nodes.

Moderator reactivity is determined from either a tabular input function of reactivity versus moderator temperature or moderator density. The arithmetic average of the coolant temperatures associated with core thermal-hydraulic nodes is used for the moderator temperature. Except for steam line break applications, when the density function is specified, the moderator density is based on the arithmetic average of the coolant specific volumes associated with the core thermal-hydraulic nodes. For steam line break applications, the moderator density is computed from the cold edge enthalpy and system pressure as described in response to Question 440.145.

440.99 (440.17) How is the moderator temperature/density calculated for the reactivity feedback?

Response:

See the response of Question 440.98.

440.100 (440.18) How is the fuel temperature for the Doppler feedback calculated?

Response:

The fuel rod temperature is calculated using the model presented in Section 10 of Reference 13. The temperatures calculated for the three radial nodes are then used for the Doppler feedback calculations. This is done by calculating the Doppler feedback for each of the three fuel rod node temperatures and averaging the reactivities. This average is then used in the kinetics calculations.

440.101 (440.19) Describe in detail the 3-D reactivity feedback model used for steam line breaks.

Response:

The 3-D reactivity contributions used in the CESEC code for steam line break analysis (pp. 10-1, 2 of Ref. 13) are calculated via the HERMITE code. The majority of the physical models within the current version of the HERMITE code are described in Reference 8. The only portion of that code in which the physical model has changed is in the area of the core thermal hydraulic calculation. There, the closed channel model described in Reference 8 has been replaced with the same core-wide open channel model described in the TORC code (Reference 9, 14). Cross-sections are generated via the DIT code (Reference 10).

A three-dimensional quarter-core HERMITE model is assembled and depleted to the end of an equilibrium cycle. This model is then expanded to full core geometry and a series of return-to-power eigenvalue calculations are performed. The most adverse control rod is assumed to be stuck in the fully withdrawn position in all return-to-power cases.

The reactivity insertion from hot full power to each return-to-power condition is then computed. A corresponding reactivity insertion is computed via traditional steam line break methods, using isothermal two dimensional HERMITE calculations. A best estimate reactivity credit is defined as the difference between the standard 2D

reactivity insertion and the more precise 3-D reactivity insertion. A multiplicative conservatism factor is then applied within the CESEC code.

As described on page 10-2 of Ref. 13, these reactivity credits are input to CESEC as tabular functions of normalized core flow fraction, normalized fission power to normalized core flow ratio, and temperature tilt. In the dynamic calculation the normalized flow and fission power are calculated by dividing core flow and fission power by the flow and fission power values, respectively, that were used to normalize the results of the HERMITE calculations. The temperature tilt is the difference between the hot and cold edge temperatures at the core inlet plane. Test results (Ref. 11) indicate that the temperature of the fluid at the very edge of the core directly under one steam generator loop would have very little contribution from the fluid of the opposite loop. Therefore, the temperature tilt is calculated using an algorithm which factors out the effect of reactor vessel inlet mixing:

Temperature tilt = $T(h_H, P) - T(h_C, P)$,

where

$$h_H = \frac{h_3 + h_{15}}{2} + \left(\frac{1 + F_I}{1 - F_I}\right)\left(\frac{h_{15} - h_3}{2}\right)$$

and

$$h_C = \frac{h_3 + h_{15}}{2} - \left(\frac{1 + F_I}{1 - F_I}\right)\left(\frac{h_{15} - h_3}{2}\right) ,$$

all notation being the same as that of Section 2 of Reference 13. Table interpolation routines use dynamically calculated values of nomalized core flow fraction, nomalized fission power to nomalized core flow ratio, and temperature tilt to obtain the dynamics 3-D feedback from the input tables of reactivity credits as a function of these three parameters. This 3-D feedback is added to the other feedback reactivities (moderator, Doppler, etc.) after multiplication by the conservatism factor mentioned above. An input option allows the user to activate the 3-D feedback calculation for the analyses to which 3-D feedback is appropriate.

440.102 (440.20) Explain the homogenization procedure for the third radial node of the fuel rod heat conduction model.

Response:

The homogenization procedure for the parameters for the third radial node of the fuel rod heat conduction model is described in Section 1.3 of Reference 6, in the response to Questions 240.22 and 240.23 of Reference 5, and in Section 2.2.2 of Reference 1. The temperature of each radial fuel rod is taken to be the temperature of the fuel at a reference radius for that node. For the first and second nodes this reference radius is the average of the radii of the boundaries of the nodes. For the third node the reference radius is the average of the radius at the boundary of the second radial node and the radius of the fuel pellet. The effective thermal conductance* between the second and third node, K_{23}, is calculated between the reference radii for these nodes. This conductance includes the effect of cylindrical geometry, assuming a uniform heat source within the fuel pellet, and accounts for the temperature dependence of the thermal conductivity of the fuel.

$$K_{23} = \frac{16\pi R_2^2 \ell K_F (T_{F3})}{(R_2+R_F)^2 - (R_1+R_2)^2}$$

*See Figure 10-6 of Ref. 13.

$$K_{3W} = \left\{ \frac{4R_F^2 - (R_2+R_F)^2}{\pi \ell (R_2+3R_F)^2 K_F(T_{F3})} + \frac{1}{2\pi R_F \ell h_G} \right.$$

$$+ \frac{\ln\left[R_3/(R_3-\delta_c)\right]}{2\pi \ell K_c(T_c)}$$

$$\left. + \frac{1}{2\pi R_3 \ell h_W(T_W, W)} \right\}^{-1}$$

where in addition to the parameters defined earlier:

h_G = gap conductance

R_3 = radius of fuel pin

$K_c(T_c)$ = thermal conductivity of clad at clad temperature, T_c

δ_c = clad thickness

$h_W(T_W, W)$ = film heat transfer coefficient of clad to coolant interface evaluated at the temperature, T_W, and mass flow rate, W, of the coolant

The clad temperature, T_c, is calculated using T_W, the thermal resistance between the coolant and the clad, and the heat flux at the surface of the fuel pin.

The heat capacity of the third node, $(MC)_3$, is the heat capacity of the volume of fuel pellet in this node plus the product of the heat capacity of the clad with the ratio of the clad temperature to the temperature of the third fuel rod node.

$$(MC)_3 = V_{F3}\ \rho_F(T_{F3})C_F(T_{F3}) + V_c\ \rho_c(T_c)C_c(T_c)\ \frac{T_c}{T_{F3}}$$

where in addition to the parameters defined above:

V_{F3} = volume of fuel pellet portion of node 3

V_c = volume of clad

$\rho_F(T_{F3})$ = density of fuel at temperature of fuel in node 3

$\rho_c(T_c)$ = density of clad at clad temperature

$C_F(T_{F3})$ = specific heat of fuel at temperature of fuel in node 3

$C_c(T_c)$ = specific heat of clad at temperature of clad

440.103 (440.21) Is the heat transfer correlation given by Eq. (10-1), for the clad-coolant interface, actually used for all pressures and temperatures.

Response:

Eq. (10-1) is used for calculating the heat transfer coefficient for forced convection flow of sub-cooled liquid. Calculations show that values calculated using Eq. (10-1) differ from those obtained using the Dittus-Boelter correlation (Ref. 17), by less than 4% over the pressure range from atmospheric pressure to 3200 psia for temperatures from 200 °F to a temperature just below saturation.

440.104 What is the difference between T_w and T_{w1} in Fig. 10-6?
440.22)

Response:

The equation for heat to water in Fig. 10-6 should read as follows:

$$Q_w = K_{3w} (T_{F3} - T_w) + C_w P$$

440.105 (440.23) Is Q_w in Fig. 10-6 the source term used in the thermal-hydraulic equations of Appendix B?

Response:

The Q_w in Figure 10-6 is the source term used in the thermal-hydraulic equation of Appendix B:

$$Q_5 = Q_{17} = 0.5\ Q_w$$

Section 11.0

440.106 (440.24) Is the letdown fluid temperature at the heat exchanger user input as stated by Section 11.0 or calculated in accordance with eq. (F-3)?

Response:

For analyzing letdown line break events, the mathematical model described in Appendix F is employed. For these events the letdown fluid temperature at the regenerative heat exchanger (RHX) exit is calculated using eq. (F-3).

Under normal operating conditions the charging and letdown temperatures are selected to be those corresponding to the steam generator outlet temperature. The letdown flow rate (gpm) is a user input quantity. The user input temperature referred to in Section 11.0 is the temperature at which this letdown flow is measured.

440.107
(440.25)

In the iterative procedure described in Appendix F is the critical flow set equal to the Darcy flow? Why assume saturation at the RHX exit?

Response:

In the procedure described in Appendix F the Darcy flow in the letdown line and the critical flow rate at the break are iteratively calculated until these two values agree within a specified criterion.

The model does not assume that the letdown fluid is saturated at the RHX exit. However, the fluid enthalpy at the RHX exit is assumed to be equal to the saturation liquid enthalpy corresponding to the RHX exit temperature (from eq.(F-3)). If the fluid is, in fact, subcooled at the RHX exit, the above assumption would have a negligible effect on the results.

If the fluid is in a two-phase state, the above assumption yields conservative results, since the assumption of a lower enthalpy (i.e., saturated liquid enthalpy) results in a higher calculated critical flow rate at the break.

440.108 (440.26) What is the database for the heat transfer correlation given by eq. (F-4)?

Response:

The overall heat transfer coefficient U is dependent on the letdown and charging flow rates. UA is given by the C-E generated (Ref. 13) empirical equation (F-4) shown below.

$$(UA)^{-1} = X \cdot G_l^{-0.8} + Y \cdot G_c^{-0.8} + Z \qquad (1)$$

where,

U is the overall heat transfer coefficient, BTU/hr-ft^2 -$^\circ$F,

A is the heat transfer area, ft^2

G_l and G_c are the letdown and charging flows in gallons/minute, and

X, Y, and Z are constants dependent on the design of the regenerative heat exchanger (RHX).

The constants X, Y, and Z for the System 80 RHX were calculated using the RHX performance data shown in Table 440.108-1. The data was extracted from the general specification for the RHX for the System 80 standard design provided in Attachment 440.108-1.

UA is calculated using the data shown in Table 440.108-1 and the following equation:

$$UA = \frac{(\dot{M}_c)\ (C_{pc})\ \ (t_{co} - t_{ci})}{\Delta t_{lm}} \qquad (2)$$

where,

$$\Delta t_{lm} = \frac{(t_{li} - t_{co}) - (t_{lo} - t_{ci})}{\ln \dfrac{(t_{li} - t_{co})}{(t_{lo} - t_{ci})}}$$

$\dot{M}_c$ is the charging flow rate, lbm/hr,

C_{pc} is the average specific heat for the charging fluid, BTU/lbm - F,

t_{li} and t_{lo} are the temperatures of the letdown fluid at the RHX inlet and outlet, F, and

t_{ci} and t_{co} are the temperatures of the charging fluid at the RHX inlet and outlet, F.

The values of UA generated from Equation 2 are employed in Equation 1 to calculate the constants X, Y, and Z. For the System 80 RHX, the constants are:

$X = 7.2160 \times 10^{-5}$

$Y = 6.3085 \times 10^{-5}$

and $Z = 1.0800 \times 10^{-5}$

These constants are input into the CESEC code to calculate UA for different letdown and charging flow rates. The CESEC calculated values of UA are then employed in equation (F-) to calculate the temperature of the letdown fluid at the RHX exit, t_{lo} (Ref. 13).

$$t_{lo} = \frac{t_{ci}\left\{1-\exp\left[\frac{UA(1-R)}{\dot{M}_l C_{pl}}\right]\right\} - t_{li}(1-R)}{R - \exp\frac{UA(1-R)}{\dot{M}_l C_{pl}}} \qquad (3)$$

(Eqn. F(3) of Ref. 13).

where,

$$R = \frac{\dot{M}_l C_{pl}}{\dot{M}_c C_{pc}}$$

$\dot{M}_l$, $\dot{M}_c$ are letdown and charging flow rates, lbm/hr
C_{p_l}, C_{pc} are the average specific heats of letdown and charging fluids BTU/lbm-^oF

In order to assess the accuracy of the empirical correlation provided as equation (F-4), calculated values of t_{lo} (using Equation F-3) for various flow rates and inlet temperatures are compared in Table 440.108-2 with measured values of t_{lo}. The flow rates and temperatures in Table 440.108-2 are extracted from the general specification and the project specification for the RHX for the System 80 standard design (Attachments 440.108-1 and 440.108-2).

The comparisons provided in Table 440.108-2 indicate that the calculated values of t_{lo} agree very well with the measured steady state values (see sample calculation).

Sample Calculation:

Calculation of T_{lo} for case 3 of Table 440.108-2 is shown below.

Equation (3) uses the average specific heats of the charging and letdown fluids, i.e., specific heats at the average temperatures, $(t_{li} + t_{lo})/2$ and $(t_{ci} + t_{co})/2$. Since, at the start of the computation t_{lo} and t_{co} an not known, assumed values of C_{pl} and C_{pc} are used in the beginning and eqn. 3 is used iteratively to compute the value of t_{lo}.

In the sample calculation below, since measured values of t_{lo} and t_{co} are known, c_{pl} and C_{pc} at the average of the measured temperatures are used. The need for an iterative procedure is thus avoided.

Data (measured values):

G_c = 92 GPM	G_l = 135 GPM
T_{ci} = 130°F	T_{li} = 564.5°F
T_{co} = 419°F	T_{lo} = 382°F

Calculation:

Average Temperatures:

$\bar{T}_c$ = 274.5°F and $\bar{T}_l$ = 473.3°F

Specific heats at the average temperatures and assumed pressure of 2000 psia are obtained from Ref. 36.

C_{pc} = 1.0091 BTU/lbm°F

C_{pl} = 1.1235 BTU/lbm°F

From eqn. (1)

$$(UA)^{-1} = 1.3920 \times 10^{-5}$$

or $UA = 7.1839 \times 10^{4}$ BTU/hr - °F

$$R = \frac{\dot{M}_l C_{pl}}{\dot{M}_c C_{pc}} = \frac{G_l}{G_c} \quad \frac{C_{pl}}{C_{pc}} = \underline{1.6337}$$

$\dot{M}_l$ = 67,242.7 lbm/hr (using ρ = 62.104 lbm/ft^2) (Ref. 36).

Using UA, R and $\dot{M}_l$ in eqn. (3) we obtain t_{lo} = 383.4°F which agrees well with the measured t_{lo} of 382°F.

Table 440.108-1: Data Base Used In Calculating the Values of X, Y, and Z

	CHARGING (SHELL SIDE)			LETDOWN (TUBE SIDE)		
Case No.	Flow G_c (gpm @ 120°F)	Inlet temp t_{ci} (°F)	Outlet temp t_{co} °F	Flow, G_l (gpm @ 120°F)	Inlet temp t_{li} (°F)	Outlet temp t_{lo} (°F)
1	61.6	120	445	72.4	564.5	310
2	61.6	120	488	135	564.5	414
3	105.6	120	348	72.4	564.5	258

Table 440.108-2: Comparison of Measured and Calculated Values of t_{lo}

Case No.	RHX Operating Parameters (Measured)						Calculated value using equation (F-3)
	G_c (gpm @ 120°F)	G_l (gpm @ 120°F)	t_{ci} (°F)	t_{co} (°F)	t_{li} (°F)	t_{lo} (°F)	t_{lo} (°F)
1**	44	30	120	395	564.5	185	184
2*	61.6	72.4	120	445	564.5	310	311
3**	92	135	130	419	564.5	382	383
4*	105.6	135	40	373	564.5	330	329

* From Attachment 1

** From Attachment 2

ATTACHMENT 440.108-1

STEADY STATE PERFORMANCE DATA* FOR SYSTEM 80 RHX

4.1.2 Operating Modes

Tube side letdown and shell side charging flows are controlled to satisfy operating conditions. Typical flow combinations listed below include Mode [3] which is the thermal sizing condition and Mode [3] which is the normal operating condition.

Mode No.	Shell Side (Charging)				Tube Side (Letdown)			
	Flow gpm @ 120°F	Temperature °F In	Out	P, psi	Flow, gpm @ 120°F	Temperature, °F In	Out	P, psi
1	61.6	120	328	8.5	30	564.5	163	2.6
2	61.6	130	334	8.5	30	564.5	172	2.6
3	61.6	120	445	8.6	72.4	564.5	310	13.3
4	61.6	130	447	8.6	72.4	564.5	315	13.3
5	61.6	120	488	8.7	135	564.5	414	44.1
6	61.6	130	489	8.7	135	564.5	417	44.1
7	105.6	120	348	24.2	72.4	564.5	258	13.2
8	105.6	130	353	24.2	72.4	564.5	264	13.2
9	105.6	40	373	24.3	135	564.5	330	42.8
10	105.6	120	248	24.2	30	564.5	145	2.6
11	44	120	385	4.4	28.4	564.5	178	2.4
12	44	40	351	4.5	28.4	564.5	110	2.4

* EXTRACTED FROM GENERAL SPECIFICATION FOR RHX

ATTACHMENT 440.108-2

STEADY STATE PERFORMANCE DATA* FOR SYSTEM 80 RHX

4.2.4 Operating Modes

Tube side letdown and shell side charging flows are controlled to satisfy operating conditions. Typical flow combinations listed below include mode 1 which is the thermal sizing condition and mode 5 which is the normal operating condition.

Mode	Shell Side (Charging)				Tube Side (Letdown)			
No.	Flow, gpm at 120°F	Temperature, °F In	Out	ΔP, psi	Flow, gpm at 120°F	Temperature, °F In	Out	ΔP, psi
1	44	130	525	5.2	135	564.5	450 Max.	48.1
2	48	130	520	6.2	135	564.5	441	47.9
3	92	130	419	22.4	135	564.5	382	46.8
4	44	120	508	5.2	84	564.5	379	19.3
5	48	120	496	6.2	84	564.5	368	19.2
6	92	120	389	21.9	84	564.5	295	18.8
7	44	120	440	5.2	40	564.5	233	4.75
8	44	40	415	5.2	40	564.5	177	4.75
9	48	120	422	6.1	40	564.5	225	4.75
10	92	120	301	21.8	40	564.5	176	4.75
11	44	120	395	5.2	30	564.5	185	2.8
12	92	120	266	21.9	30	564.5	148	2.8

* EXTRACTED FROM PROJECT SPECIFICATION FOR RHX

Section 13.0

440.109 (440.27)

(a) Why does the suppression factor S, given by eq. (13-9) not correspond with the formula given in Table 2 of the Hoeld+ paper referenced?

(b) Provide references/explanation for the difference in functional dependence between Chen's suppression factor* $f(Re_R F^{1.25})$ and Hoeld's expression $f(1 - x)\ Re_R F^{-1.25}$.

(c) Justify the choice of Hoeld's formula for the Reynold's number factor, F, eq. (13-8) over the original Chen values.

Response:

The suppression factor S introduced in Chen's correlation for the two-phase flow is a function of $Re_b \cdot F^{1.25}$ (Reference 24). In the Hoeld paper (Ref. 25), he formulated the factor as

$$S = 1/[1+(1.63)(10^{-5})(1-X)\ Re_b\ F^{1.25}]$$

Note that the exponential 1.25 was misprinted as -1.25. The (1-X) term is accounted for a mixture. If the mixture quality equals 0, F=1.

The CESEC code uses this formula for calculating the primary side heat transfer for a condition of two-phase flow with boiling (reverse heat transfer). CESEC will be modified as indicated above. However, no significant differences are expected in the consequences of transients analyzed with the incorrect exponent,

since boiling occurs in the primary side of the steam generator tubes for only very limited portions of a few transients analyzed with CESEC.

In order to solve for the heat transfer coefficient using the Chen correlation it is necessary to determine the Reynolds-number Factor, F. The open literature prior to the Hoeld paper recommended a lookup of the value from a graph or table. Since Hoeld was generating a digital computer code, it was more practical to use a fit to Chen's data for use in the code. The Hoeld paper provides a fit to the Chen data for the Reynolds-number Factor as a function of the Martinelli parameter, X_{tt}. It is of the form

$$F = 1.0 + 1.6\ (1/X_{tt})^{0.8174}$$

When the Hoeld functional fit is compared to the Chen data (Reference 37), reasonable agreement is observed (See Figure 440.109-1). For these reasons the Hoeld expression for the Reynolds-number Factor is used in the CESEC-III code.

+A. Hoeld, "A Theoretical Model for the Calculation of Large Transients in Nuclear Natural Circulation U-Tube Steam Generators (Digital Code UTSG)," Nuclear Eng. and Design, 47 , pp. 1-23, 1978.

*J. C. Chen, "Correlation for Boiling Heat Transfer to Saturated Fluids in Convection Flow," I&EC Process Design and Development, 5 , pp. 322-329.

FIGURE 440.109-1
REYNOLDS-NUMBER FACTOR
VS
RECIPROCAL MARTINELLI PARAMETER

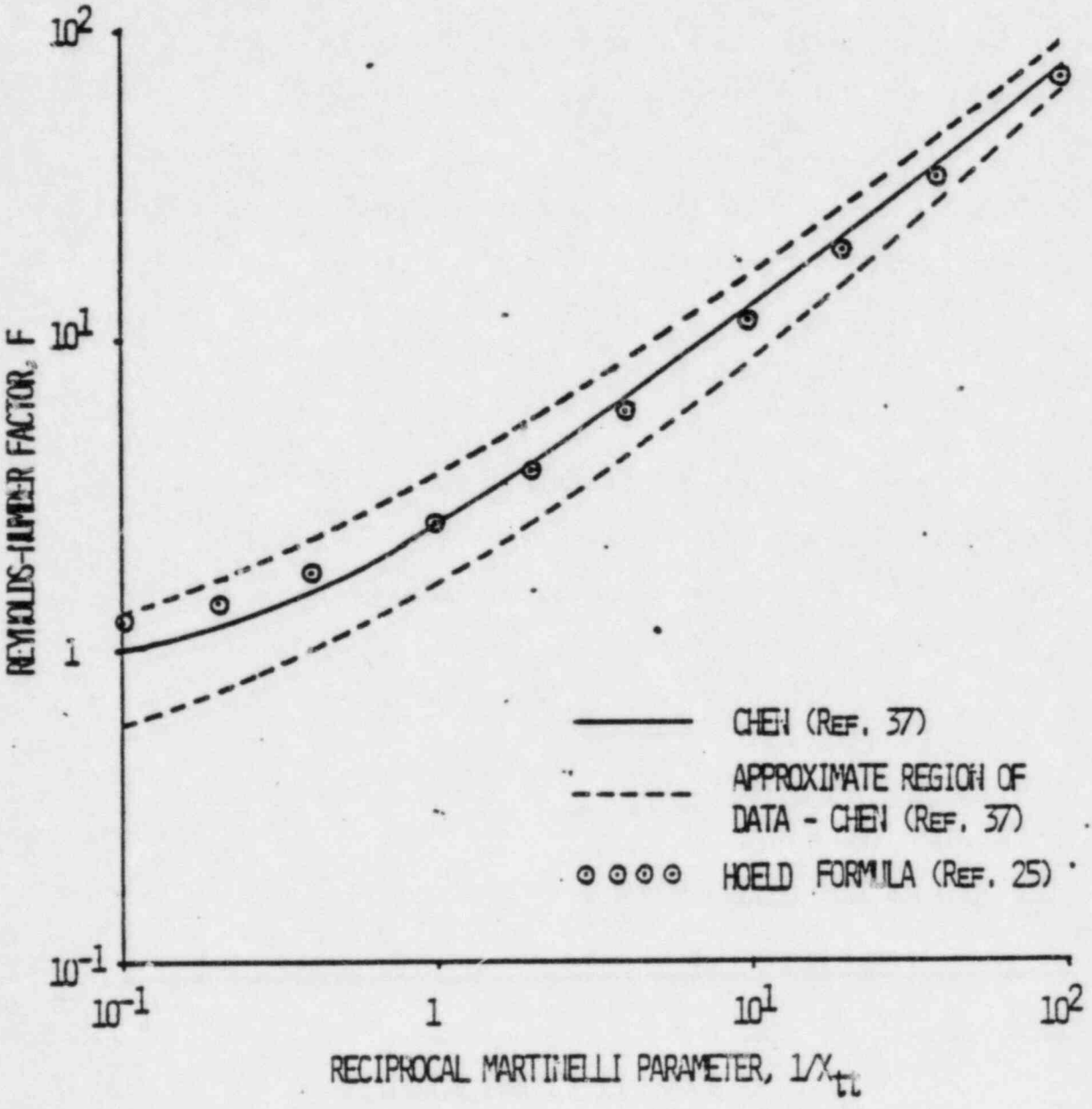

where:

$K_F(T_{F3})$ = thermal conductivity of fuel at the temperature of the fuel in node 3, T_{F3}

ℓ = length of axial node

R_1 = radius of boundary between nodes 1 and 2

R_2 = radius of boundary between nodes 2 and 3

R_F = radius of fuel pellet

The effective thermal conductance between the third node and the reactor coolant, K_{3w}, is calculated between the reference radius of the third node and the coolant. This conductance includes the conductance of the fuel from the reference radius to the pellet surface, based on the same assumptions used for the conductance between the second and third nodes, and the conductances of the gas gap, the clad, and the fluid film on the clad surface.

440.110 (440.28) Justify the use of the Dittus-Boelter correlation, eq. (13-3) for film heat transfer.

Response:

Equation (13-3), the Dittus-Boelter correlation is used during subcooled flow to calculate the heat transfer coefficient. The correlation is not used during film boiling heat transfer.

The physical properties of water required for all of the heat transfer correlations used in CESEC are obtained using the relationships given in Reference 31.

440.111 (440.29)

(a) Justify the assumption of two phase flow with condensation in the steam generator primary for all cases of forward heat transfer.

(b) Explain why the extrapolation of the Akers, Deans, and Crosser correlation to the water system is valid.

Response:

(a) CESEC uses the correlation for two-phase flow with condensation, Equation (13-4), for heat transfer from the reactor coolant to the steam generator tubes (forward heat transfer only) whenever the reactor coolant in the steam generator tubes is saturated.* Under such conditions heat transfer can be expected to involve a condensation component, since in order for heat transfer to take place in the forward direction the tube walls and any liquid film on the inside surface of the tube walls must be at a lower temperature than that of vapor phase present in the node, which will be saturated and at the bulk fluid temperature.

(b) The Akers, Deans, and Crosser correlations has been demonstrated by C-E in Reference 30, Section 3.5, to be valid in the water system.

---

*See Section 13 of Ref. 13 for a discussion of the correlations used for other conditions.

440.112 (440.30) (a) Present the database for C-E's modification of the Rohsenow pool boiling correlation, eq. (13-10), and discuss the range of validity.

(b) Should the term (P-800) be (P_{sec} - 800) in the second expression for K_R on page 13-5?

Response:

(a) The modified Rohsenow pool boiling correlation (Equation 13-10, Reference 13) is used in the calculation of the secondary side heat transfer coefficient during forward heat transfer. The coefficient K_r in the correlation is a function of the pressure on the secondary side of the steam generator.

For pressures less than 800 psia, K_r has been compared to the experimental data from which it was generated using Equation 1.

$$E = \left[\frac{1}{N-K-1} \sum_{x=1}^{N} \left(\frac{K_{exp} - K_{cor}}{K_{cor}} \right)^2 \right]^{1/2} \qquad (1)$$

where:

E = Difference between correlation and experiment, %

N = Number of data points

K = Number of undetermined coefficients in correlation

K_{exp} = Experimental data point

K_{cor} = Coefficient as calculated from correlation

The difference between the correlation for K_r and the experimental data using Equation 1 was 7.2% for data taken over the following ranges.

Pressure 300 - 900 psia

Heat Flux 30,000 to 52,000 BTU/hr-ft^2

The correlation for K_r which is used for pressures greater than 800 psia was based on preliminary results from experiments performed at C-E. When the correlation is compared to a more reliable set of C-E data, a 30.4% difference between the correlation and the experimental data using Equation 1 results. The experimental data base for this comparison has the following ranges.

Pressure 800 - 1200 psia

Heat Flux 27,000 - 86,000 BTU/hr-ft^2

Although both correlations differ from the experimental data, the differences are accounted for in the initialization scheme by adjusting tube resistance and wall fouling resistance term in the calculation of the overall heat transfer coefficient.

(b) The term (P-800) should be (P_{sec} - 800).

440.113 (440.31) Justify the assumption of free convection in the steam generator secondary during reverse heat transfer.

Response:

If the temperature of the secondary side exceeds that of the primary side, then reverse heat transfer (secondary to primary) exists. During this mode of heat transfer, free convection on the secondary side is assumed to exist. The appropriateness of this assumption has been established by the NRC acceptance of the model used for small break LOCA analysis (References 26 & 27) and of the CEFLASH-4AS computer code (References 28 & 29) which utilizes the model. The McAdams correlation used in CESEC (Eq. 13-11 of Ref. 13) for this heat transfer mode is the same as the correlation used in CEFLASH-4AS (Section 2.2 of Ref. 29), as approved by the NRC.

Section 15.0

440.114 (440.32) Is flow through the valves of the steam system assumed to be choked even when the sink pressure is higher than the throat pressure?

Response:

When the sink pressure is higher than the throat pressure, the flow through the valves of the steam system is not assumed to be choked and the orifice equation is used to calculate the mass flow rate. The throat pressure is determined from correlations appropriate to the critical flow correlation used. The turbine is represented by an effective flow area with critical flow and zero sink pressure. When the turbine is tripped the effective flow area is zero.

For steam generator tube rupture events flow rate is calculated using the appropriate correlation. The mass and energy removal from the primary coolant due to this flow is accounted for in the external flow terms of the thermal hydraulic equations (Eq. B-28 of Ref. 13) for the steam generator tube nodes. The addition of this mass and energy to the secondary is accounted for in the "leakage" terms, W_L and h_L, of the steam generator shell side mass and energy balance equations (Figure 13-1 of Ref. 13). It should be noted that these "leakage" terms are specifically for the steam generator tube rupture event. Ordinary operational steam generator tube leakage up to the Technical Specification limit is neglected in analyses done with CESEC (p. 16-4 of Ref. 13).

440.115 (440.33) Justify the expression for A_{TUB} in Fig. 15-1A.

Response:

All flow processes in the secondary system header simulator of Figure 15-1A (of Ref. 13) are assumed to be isenthalpic. The steam flow through the turbine is

$$W_{TUB} = A_{TUB} P_{HEAD} \frac{1977.6}{h_g - 185}$$

Turbine power is $W_{TUB} \times (h_g - h_\ell)$,

where h_ℓ = effective enthalpy of fluid leaving turbine. Turbine power, $P_{TBD} f'_D(t)$, at time t equals the steam power.

Therefore $P_{TBD} f'_D(t) = W_{TUB} (h_g - h_\ell)$

$$= A_{TUB} P_{HEAD} \frac{1977.6}{h_g - 185} (h_g - h_\ell)$$

$$\text{This yields } A_{TUB} = \frac{P_{TBD}}{\frac{1977.6}{h_g - 185} P_{HEAD} h_g} \left[\frac{h_g}{h_g - h_\ell} f'_D(t) \right]$$

The time function power demand fraction, $F_D(t)$, in Fig. 15-1a is therefore equal to $\left[\frac{h_g}{h_g - h_\ell} f'_D(t) \right]$. This quantity is input to the code as a table.

440.116 (440.34) Correct the equation for W_{gL} in Fig. 15-1A.

Response:

The equation for W_{gL} in Fig. 15-1A should read

$$W_{gL} = F_{RC} \left(\frac{P_{SECL} - P_{HEAD}}{v_L} \right)^{1/2}$$

440.117 (440.35) Justify the use of CRITCO for steam discharge flow when the reference+ quoted in the CESEC report is for two phase mixtures.

Response:

Calculations were done to show the correlation between the Darcy formulation for critical flow (last equation on p. 2-15 of Ref. 22) and the CRITCO (Ref. 23) formulation over the pressure range of interest (100-1000 psia) for the steam line break incident. With an average deviation between the Darcy and CRITCO formulations of about 1.7% over the pressure of interest, these two formulas correlate closely. In this comparison for the steam line break incident, the flow path geometry was used to determine the critical flow constants in the Darcy formulation.

For flow through valves the flow path geometry is accounted for by a normalization during code initialization. The code calculates an effective, full-open design valve flow area based on full-open design steam flow at design pressure. Then during the dynamic calculation, the steam flow rate is determined using this area, the pressure, and the fractional valve opening.

+ A. N. Nahavandi and M. Rashevsky, "Computer Program for Critical Flow Discharge of Two Phase Steam-Water Mixtures," CVNA-128, February, 1962.

440.118 (440.36) Is an orifice coefficient used in eq. (16-4) only when the steam generator tube rupture option is selected?

Response:

The orifice equation, (16-4) is of the following form:

$$G = (C \Delta P \rho)^{1/2}$$

where,

G = Mass flow rate per unit area ($lbm/sec/ft^2$)

C = 2 X acceleration due to gravity = $64.4 \left(\frac{lbm - ft}{lbf - sec^2} \right)$

ΔP = source to sink pressure drop (lb/ft^2)

ρ = fluid density (lbm/ft^3)

When the steam generator tube rupture option is selected the right hand side of the above equation is multiplied by a coefficient which accounts for the friction and geometric losses. For other options such as the steam line break option, this coefficient is assumed to be unity. (See page 16-3 of Ref. 13).

Section 17.0

440.119
(440.37) Show why the steam generator load dependency of the steam generator water level, required in the steady state situation, is not needed to determine level during transients.

Response:

The downcomer water level for the steam generator is calculated during the transient using the load dependent model described in Section 17 of Reference 13. The model is used only for the determination of the low water level trip and is valid for steady state or near steady state conditions on the load demand. Since the model is not valid during periods of rapidly changing load demands, the low level trip is not, in general, used as the primary trip for core protection. Other trips such as high pressurizer pressure or low DNBR are the primary trips credited for Chapter 15 analysis. When the low level trip is credited, the setpoint for the trip is conservatively selected.

Appendix B

440.120 (440.31) Equations (B-31), (B-33), (B-35) and B-54) should be corrected.

Response:

(B-31) $(\beta_2 + \alpha_2 h_{\frac{1}{2}}) W_{1,2} - (\beta_2 + \alpha_2 h_2)(1 + F_I) W_{2,3} + (\beta_2 + \alpha_2 h_{\frac{14}{2}}) W_{14,2}$

$\underline{+ \delta_2 \dot{P} = \varepsilon_2}$
$+$

(a second line which ends Eq. (B-31) was missing)

(B-33) $- (\beta_4 + \alpha_4 h_{\frac{4}{2}}) \underline{W_{4,2}} + \delta_4 \dot{P} = \varepsilon_4 - (\beta_4 + \alpha_4 h_{\frac{12}{4}}) W^R_{P2}$
$+$

(error in first term: Was $W_{4,12}$, should be $W_{4,2}$)

(B-35) $(\beta_6 + \alpha_6 h'_5) W_{5,6} + (\beta_6 + \alpha_6 h_3) \underline{F_B} W_{3,5} - (\beta_6 + \alpha_6 h_6)(1 + F_o + F_H) W_{6,7}$
$+$

$+ \delta_6 \dot{P} = \varepsilon_6$

(error, was F_R, should be F_B)

(B-54) $(\beta_{25} + \alpha_{25} h_{\frac{6}{25}}) F_H \underline{W_{6,7}} + (\beta_{25} + \alpha_{25} h_{\frac{18}{25}}) F_H W_{18,19} - (\beta_{25} + \alpha_{25} h_{25}) W_{25}$
$+$

$+ \delta_{25} \dot{P} = \varepsilon_{25}$

(error in second term: was $W_{6,25}$, should be $W_{6,7}$)

440.121 (440.39) Is reverse flow allowed in the core?

Response:

The CESEC code does not allow reverse flow in the core.

440.122 (440.40) Is $W_{25} = 2W_{25,7}$?

Response:

$$W_{25,7} = W_{25,19} = 0.5W_{25}$$

440.123 (440.41) Describe the algorithm CESEC uses to trace the state of the pressurizer and to maintain continuity as the state changes. Is there an automatic time step adjuster?

Response:

The continuity of the state changes of the pressurizer fluid is controlled using the algorithms described in Section 4.2.5.3 of Reference 3. There is no automatic time step adjustment due to the pressurizer status change in CESEC. The user is furnished at each major edit with a print-out of the accummulated non-conservation of mass and energy in the pressurizer (and in the RCS) up to that time. If the small discontinuities which may result from state changes cause significant non-conservations of mass and/or energy, the user can re-run the case with smaller time steps.

The initially pre-determined values of fluid mass and enthalpy are associated with the pressurizer fluid status defined as saturated liquid and vapor.

At the beginning of each time step the actual fluid mass and enthalpy values are updated based on the pressurizer status, i.e., the status determined at the end of the previous time step.

At the end of each time step the pressurizer status is determined based on the vapor and liquid mass and enthalpy check. If the current status differs from that determined at the end of the previous time step, the necessary adjustment takes place and an appropriate message is given to the user. The adjustment is performed in order to maintain the continuity of the pressurizer status throughout the transient.

440.124 (440.42) Justify the identification, in state 8, of W_B with the vapor portion of the critical flow through the pressurizer valve. How is this consistent with the absence of W_B in state 7?

Response:

No boiling is assumed for pressurizer state 7 which is defined as subcooled liquid without presence of a steam region. However, when the pressurizer state is checked (at the end of each time step) boiling can appear (see the response to Question 440.123) in which case the pressurizer state is changed to 8 if $W_B \leq W_{valve}$ or to 4 if $W_B > W_{valve}$. Since the valves are located near the top of the pressurizer, for the condition $W_B \leq W_{valve}$, it is assumed that all steam generated from boiling is removed through the valves. Therefore the boiling flow in state 8 is identified with the vapor portion of the valve flow at the valve entrance. Note that this is used to determine the enthalpy of the fluid entering the valves, not the vapor fraction directly. Flashing in the valves will in general increase the vapor fraction in the flow exiting the valves.

440.125 (440.43) Provide references for the two phase pressure drop correlations eqs. (C-1) - (C-5) and a comparison with the Barcozy+ or Chisholm* correlation.

Response:

Equations (C-1) through (C-5) provide the two-phase multiplier for the frictional pressure drop term for pressures less than 250 psia. The appropriateness of these equations has been established by the NRC acceptance of the model (Section III. C.2.b of Ref. 15) and of the CEFLASH-4A computer code (Section III. B.18 and Appendix N, of Ref. 16) which utilizes the model.

+ C. J. Baroczy, "A System Correlation for Two Phase Pressure," AIChE reprint #37. Paper presented at the 8th Nat. Heat Transfer Conf., Los Angeles, Aug., 1965.

* D. Chisholm, "The Influence of Mass Velocity on Frictional Pressure Gradients During Steam-Water Flow," Paper 35 presented at the 1968 Thermodynamics and Fluid Mechanics Convention, Bristol, 1968.

440.126 (440.44) Are the CEFLASH-4A water properties applicable to the supercritical region? Provide a copy of the report+

Response:

The McClintock and Silvestri routines (Ref. 31) are used to determine water properties in CESEC (p.8-1, Ref. 13). Water property derivatives are determined using CEFLASH-4A routines (p. 8-2, Ref. 13). The CEFLASH-4A water property derivatives are limited to subcritical pressure regions. The transients which are studied in the safety analysis reports stay within the applicable pressure range. ATWS transients, which may go beyond this range, would bear further investigation to determine the errors encountered by use of the CEFLASH-4A water property derivatives. However significant errors are not expected, even for ATWS transients. At the present time there is no ATWS licensing requirement. CESEC-III is not being used for ATWS evaluations.

A copy of the requested document + has been transmitted.

+CENPD-133, "CEFLASH-4A, A FORTRAN IV Digital Computer Program for Blowdown Analysis," August, 1974.

440.127 (440.45) Explain why eq. (D-12A) can be neglected.

Response:

The set of equations which appear in Section 5.0 and Appendix D of the CESEC report have been approved by the NRC for usage in CEFLASH-4A (Reference 16). These equations appear, respectively, in Section III.B.3 and Appendix I of Ref. 16.

Equation D-11 as explained in Ref. 16 and Appendix D of the CESEC report can be rewritten in terms of two linear differential equations of the first order. The solution of these equations then represents the total solution to Equation D-11. Equation D-12B relates the exit fluid conditions of the node to the nodal average fluid conditions, while Equation D-12A yields the relationship between inlet and average node enthalpies. The solution of Equation D-12A provides numerically for the proper heating of the fluid as it exits the node for steady state and transient conditions. Therefore, Equation D-12A may be neglected from a numerical standpoint.

440.128 (440.46)

(a) How is the reference exit temperature in the steam generator node calculated and how is it used?

(b) How is the exiting enthalpy computed?

Response:

(a) The reference exit temperature used in CESEC is Tsec, the temperature of fluid in the secondary side of the steam generator. This reference temperature is applied to ensure that the heat transfer between the primary and secondary sides has not violated the second law of thermodynamics. In other words, it is used as a physical bound for the calculated exiting temperature of the primary side. For example, in the situation of heat transfer from primary to secondary, the exiting temperature of the primary side must be greater than or equal to Tsec. For the situation of reverse heat transfer, secondary to primary, the exiting temperature of the primary side must be less than or equal to Tsec. Upon violation of the 2nd law of thermodynamics, the exiting enthalpy is set equal to the node enthalpy (see Equation (D-15)). This updated value of exiting enthalpy is then used in either Equation (D-13) or (D-14), depending on the flow condition, to solve for the corrected heat transfer rate between primary and secondary, Q. At this point, the newly calculated heat transfer rate is compared to the original which is calculated by the steam generator algorithm (see Equation (13-1)). If the direction of heat transfer predicted by both calculations is the same, then the corrected heat transfer rate and the updated exiting enthalpy (node enthalpy) will be used for that

time step. If the direction of heat transfer predicted by both calculations is not the same, then the heat transfer rate is set equal to zero for that time step. These steps are presented in outline form in the detail at step G(8) of figure 440.128-1.

(b) The exiting enthalpy is calculated by using either Equation (D-13) or (D-14).

Figure 440.128-1

CESEC DYNAMIC CALCULATION SEQUENCE

A. Determine time step size.

B. Calculate parameters for Runge-Kutta-Merson (Ref. 35) integration in the interval between t - Δt and t for

- fuel temperature
- steam generator secondary parameters
- reactor kinetics

C. Calculate reactivity at time t

D. Integrate pump and flow model equations over interval from t -Δ t to t

E. Calculate values of parameters at time t for

- pressurizer
- feedwater system
- steam system

F. Determine values of parameters and their derivatives at time t (complete Runge-Kutta-Merson integration) for

- fuel temperature
- steam generator secondary parameters
- reactor kinetics

G. Integrate RCS thermal hydraulics equations

(1) calculate values of coefficients and right-hand side of thermal hydraulics equations

(2) solve thermal hydraulic equations for flows and rate of change of pressurizer pressure

(3) if surge line pressure drop iteration scheme is not converged return to (1) and repeat, otherwise calculate surge line pressure drop and continue with (4)

(4) use flows and rate of change of pressurizer pressure to determine rates of change of enthalpies

(5) use Euler integration to determine pressurizer pressure and enthalpies at $t + \Delta t$

(6) calculate RCS pressure from pressurizer pressure and surge line pressure drop

(7) calculate other thermodynamic properties from pressures and enthalpies

(8) calculate the exiting enthalpy for reactor core and steam generator tube nodes

(a) use enthalpy transport algorithm to calculate existing enthalpies

(b) check for 2nd law violation for steam generator tube nodes, if none continue with step (f), otherwise continue with step (c)

(c) set exit enthalpy equal to node average enthalpy

(d) calculate a primary to secondary heat transfer rate which is consistent with exit enthalpy

(e) check for inconsistency in heat transfer direction, if consistent continue with step (f), otherwise set heat transfer rate equal to zero before continuing with step (f)

(f) integration of thermal hydraulics is complete and main calculation is continued at step H.

H. Integrate wall heat equations

I. Calculate reactor protective system trip action times

J. Integrate boron transport equations

K. Print minor or major edit if called for at this time

L. Continue at A unless time equals the run end time

440.129 (440.47) Prove that eq. (E-4) converges.

Response:

Convergence of Equation (E-4) is a necessary condition for the execution of CESEC. The equation is known to converge within the upper limit specified within the code on the number of iterations. If this limit is exceeded, code execution is terminated.

440.130 (440.48) How is the moderator feedback divided between the void feedback and the density feedback?

Response:

Void formation is not a significant concern in non-ATWS events. In ATWS calculations, the void contribution to moderator reactivity is separated from the density contribution as follows.

When there is significant void formation in the core, the density contribution to moderator reactivity is evaluated at the core average two-phase density of the coolant under saturated conditions at the given pressure (P) and temperature (T). An input table of moderator reactivity vs. moderator density is interpolated for this purpose.

The method of estimating the void contribution consists of (1) calculating the void distribution throughout the core, and (2) flux and volume weighting the point-wise reactivity contributions to obtain the core average void reactivity. With a knowledge of void distribution and hence the density distribution in the core, spatially dependent void reactivity R(z) is given by the relation:

$$R(Z)_{void} = R\left[D(Z)_{P,T} \right] - (D_{P,T})$$

where P = system pressure (psia)

T = saturation temperature at pressure P (F)

$D_{P,T}$ = core-average two-phase density when coolant is

saturated at pressure P and temperature T.

$\rho(D_{P,T})$ = reactivity contribution due to the core-average two-phase moderator density.

$D(Z)_{P,T}$ = local two-phase fluid density corresponding to the given P, T and the local void fraction.

R[D(Z)] = local point-wise reactivity interpolated from an input table at density D(Z).

The above formula is flux and volume integrated over the core to obtain the core average void reactivity ρ_V. (Ref. 2, Section 2.3 and Ref. 6, Section 1.4).

440.131 (440.49)

(a) Provide additional information about the core coolant flow and temperature calculation as the connection between COREQ and LOOPEQ is not clear. Which moderator temperature and density is used for the reactivity feedback?

(b) What fraction of instantaneous core power is absorbed by the coolant?

Response:

(a) COREQ is the CESEC-ATWS routine responsible for reactor kinetics and fuel heat transfer calculations. Briefly, it solves the point kinetic equations, and performs decay heat calculations to arrive at the total core power. Alternatively, core power can be specified as an input function of time, and the ANS decay heat curve option is available after long term operation.

In the heat transfer part of COREQ the standard heat conduction equation for the core average channel is solved to obtain the temperature distribution and core heat flux at each time step. The heat conduction model uses three equal volume radial nodes in the fuel rod, and one node in the coolant channel. Core coolant flow is an input constant to this calculation (Ref. 6, Section 1.3).

LOOPEQ does not perform any calculations in CESEC-ATWS. This routine was retained for initializing certain parameters such

as RCS temperatures and flows. There is no direct connection between COREQ and LOOPEQ.

Moderator reactivity is determined in the code at core-average moderator temperature and density by interpolating input reactivity tables.

(b) The fraction of instantaneous core power liberated in the moderator is a plant specific input parameter. Typically for a PWR, the value is around 2.5%.

440.132 (440.50) Justify the reactivity flux weighting method (i.e., flux or flux**2).

Response:

Although provision for reactivity flux weighting exists in the void reactivity model, this option has not been utilized. In analyses performed to date, only one axial node is specified for the core in the input, and as such flux weighting is immaterial.

440.133 (440.51) Why does the void reactivity calculation employ static quality when the Martinelli-Nelson correlation+ referred to uses flowing quality?

Response:

The void reactivity calculation option has not been exercised in CESEC-III. It has been used only in ATWS analyses.

Martinelli-Nelson correlation is used to estimate the void fraction when system pressure falls below 1850 psia. At pressures of 1850 psia and higher, the void formation is simply given by the homogeneous model based on static quality.

In ATWS events the critical parameter is the RCS peak pressure which is in the region of 2900-4000 psia for C-E plants. Thus, Martinelli-Nelson correlation is of no concern in predicting the severity of ATWS events. The correlation comes into play only during the depressurization phase when system pressures are below 1850 psia and power levels are low (< 10% design).

The question of static vs. flowing quality in Martinelli-Nelson correlation has no effect on the conclusions of the safety analysis. Therefore, the use of static quality derived from the enthalpy distribution throughout the calculation is a simplifying assumption which is entirely adequate. Additionally, a comparison of total reactivity for a range of representative cases shows good agreement between CESEC and PDQ-TH which is the industry-wide production code for reactor physics calculations. This comparison

confirms the adequacy of using static quality throughout in the void reactivity calculations. (See Section 2.0, Reference 6).

+N. C. Sher, "Review of Martinelli-Nelson Pressure Drop Correlation," Westinghouse Electric Corp., Report WAPD-TH-219 (July 1956).

440.134 (440.52)

(a) Is the quantity Q used in T_{eff} for the Doppler an input constant.

(b) How is it determined?

Response:

(a) Doppler reactivity is interpolated from an input table of reactivity vs effective fuel temperature T_{eff}. The quantity Q used in the expression for T_{eff} is not an input constant. It is defined as the ratio

$$Q = \frac{\text{Core heat flux (t)}}{\text{Design power}}$$

Design power is an input to the code, while core heat flux is calculated at each time step.

(b) Average core heat flux is computed in CESEC by solving the heat conduction equation for an average fuel rod surrounded by moderator. In the steady state, core heat flux equals the total fission power (Mwt), and Q is a constant. In a power transient, however, the heat flux from the fuel lags behind the total fission power, and Q, the core heat flux expressed as a fraction of input design power becomes time-dependent. Details of the fuel heat conduction model are found in Ref. 6, Section 1.3 and related references.

440.135 (440.53) Justify the CESEC/PDQ-TH calibration scheme for weighting factors.

Response:

A comparison of total reactivity as calculated by CESEC-ATWS and PDQ-TH for several realistic cases, shows that there is good agreement between the two codes, and hence, demonstrates the adequacy of the CESEC reactivity model. Thus, weighting factors to adjust reactivities are no longer used (Ref. 6, Section 2.0).

440.136 (440.54) Explain why in the formulation of the T/H nodal equations the pressure p is used but in the determination of water properties the pressure $p + \Delta p_{surge}$ is utilized.

Response:

Although for a different number of nodes, the CESEC-ATWS code uses the same thermal-hydraulic formulation as the CESEC-III version. Therefore, refer to the response to Question 440.87 for the response to this question.

440.137 (440.55) Present the derivation/assumptions used to reduce the T/H nodal equations to a 19 equation set.

Response:

The derivation for the 19 equation set utilizes the same assumptions as are used for CESEC-III, but with different variable names. The derivation for the 19 equation set is presented in Section 4.2 of Reference 3.

440.138
(440.56)

In the T/H model is the instantaneous core power entirely absorbed by the coolant with no heating of the fuel?

Response:

The CESEC-ATWS code uses the same formulation as the CESEC-III version. The instantaneous core power is used in the solution of the heat conduction equation for the fuel rod. A discussion of the solution model is presented in Section 10.2 of Reference 13.

440.139 (440.57) Are the sprays 100% efficient?

Response:

The pressurizer sprays are 100% effective in the CESSAR-ATWS code.

440.140 (440.58) Discuss the DNBR calculation in more detail; in particular the open/closed channel aspect.

Response:

The CESEC-ATWS code had the capability of calculating DNBR. This calculation is used only to determine trends in DNBR and not for safety analysis. Refer to question 440.84 for the details of the DNBR methodology.

440.141 (440.59) Describe the modelling of the steam bubble. What effect does the assumption of a uniform RCS pressure have?

Response:

The CESEC-ATWS code does not explicitly model the formation of voids in the upper head region which may occur during events with rapid primary system depressurization or overcooling.

SAR Chapter 15 depressurization and overcooling transients, which have a potential for causing void formation due to pressurizer drain, or depressurization to saturation conditions, are increased heat removal by the secondary system events (e.g., steam line break) and the decrease in primary system inventory events (e.g., steam generator tube rupture). Analyses of these transients have been conducted (Ref. 18) to evaluate the impact of void formation in the reactor vessel upper head region on system response and in terms of meeting criteria as specified by the SRP guidelines.

The limiting Chapter 15 accident with respect to void formation for the increase in heat removal events is the steam line break. For the decrease in inventory events the steam generator tube rupture is limiting. The limiting anticipated operational occurrence (AOO) is the inadvertent opening of an atmospheric dump valve with loss of offsite power (limiting single failure). Conclusions from these analyses, for which the most severe depressurization is predicted, bound the rest of the SAR Chapter 15 depressurizaton and overcooling events.

The SAR analyses performed with vessel head voiding indicate that voiding is not extensive enough to initiate the uncovery of the reactor vessel hot legs. Additionally, these analyses conclude that voiding does not result in violation of the SRP requirements for C-E plants. The main impact of the vessel upper head void is a slower pressure response; since once this relatively stagnant region reaches saturation, it acts like a pressurizer. The slower pressure response can hold up the pressure for steam generator tube rupture and steam line break events. This will increase the primary to secondary leakage during a steam generator tube rupture event and reduce the safety injection flow during a main steam line break event. However, the impact of these effects does not result in a violation of the criteria specified by the SRP guidelines, even though upper head voiding has an impact upon transient values of plant parameters.

See response to Question 440.86 for assumption of a uniform RCS pressure.

440.142 (440.60) Is there only boiling heat transfer on the secondary side of the steam generator and only film heat transfer on the primary side?

Response:

In the CESEC-ATWS code, boiling heat transfer is assumed to exist in the secondary side until the quality exceeds 90%. At qualities greater than 90% no heat transfer is assumed to exist. Refer to the response to Question 440.143 for the details of the tube bundle quality calculations.

On the primary side of the tube bundle, only film heat transfer is assumed to exist.

440.143 (440.61)

(a) Explain the steam generator dryout heat transfer criterion and the calculation of UA.

(b) How is the steam flow calculated?

(c) How is tube heat transfer area related to the mass inventory, the recirculation flow, and the quality calculation?

(d) How is quality calculated?

Response:

(a) Refer to the response to Question 440.143, part C.

(b) The steam flow from the secondary side of the steam generator is determined as described in Section 15.0 of Reference 13.

(c) A model is provided in the CESEC-ATWS code to calculate the steam quality in the tube bundle region, the downcomer level, and the effective heat transfer area, for each of the two steam generators. The calculations are performed consistent with the assumptions of saturated conditions in the steam generator. For this calculation, the liquid inventory, the steam inventory, the secondary pressure, the fluid specific volume, the steam specific volume, the feedwater flow, the steam flow, and the time step increment, are the independent variables. The model calculates the steam generator downcomer level, and the fraction of total tube bundle area, which is effective in

providing heat transfer.

The steam generator is divided into five basic regions, the downcomer, the steam drum, a riser region with a perfect steam separator, a non-boiling region of the tube bundle, and a boiling region of the tube bundle. During conditions where effective heat transfer exists over the entire length of the tube bundle, the boundary between the non-boiling and boiling regions of the tube bundle and the tube bundle exit quality are calculated consistent with the total liquid and steam inventory in the steam generator. Two basic assumptions made in this calculation are the existence of saturated conditions (for both water and steam) and a linear variation of quality with height in the boiling region of the tube bundle. Although the option of specifying a non-boiling region exists, the option was never exercised. The non-boiling region terms, however, are included here for completeness.

The downcomer level is determined from hydraulic and momentum balance around the internal circulation loop of the steam generator, which is described by:

```
DCL = (H1*1./VF-1./VR) + H2*(1./VB-1./VR) + HRISER*
(1./VR-1./VG)                                              (1)

+ HTUBE*(1./VR-1./VG) + DP*144.)/(1./VF-1./VG)
```

where:

DCL = water level in the downcomer region

H1 = height of the non-boiling region of the tube bundle

H2 = height of the boiling region of the tube bundle

VF = specific volume of saturated liquid

VG = specific volume of saturated steam

HTUBE = height of the tube bundle

VB = average specific volume of the tube bundle boiling region assuming a linear variation in quality.

calculated by
1.0/((1.0/(VFG*XR)))*ALOG(((VF+VFG*XR)/VF)))

XR = tube bundle exit quality

VFG = VG - VF

HRISER = height of the riser region

VR = average specific volume of the riser region

calculated by
VF + VFG * XR

DP = momentum pressure drop

In establishing the initial steady-state conditions, the downcomer level is input, the tube bundle exit quality is calculated and Equation 1 is solved for the balancing pressure drop.

During steam generator operation in the absence of any decrease in the effective heat transfer area, the total fluid mass in the steam generator (TØTFM) is given by:

$$TØTFM = DCM + SCM + BØILM + RISEM \qquad (2)$$

where:

DCM = fluid mass in the downcomer region

= VDC/VF and VDC is the volume of the downcomer region calculated as a function of downcomer fluid level.

SCM = fluid mass in the non-boiling region of the tube bundle.

= ATUBE*H1/VF where ATUBE is the cross-sectional area of the tube bundle.

BØILM = fluid mass in the boiling region of the tube bundle

= (ATUBE*H2/(VFG*XR)*((VG/VFG)*ALØG((VF+VFG*XR)(/VF)-XR)

RISEM = fluid mass in the riser region

= ARISER*HRISER* (1.-XR)/(VF+VFG*XR)

The total steam mass in the steam generator (MSTØT) is given by:

MSTØT = BØILS + RISES + DRUMM (3)

where:

BØILS = steam mass in the tube bundle

RISES = steam mass in the riser region

DRUMM = steam mass in the drum region

Steam masses are determined from similar equations involving the appropriate volumes, qualities and specific volumes, as are the fluid masses.

The two transcendental equations, 2 and 3 are solved iteratively for XR and DCL until the total steam and fluid masses converge to the total steam and fluid masses determined by a mass and energy balance

for the secondary side.

For those transients in which the steaming rate exceeds the feedwater flow rate: as the inventory of the steam generator is depleted and the total energy input to the steam generator is sufficient to increase the quality in the steam generator, secondary side bundle. A tube bundle exit quality will eventually be reached above which a mode is switched where the exit quality is kept constant at XDNB and H2 determined from Equations 2 and 3 to define the location where XDNB was first achieved (See Figure).

A heat transfer area degradation factor is then calculated by:

ARATIO = H2/HTUBE

where ARATIO is the ratio of the tube bundle height over which effective heat transfer is maintained to the total tube bundle height. This ratio is then used to modify the effective heat transfer area in the overall heat transfer coefficient calculation. Thus, the overall heat transfer is calculated as

$$U_D A_D = U_D * A_{HTUBE} * ARATIO.$$

where:

U_D = Dynamic overall heat transfer coefficient, BTU/hr-ft - F

A_D = Effective heat transfer area, ft

A_{HTUBE} = Total heat transfer area, ft

Further information on the steam generator model in the CESEC-ATWS code is presented in Section 3.2 of Reference 2, Section 3.3 of Reference 3, and Section 4.2 of Reference 6.

(d) Refer to the response to Question 440.143, part c.

QUALITY AND HEAT TRANSFER PROFILE
DURING SECONDARY SIDE DRYOUT

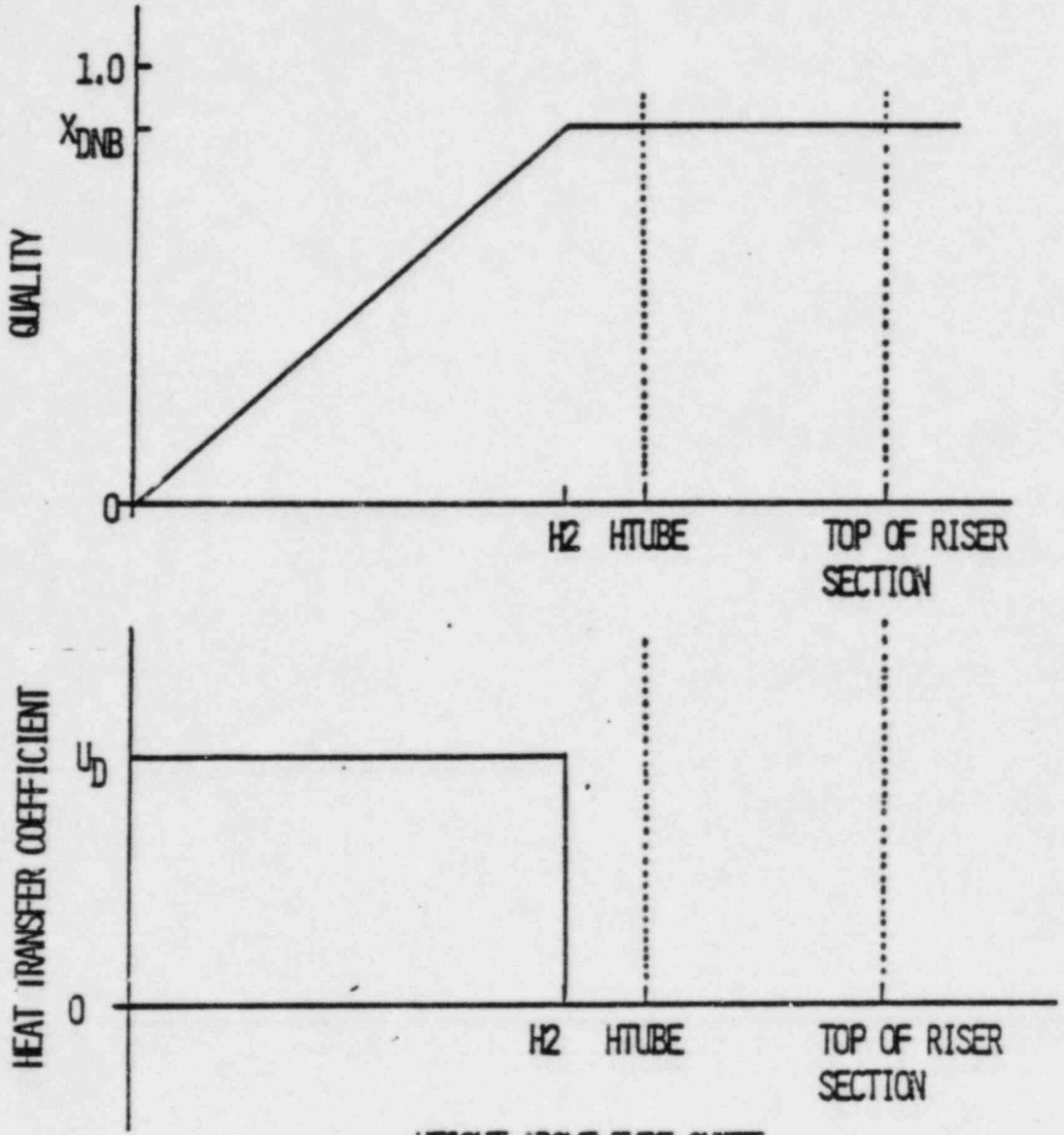

440.144 (440.62) Is it correct that the heat transfer in the steam generator is

$$Q = \begin{cases} \dfrac{UA\,(T_i - T_s)}{\ell n \dfrac{(T_i - T_s)}{(T_o - T_s)}} & UA = 1.0\ UA \text{ forward transfer} \\ & \quad = \text{input reverse transfer} \\ & \text{when } T_i > T_s \text{ and } T_o < T_{-s} \\ UA\left(\dfrac{T_i + T_o}{2} - T_s\right) & \text{with } UA = 0.8\ UA \text{ of previous timestep} \end{cases}$$

where UA = overall heat transfer coefficient

T_i = primary side inlet temperature

T_o = primary side outlet temperature

T_s = secondary side temperature

Response:

Yes, the heat transfer in the steam generator is governed by these equations in the CESEC-ATWS version of the code.

440.145 (440.63) (a) Does the code use the cold edge temperature or the cold leg temperature for the moderator feedback?

(b) How is the cold edge temperature calculated?

Response:

(a) For conservatism in the analysis of steam line break initiated events, the code has an option which allows the user to specify that the cold edge density will be used for moderator feedback calculations.

(b) The cold edge density is determined from the RCS pressure and the cold edge enthalpy, h_{edge}. The cold edge enthalpy is defined as the enthalpy of the fluid from the cold legs of the loop with the ruptured steam generator, with the addition of core heat up to the core axial midplane, and without the effect of mixing with fluid from the other loop. Using the notation used in Section 2 of Ref. 13,* and choosing SG2 as the steam generator with the ruptured steam line, an expression for h_{edge} can be written for steady state:

$$h_{edge} = h_1 + \frac{Q}{4W_{3,5}} \quad , \qquad (440.145\text{-}1)$$

where Q is the total core heat generation rate and where it is assumed that $h_1 = h_4$ due to steady-state conditions.

* See also Figure 440.145-1

/b/

The following also hold true at steady-state:

$$W_{16,14} = W_{13,14} = W_{1,2} = W_{4,2}\ ,\ W_{14,15} = W_{2,3}\ ,$$

$$W_{15,17} = W_{3,5}\ ,\ \text{and}\ h_{13} = h_{16}.$$

Mass and energy balances can be written on nodes 3 and 15 and solved using the foregoing steady-state relationships together with the coolant heatup from node 3 to 5 and from node 15 to 17, to yield the enthalpies at nodes 5 and 17:

$$h_5 = \frac{h_1 + h_{13} F_I}{1 + F_I} + \frac{Q}{4W_{3,5}} \qquad (440.145\text{-}2)$$

$$h_{17} = \frac{h_{13} + h_1 F_I}{1 + F_I} + \frac{Q}{4W_{3,5}} \qquad (440.145\text{-}3)$$

Simultaneous solution of Eqns. (440.145-1), (440.145-2) and (440.145-3) yields the algorithm used in CESEC to calculate cold edge enthalpy:

$$h_{edge} = \frac{h_5 - h_{17} F_I}{1 - F_I} = \frac{h_5 + h_{17}}{2} - \frac{(1 + F_I)}{(1 - F_I)} \left(\frac{h_{17} - h_5}{2} \right)$$

(440.145-4)

FIGURE 440.145-1

SCHEMATIC OF C-E NSSS

SHOWING APPROXIMATE CESEC NODALIZATION

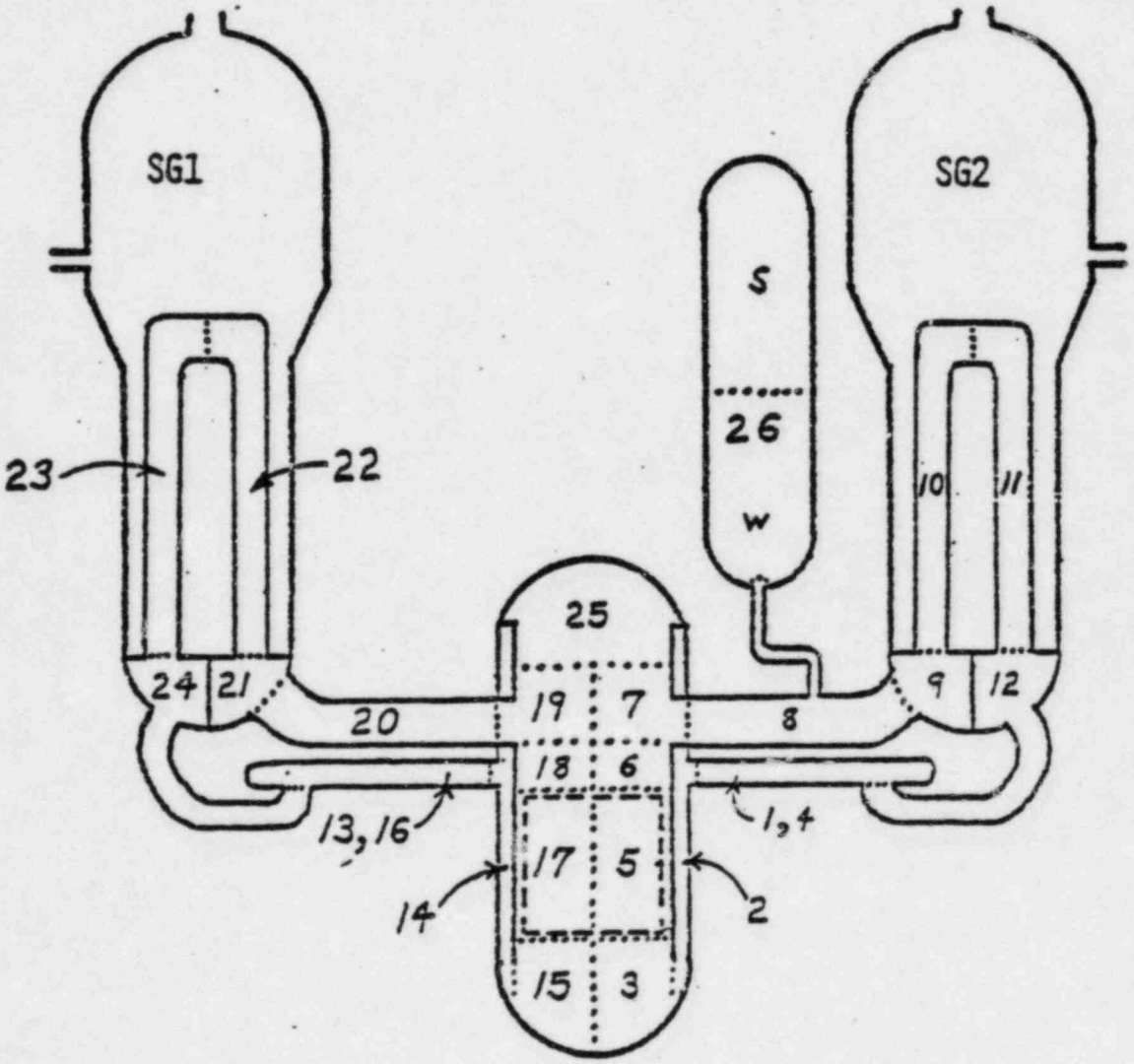

440.146 (440.64) Is there an iteration between the pump flow calculation and the energy/mass balance calculations?

Response:

There is no iteration between the pump flow calculation and the thermal hydraulic equations.

440.147 (440.65)

(a) How is the input flow fraction for the outlet plenum to closure head flow determined?

(b) Are the plena crossflows or the bypass flows user specified? If so what is the basis for the input valves?

Response:

(a) The method used to determine the fraction of flow from the outlet plenum to the closure head, F_H, is based on flow net calculations. All possible flow paths are determined and the loss coefficients for each component in each flow path is calculated. The loss coefficient calculations are generally based on published experimental data. Invoking conservatism of momentum and mass, the flow net equations are solved for each node. The results of these flow net calculations are mainly used for ECCS analysis and are quite detailed. All the fractions of flow from all flow paths leading from the outlet plenum to the upper head are summed to produce the input value of F_H for CESEC.

(b) Certain plena crossflows and the bypass flows are calculated using input flow fractions. The plena crossflows $W_{2,14}$ and $W_{7,19}$ (see footnote on page 2-2 and Figure 2-1 of Ref. 13) are determined directly from the solution of the thermal hydraulic equations. The other plena crossflows are determined as described on page 2-2 of Reference 13, with the factors F_I and F_O being user specified values which are determined as

described in response to Question 440.150. The bypass flows are calculated using the input flow fraction F_B:

$$W_{3,6} = F_B W_{3,5}$$

$$W_{15,18} = F_B W_{15,17}$$

The bypass fraction, F_B, used for CESEC calculation is taken to be equal to the design value. However, bypass flows are calculated in considerable detail, using methods similar to those used to calculate F_H, to ascertain that the total bypass flow does not exceed the design value.

440.148 (440.66) How is the UA parameter used in the steam generator heat transfer determined at the minimum mass inventory [for CESEC-SLB]?

Response:

UA is set equal to a value sufficient to transfer enough heat to raise any incoming feedwater to saturation enthalpy at the minimum mass inventory in CESEC-SLB.

440.149
(440.67)

It is our intent that CESEC-III be used for future analyses instead of CESEC-I or CESEC-II. Please demonstrate that CESEC-III is capable of performing the required analyses by submitting an analysis of the following transients for the CESSAR design using CESEC-III:

(a) steamline break,

(b) feedwater line break,

(c) loss of feedwater ATWS, and

(d) steam generator tube rupture.

The results obtained with CESEC-III should be overlaid with the results obtained with CESEC-I and CESEC-II.

Response:

(a) Comparisons of CESEC-I, CESECII, and CESEC-III for Steam Line Break Analyses.

Introduction:

Comparisons of results obtained using CESEC-I, CESEC-II, and CESEC-III for a full power large steam line break (SLB) with concurrent loss of offsite power are presented in Figures 440.149A-1 through 12. The comparisons between CESEC-I and

CESEC-III have been made for Waterford Unit 3 and are shown in Figures 440.149A-1 through 6. Table 440.149.a-1 presents the initial conditions and Table 440.149.a-2 presents the sequence of events for this CESEC-I/CESEC-III comparison. The CESEC-I results presented here are the same as those given in the Waterford Unit 3 FSAR. Figures 440.149A-7 through 12 present comparisons between CESEC-II and CESEC-III for System 80. Table 440.149.a-3 presents the initial conditions and Table 440.149.a-4 presents the sequence of events for this CESEC-II/CESEC-III comparison. The results obtained using CESEC-III are those presented in CESSAR-F. For each case, plots of reactivity, core power, RCS pressure, reactor coolant temperatures, reactor coolant flow rate, and minimum post-trip DNBR are presented versus time. The first five of these parameters are calculated directly by CESEC. A separate calculation, using CESEC output is used to determine DNBR.

The differences between results obtained using CESEC-III compared with those obtained using CESEC-I or CESEC-II are due to the presence of improved models in CESEC-III. For these SLB transients the most important effects are due to the improved/new models for

- reactor coolant pumps/flow
- reactor vessel upper head
- 3D reactivity feedback
- heat transfer from the metal walls of the RCS

The effect of each of these models upon the transient results will be discussed first with respect to comparison of CESEC-I with CESEC-III for Waterford and then with respect to the comparison of CESEC-II with CESEC-III for System 80.

CESEC-I/CESEC-III comparison

The major reason for those differences which exist between the CESEC-I and CESEC-III results for Waterford are due to the differences in reactor coolant flow. CESEC-I uses an input table of flows. CESEC-III uses the pump/flow models to calculate flow. This model has been shown to yield very good agreement with test results (Fig. I-2 of Ref. 13). The initially higher loop flows in the CESEC-I analysis causes a more rapid transport of the effect of the cooldown to the moderator density. This results in an early return-to-power in the CESEC-I analysis. The associated fluid heating, together with reactor coolant flows which by this time are lower than those calculated by CESEC-III, results in a marked increase in reactor average and outlet temperatures. CESEC-III shows lower core inlet -- and consequently average and outlet -- temperatures due to the appreciable higher flow rate from the loop with the affected steam generator compared with that from the other (hotter) loop. Overall moderator reactivity values

are very similar for both code versions since both base moderator reactivity on a cold edge density. CESEC-III calculates this density as described in the response to Question 440.145. The method for determination of cold edge density in CESEC-I is presented in Section 2.2.9.3 of Ref. 1.

The RCS pressure decrease with NSSS cooldown calculated by CESEC-III shows the effect of upper head voiding. The CESEC-I and CESEC-III pressure transients are essentially identical until flashing begins in the upper head node of the CESEC-III model. Without the influence of an upper head model RCS pressure, as calculated by CESEC-I, continues to fall until the pressurizer empties and hot leg saturation occurs. Thereafter the RCS pressure in CESEC-I follows the hot leg saturation temperature until pressurizer level is re-established.

The Waterford CESEC-III analysis illustrates the 3D reactivity results upon an SLB transient. As the power-to-flow ratio and the temperature tilt across the core (see the response to Question 440.101) increase during the cooldown/return-to-power portion of the transient, 3D effects contribute a small amount of negative reactivity to help reduce the return-to-power.

For the analysis presented here wall heat transfer effects were included mainly in the upper head node of the reactor vessel. This increased the amount of void formation in the upper head and reduced the rate of decrease of RCS pressure. For the balance of the RCS only those components which could contribute

to heating of the RCS coolant over very long time periods were included. The effect upon the SLB transient of this heating over the time span shown here was small.

The minimum post-trip DNBR is affected by core power, core flow, core inlet temperature, and RCS pressure. Due to the very large radial neutron power peaking factors associated with the DNBR analyses for the post-trip portion of SLB events with an assumed stuck CEA, the most important parameter for these analyses is usually the core power at time of return-to-power. The lower return-to-power is the major factor in the higher DNBR calculated from the CESEC-III results. The slightly higher core flow and lower core inlet temperature had a smaller contribution. The effect of RCS pressure was negligible.

CESEC-II/CESEC-III comparison

Similar to the comparison between CESEC-I and CESEC-III for Waterford, a significant reason for differences between CESEC-II and CESEC-III results for System 80 is the difference between reactor coolant flow in the two analyses. However, both the effect of the upper head model and the wall heat model are more evident for System 80, the upper head model having the most significant effect. The 3D reactivity model was not used in this analysis.

CESEC-II uses an input table of flows, as does CESEC-I. The effect of the large natural circulation driving heads caused by

the cooldown is to produce higher core flow in the CESEC-III results after reactor coolant pump coastdown. This causes a lower core T and a more rapid cooldown with earlier steam generator dryout. The presence of heat from the walls of the RCS compensates for the more rapid cooldown due to the higher natural circulation flow to yield a net cooldown rate which is slightly less than that calculated using CESEC-II. Further, this wall heat yields minimum transient temperatures from CESEC-III which are somewhat greater than those determined by CESEC-II.

The effect of the upper head node upon RCS pressure is much more pronounced for System 80 due to the much larger upper head volume than that present in other C-E NSSSs. The marked reduction in rate of depressurization at the point of initiation of void formation in the upper head model of CESEC-III yields a safety injection flow which is both delayed in time and reduced in amount compared with that calculated by CESEC-II. This causes a larger calculated post-trip total reactivity and resulting return-to-power for CESEC-III than for CESEC-II.

As for the Waterford analysis the major effect upon the calculated post-trip minimum DNBR for System 80 is the core power. The impact of the other relevant parameters is small due to the lack of a return-to-power in the CESEC-II analyses.

Summary:

The CESEC-I/CESEC-III comparison and the CESEC-II/CESEC-III comparison demonstrate that CESEC-III models important effects for SLBs more completely than did either CESEC-I or CESEC-II. Further the CESEC-I/CESEC-III comparisons demonstrates that the conclusions reached in SLB analyses done using CESEC-I would not be changed by analyses done with CESEC-III. No FSAR analysis uses CESEC-II for SLB events.

(b) Of all the decreased heat removal events analyzed in Section 15.2 of the FSAR, the feedwater line break event is limiting in terms of primary overpressurization. Combustion Engineering's Chapter 15 feedwater line break analyses used either the CESEC-II or the CESEC-III codes. CESEC-I was not used to analyze feedwater line break transients. Therefore, in response to this event or section only the results of the CESEC-II and CESEC-III codes are compared.

A comparison of these two codes was made with the basis being the feedwater line break transient for a System 80 plant. The limiting case feedwater line break for the System 80 plants is found in Appendix 15B of the CESSAR FSAR. The Appendix 15B results were obtained using the CESEC II computer code, and are provided as the CESEC II portion of this question response.

The CESEC-III code was run using the same initial conditions that were assumed for the Appendix 15B case, and are listed in

Table 440.149.b-1. The resulting sequence of events for the two codes are provided for comparison in Table 440.149.b-2.

Figures 440.149.b-1 through 440.149.b-8 show the results of the analyses over the time frame of maximum RCS pressurization.

The results presented show very good agreement between the CESEC-II and CESEC-III computer codes. A discussion of the differences in the results of the codes follows.

There is a small difference between the two codes in terms of RCS pressure vs time (Fig. 440.149.b-1). CESEC-II does not model the elevation pressure drop between the pressurizer and the hot leg centerline, while CESEC-III does. This accounts for approximately a 10 psia difference in RCS pressure, with the CESEC-III results being higher. In neither the CESEC-II or CESEC-III curve of RCS pressure vs time is the reactor coolant pump head included. However, these effects are accounted for separately in the results specified in Table 440.149.b-2.

A slight difference between the two codes occurs in the plots of steam generator pressure vs time (Figures 440.149.b-7 and 440.149.b-8). These differences can be attributed to the slightly higher primary flow rate calculated in the CESEC-III code than was input into the CESEC-II code. The differences can also be attributed in part to the modeling of the primary to secondary heat transfer rate. These phenomena cause the

steam generator pressure to be initialized at a value about 15 psia greater in CESEC-III than in CESEC-II. The differences in the plot of steam generator pressure vs time occurring beyond 45 seconds in the transient can be attributed to the differences in secondary safety valve modeling of the two codes, although the averaged responses are nearly identical.

A small difference in the RCS temperature vs time plot exists (Figure 440.149.b-3). This is due to the slight differences in primary coolant flow rate. The CESEC-III code's pump model predicts slightly higher flowrates than were input into the CESEC-II code. This causes the initial temperature rise across the core to be lower for the CESEC-III code.

As demonstrated by the figures provided, the CESEC-II and CESEC-III feedwater line break predictions are in very good agreement.

(c) At the present time, there is no ATWS licensing requirement. CESEC-III is not used for ATWS evaluation.

(d) For all decrease in primary system inventory events, Chapter 15.6 events, for which the pressurizer fluid is calculated to drain into the hot leg, or the system pressure drops below the saturation pressure of the hottest fluid in the system, the hottest fluid will be located in the relatively stagnant upper head region of the reactor vessel. The CESEC-I code, used in the Waterford Unit 3 FSAR Chapter 15.6 analyses, did not

explicitly model the steam formation in the reactor vessel upper head region. The CESEC-II code, used in the FSARs for St. Lucie Unit 2 and CESSAR FSARs Chapter 15.6 analyses also did not explicitly model the steam formation in the reactor vessel upper head region. The latest version of CESEC, namely CESEC-III, appropriately models steam formation and collapse in the upper head region of the reactor vessel. Heat transfer from metal structures to the reactor coolant system (RCS) fluid is modeled in this region in addition to flashing of the reactor coolant into steam during the depressurization of the RCS. Following the reactor coolant pump (RCP) coastdown due to loss of offsite power or manual shutdown following SIAS, thermal hydraulic decoupling of the upper head region is characterized in CESEC-III by progressively decreasing flow to the upper head from the upper plenum region.

The limiting event with respect to void formation in the decrease in primary system inventory event category is the steam generator tube rupture event. The effect of upper head voiding on the consequences of this event has been evaluated in support of the Waterford Unit 3, St. Lucie Unit 2, and CESSAR-F SARs. Analyses for this event bound all other other events for which void formation is less limiting and/or non-existent in the above event category. This is due to slower cooldown rates, RCS pumps on, and/or higher minimum RCS pressures for the other events in the category. The major concern for this event is the primary to secondary leakage and, consequently, the secondary side activity releases.

The loss of primary coolant for a double-ended tube rupture results in a steady decline in RCS pressure. This steady pressure decline continues until the reactor trips (e.g., low pressurizer pressure). Subsequent to reactor trip the RCS pressure drops very quickly and the pressurizer empties. Voids due to flashing begin to form in the reactor vessel upper head region after the RCS pressure reaches the saturation temperature of the fluid. The RCPs are shutoff subsequent to a SIAS. The thermal hydraulic decoupling of the upper head from the rest of the RCS subsequent to the RCPs shutoff and the effect of the metal structure heat transfer from the reactor vessel walls and internals, enhances the void formation in the upper head regions through boiloff.

The analyses presented for the double-ended break of a steam generator tube event assume initiation from a full power condition with the assumptions of loss of offsite power subsequent to generator trip, one percent of the full power core/upper plenum flow into the upper head up to the time that the RCPs are shutoff, RCPs shutoff coincident with loss of offsite power, and the most reactive CEA in its fully withdrawn position.

The effect of the reactor vessel upper head voiding upon the system response is illustrated in Figures 440.149.d-1 through 440.149.d-4. Figures 440.149.d-1 and 440.149.d-2 show the results for the Waterford plant and Figures 440.149.d-3 and 440.149.d-4 show the results for System 80. The solid lines

and dashed lines represent, respectively, the case for which the reactor vessel upper head fluid is explicitly modelled (CESEC-III) and the case for which the upper head region is mixed completely with that of the reactor vessel outlet plenum (CESEC-I and CESEC-II). The maximum allowable initial pressurizer liquid volume was assumed for these analyses. The radiological consequences of the steam generator tube rupture event are more adverse when maximizing this parameter. However, they still satisfy the SRP guidelines.

Figures 440.149.d-2 and 440.149.d-4 illustrate the reactor vessel upper head response. The amount of voids formed is definitely not large enough to expand the steam bubble beyond the top elevation of the hot legs. The duration of the voids will be a function of the rate of RCS cooldown and the safety injection flow rate. The slower RCS pressure decay for the case for which the upper head is explictily modelled (see Figures 440.149.d-1 and 440.149.d-3) results in a delayed SIAS and a corresponding delay in the time at which delivery of the HPSI flow beings. The slower pressure decay for this case is caused by the voids as after the pressurizer empties, the reactor vessel upper head behaves as a pressurizer. For System 80 with the upper head not modelled the relatively large amount of HPSI flow results in the crossing of the RCS pressures late in the transient as shown in Figure 140.149.d-3. For this plant class the HPSI shutoff head is higher than for the 3410 plant class which causes this dissimilarity in behavior.

Tables 440.149.d-1 and 440.149.d-2 summarize the integrated primary to secondary leakages the integrated releases through the main steam safety valves (MSSVs), and the trip times for the cases analyzed. When the upper head region is explicitly modelled, the results are more adverse. However, the radiological consequences satisfy the SRP acceptance criteria. The more adverse results are due to the relatively higher RCS pressures and primary to secondary heat transfer for the case the upper head region is explicitly modelled.

In summary, void formation in the upper head will occur for the SGTR event. However, the consequences of a steam generator tube rupture as demonstrated in the Waterford Unit 3, St. Lucie Unit 2, and CESSAR-F SARs satisfy the SRP acceptance criteria when the reactor vessel upper head region is explicitly modelled.

TABLE 440.149.a-1

CESEC-I/CESEC-III COMPARISON
WATERFORD UNIT 3
ASSUMPTIONS FOR A STEAM LINE BREAK AT FULL POWER INSIDE CONTAINMENT WITH DOUBLE ENDED RUPTURE OF THE STEAM LINE

Parameter	Assumptions
Initial core power level, Mwt	3478
Core inlet coolant temperature, F	560
Core mass flowrate, 10^6 lbm/hr	124.3
Reactor coolant system pressure, psia	2000
One pin radial peaking factor, with uncertainty	1.3
Initial core minimum DNBR	1.29
Steam generator pressure, psia	962.4
Doppler coefficient multiplier	1.15
Moderator coefficient multiplier	1.10
CEA worth for trip, $10^{-2} \Delta\rho$	-8.55
Steam bypass control system	Inoperative
Pressurizer pressure control system	Inoperative
High pressure safety injection pumps	One pump inoperative
Core burnup	End of first cycle
Blowdown fluid	100% steam
Break area, ft^2	7.88

TABLE 440.149.a-2

CESEC-I/CESEC-III COMPARISON
WATERFORD UNIT 3
SEQUENCE OF EVENTS FOR A STEAM LINE BREAK AT FULL POWER
INSIDE CONTAINMENT WITH DOUBLE ENDED RUPTURE OF THE STEAM
LINE AND CONCURRENT LOSS OF OFFSITE POWER

Time (Sec)		Event
CESEC-I	CESEC-III	
0.0	0.0	Steam line break upstream of the main steam isolation valve initiated; loss of offsite ac power occurs
2.06	2.10	Low steam generator pressure trip signal and MSIS initiated; main steam isolation valves begin to close; feedwater isolation valves begin to close
5.06	5.10	MSIVs closed
14.9	30.4	Pressurizer empties
16.2	19.2	Low RCS pressure initiates SIAS
22.1	22.1	MFIVs closed
34.2	37.2	High-pressure safety injection pump reaches full speed
99.7	110.0	Affected steam generator empties
255.9	237.5	Safety injection boron begins to reach core
337.4	147.5	Pressurizer liquid level re-established

TABLE 440.149.a-3

CESEC-II/CESEC-III COMPARISON
SYSTEM 80
ASSUMPTIONS AND INITIAL CONDITIONS FOR A LARGE STEAM LINE BREAK DURING FULL POWER OPERATION WITH CONCURRENT LOSS OF OFFSITE POWER

Parameter	Assumed Value
Initial Core Power Level, MWt	3876
Initial Core Inlet Coolant Temperature, F	570
Initial Core Mass Flow Rate, 10^6 lbm/hr	148.8
Initial Pressurizer Pressure, psia	2400
Initial Pressurizer Water Volume, ft^3	1100
Doppler Coefficient Multiplier	1.15
Moderator Coefficient Multiplier	1.10
Axial Shape Index	+.3
CEA Worth for Trip, 10^{-2} $\Delta\rho$	-8.8
Initial Steam Generator Inventory, lbm, affected intact	182000 148000
One High Pressure Safety Injection Pump	Inoperative
Core Burnup	End of Cycle
Blowdown Fluid	Saturated Steam
Blowdown Area for Each Steam Line, ft^2	1.283

TABLE 440.149.a-4

CESEC-II/CESEC-III COMPARISON
SYSTEM 80
SEQUENCE OF EVENTS FOR A LARGE STEAM LINE BREAK DURING FULL POWER OPERATION WITH CONCURRENT LOSS OF OFFSITE POWER

Time (Sec) CESEC-II	Time (Sec) CESEC-III	Event	Setpoint or Value CESEC-II	Setpoint or Value CESEC-III
0.0	0.0	Steam Line Break and Loss of Offsite Power Occur		--
0.6	0.6	Low DNBR Trip Condition Occurs, Projected DNBR		1.19
0.75	0.75	Trip Breakers Open		--
1.09	1.09	CEAs Begin to Drop		--
*	8.0	Voids Begin to Form in RV Upper Head		--
8.2	8.3	Main Steam Isolation Signal, psia		810
13.2	13.3	MFIVs Close Completely		--
13.2	13.3	MSIVs close completely		--
13.2	13.3	EFW Initiated to Intact Steam Generator		--
18	120	Pressurizer Empties		--
19	178	Safety Injection Actuation Signal, psia		1600
49	208	Safety Injection Flow Begins		--
390	237	Affected Steam Generator Empties		--
211	259	Maximum Transient Reactivity, 10^{-2} $\Delta\rho$	-0.02	+0.09
**	277	Minimum Post-Trip DNBR	**	2.7
80	280	Safety Injection Boron Begins to Reach Reactor Core		--

* No upper head node in CESEC-III

** No minimum, see Figure 440.149.a-12

Figure 440.149.A-1
FULL POWER LARGE STEAM LINE BREAK WITH
CONCURRENT LOSS OF OFFSITE POWER
REACTIVITY vs TIME

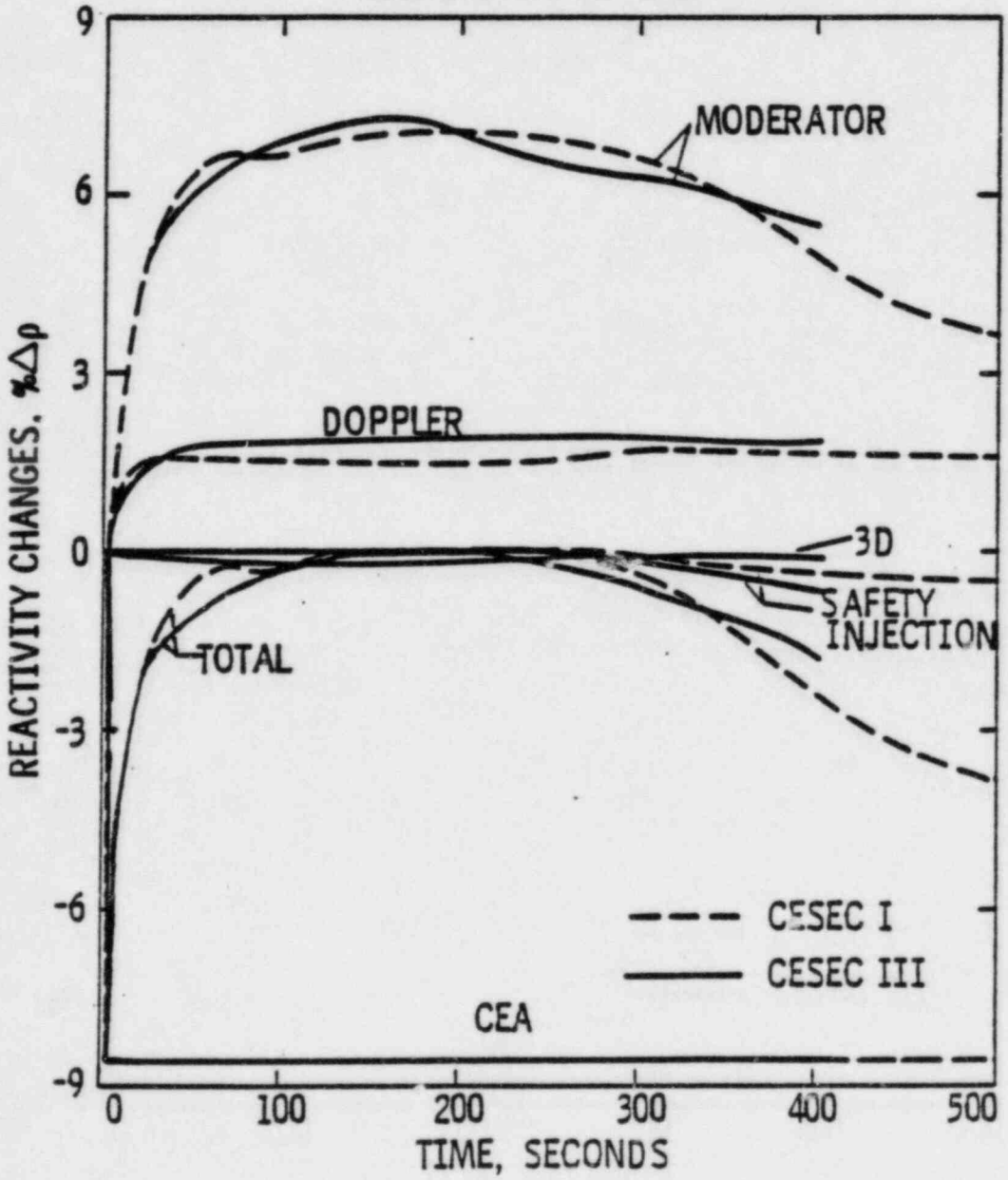

Figure 440.149.A-2
FULL POWER LARGE STEAM LINE BREAK WITH
CONCURRENT LOSS OF OFFSITE POWER
CORE POWER vs TIME

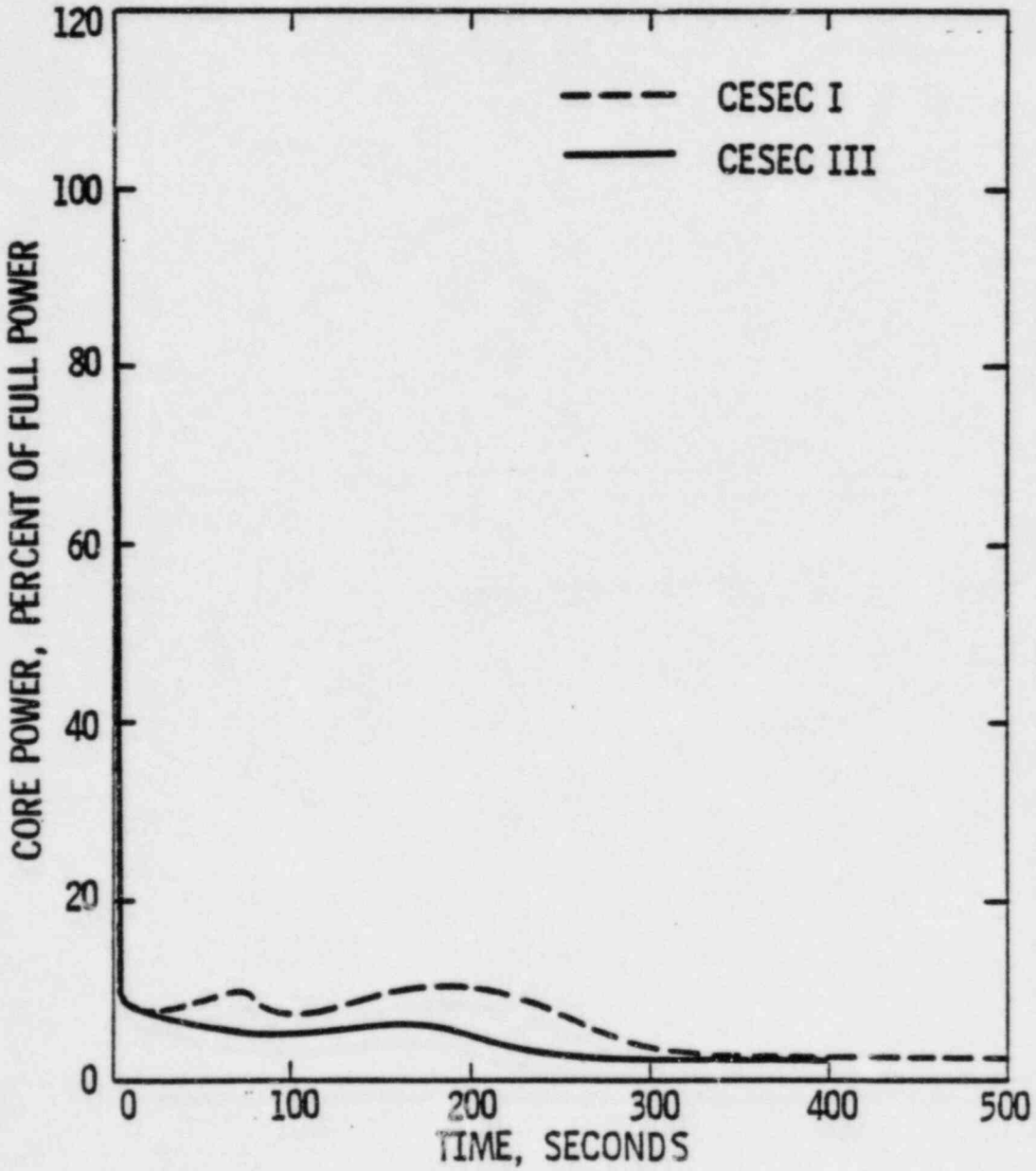

Figure 440.149.A-3
FULL POWER LARGE STEAM LINE BREAK WITH
CONCURRENT LOSS OF OFFSITE POWER
RCS PRESSURE vs TIME

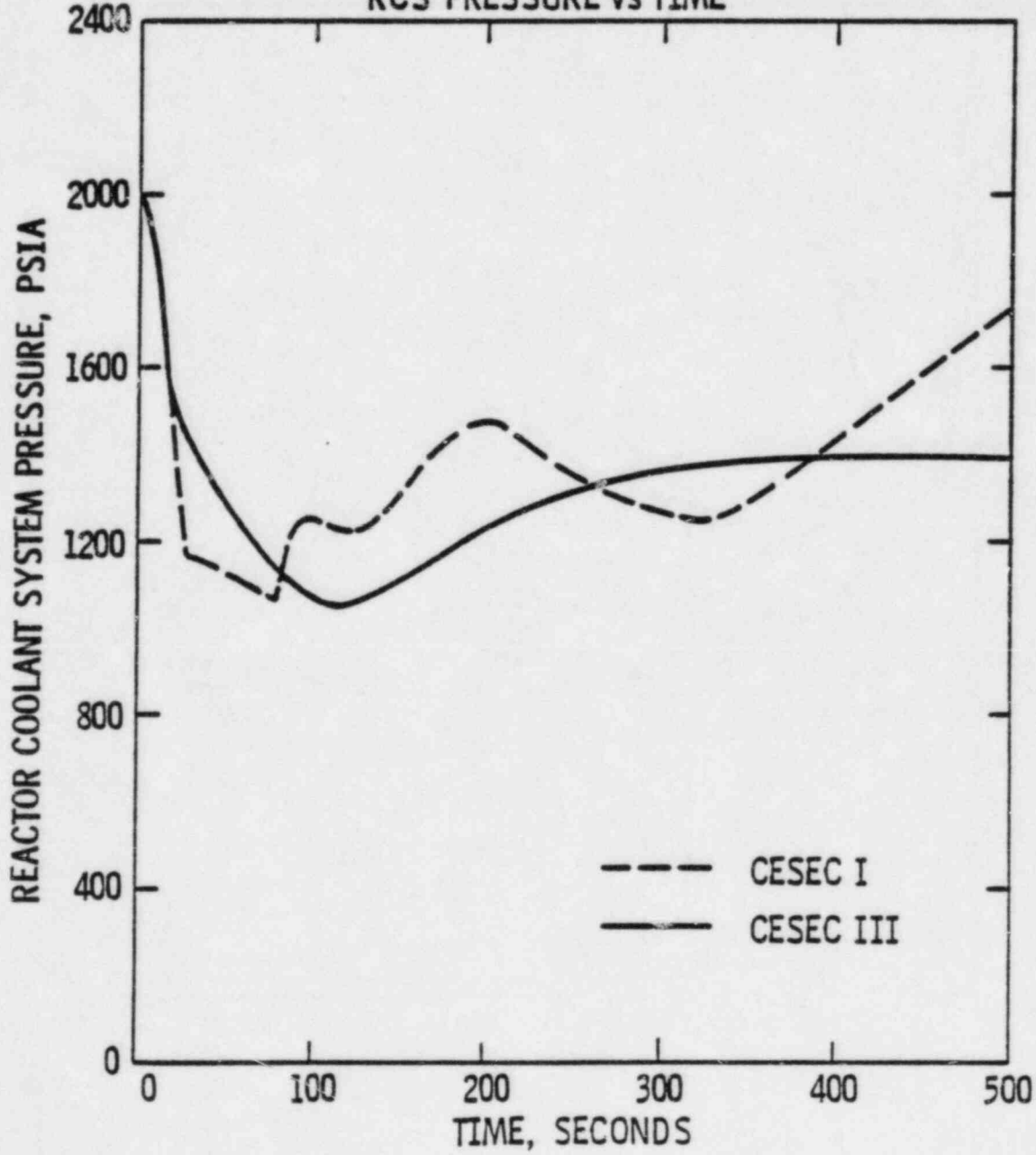

Figure 440.149.A-4
FULL POWER LARGE STEAM LINE BREAK WITH
CONCURRENT LOSS OF OFFSITE POWER
TEMPERATURE vs TIME

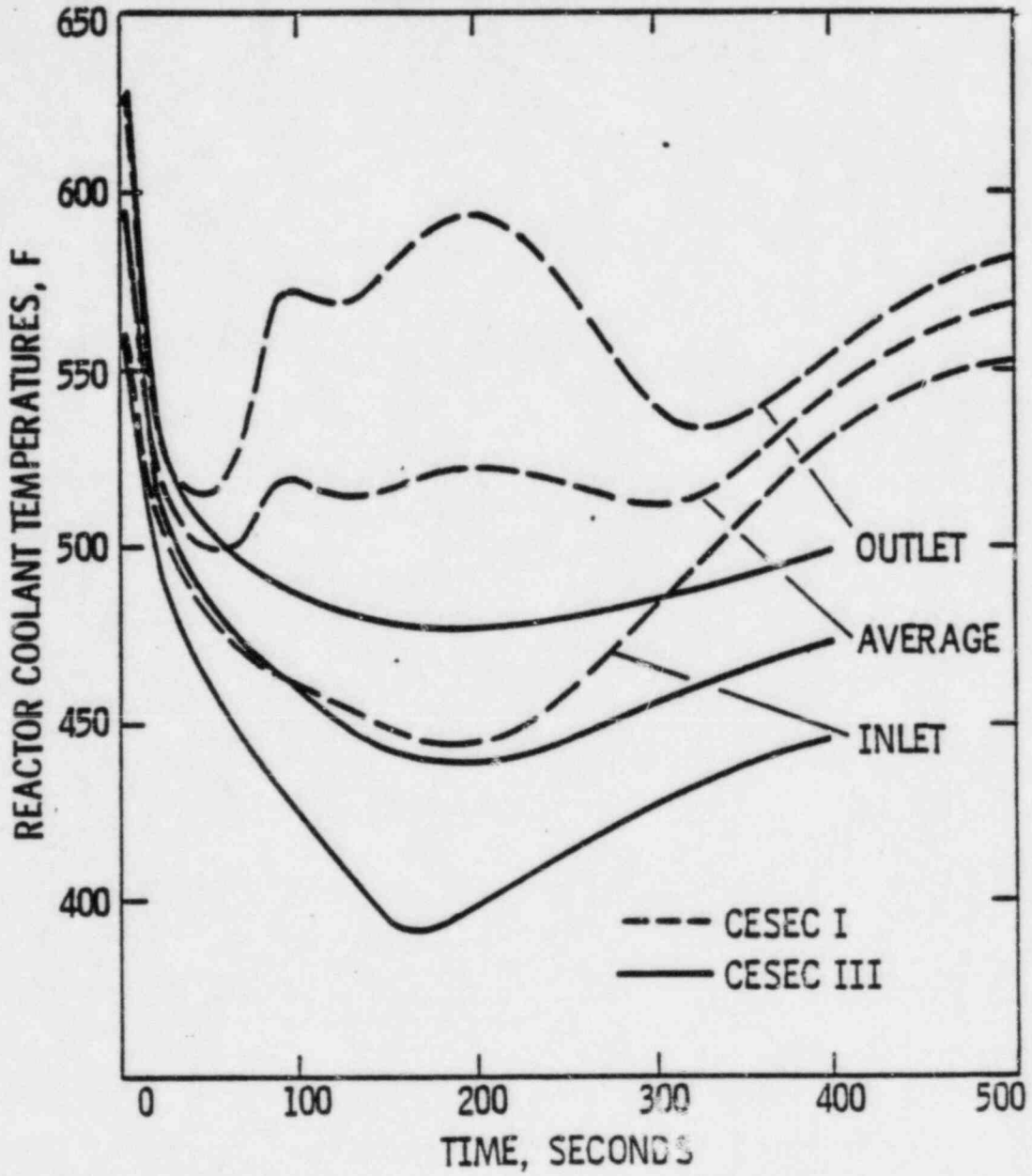

Figure 440.149.A-5
FULL POWER LARGE STEAM LINE BREAK WITH
CONCURRENT LOSS OF OFFSITE POWER
FLOW RATE vs TIME

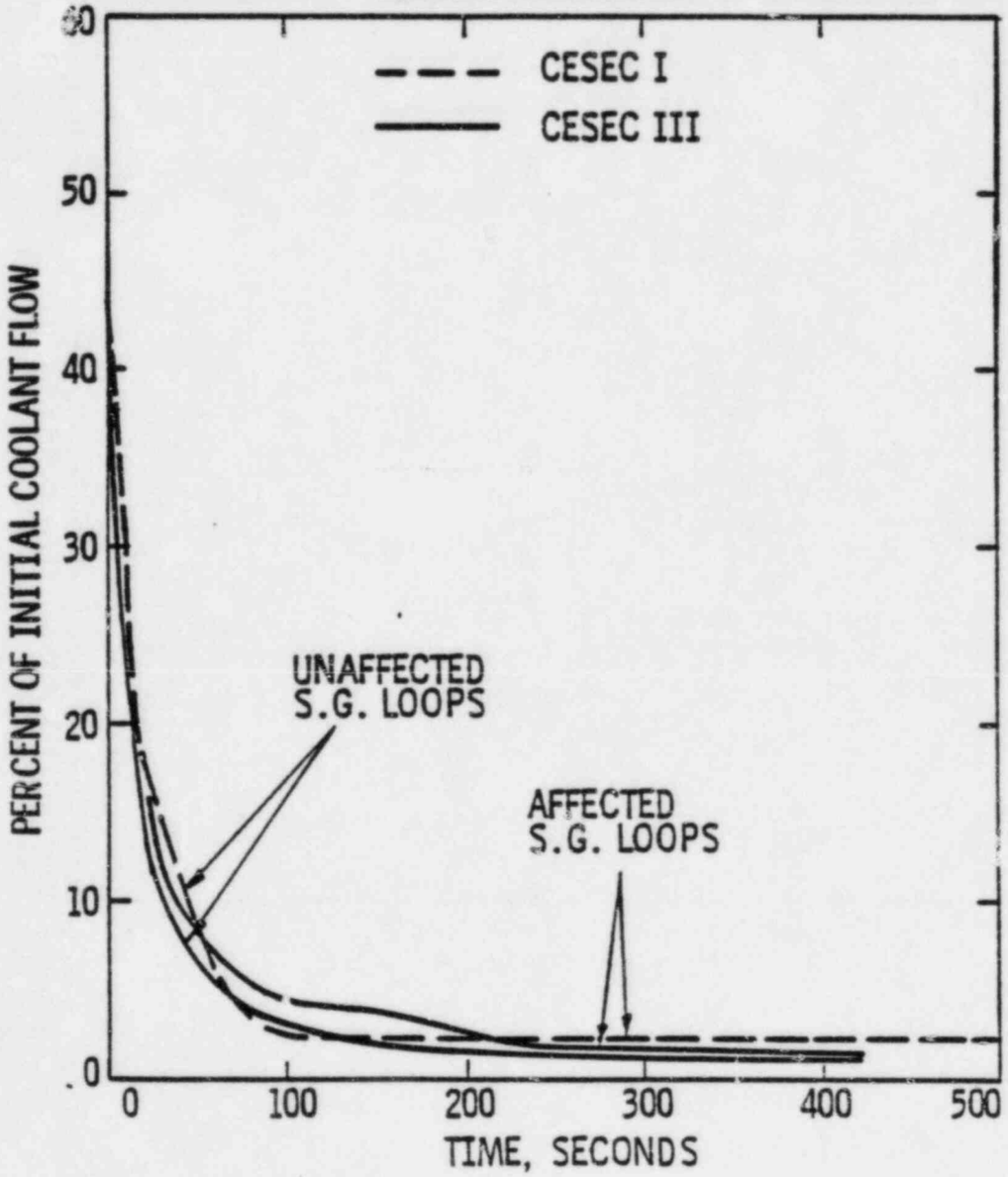

Figure 440.149.A-6
FULL POWER LARGE STEAM LINE BREAK WITH
CONCURRENT LOSS OF OFFSITE POWER
MINIMUM POST-TRIP DNBR vs TIME

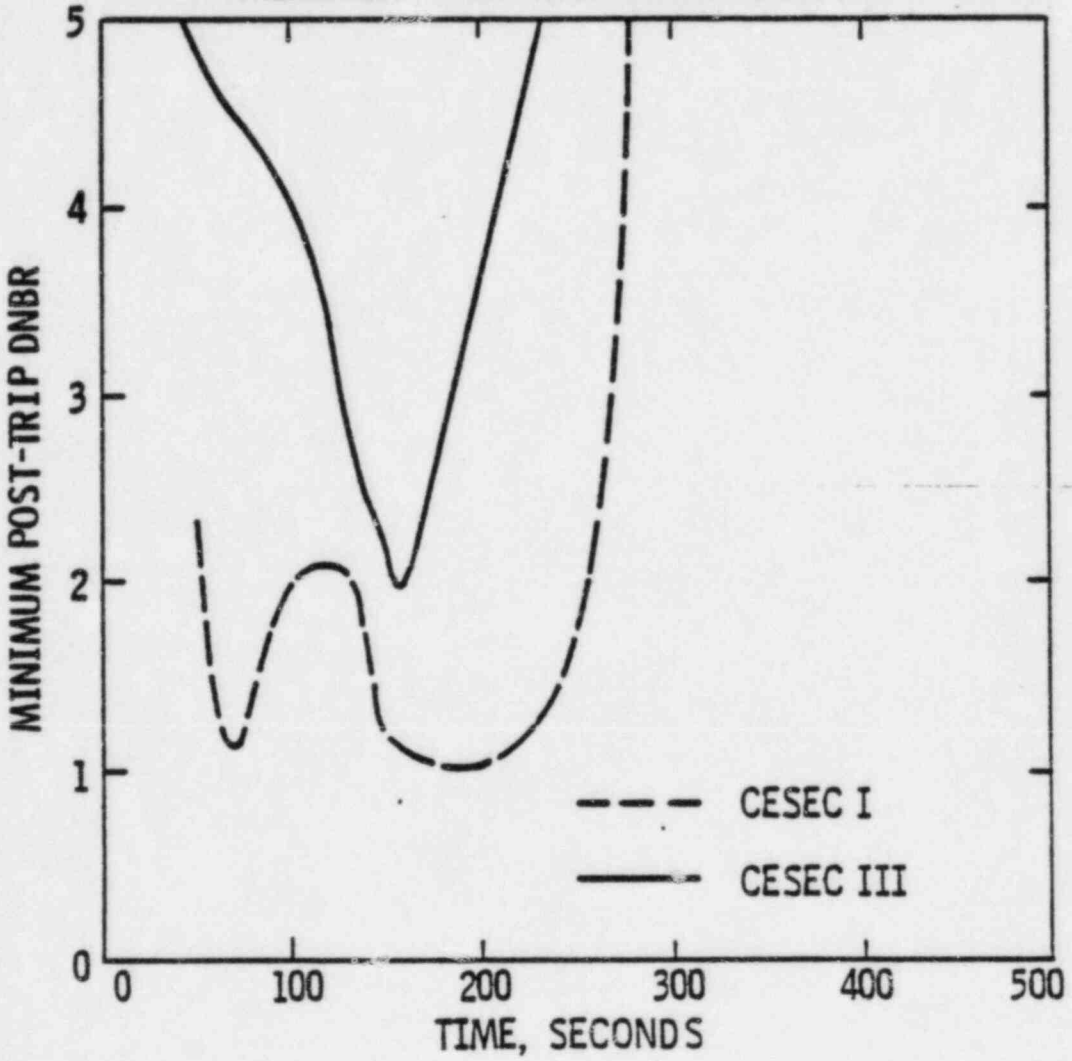

Figure 440.149.A-7
FULL POWER LARGE STEAM LINE BREAK WITH
CONCURRENT LOSS OF OFFSITE POWER
REACTIVITY CHANGES vs TIME

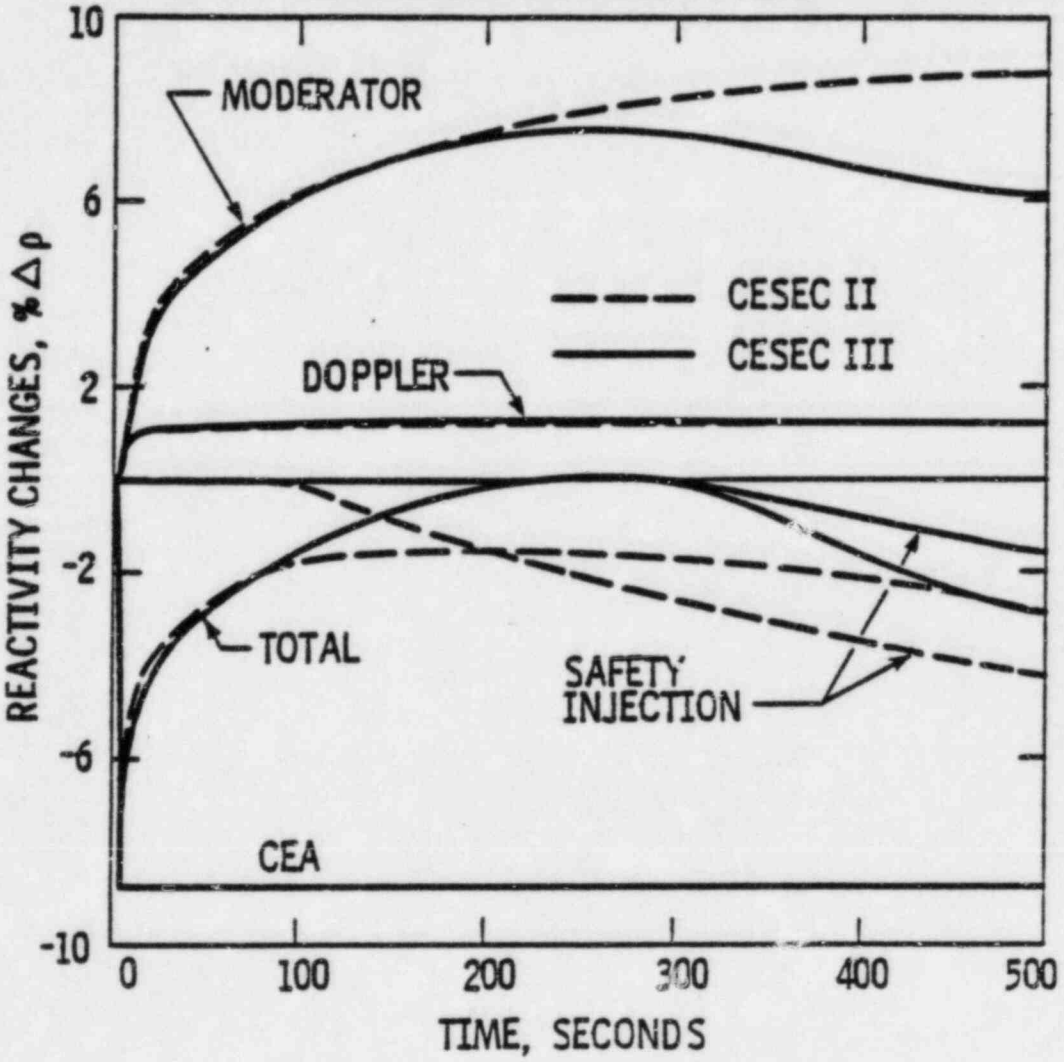

Figure 440.149.A-8
FULL POWER LARGE STEAM LINE BREAK WITH
CONCURRENT LOSS OF OFFSITE POWER
REACTOR COOLANT TEMPERATURES vs TIME.

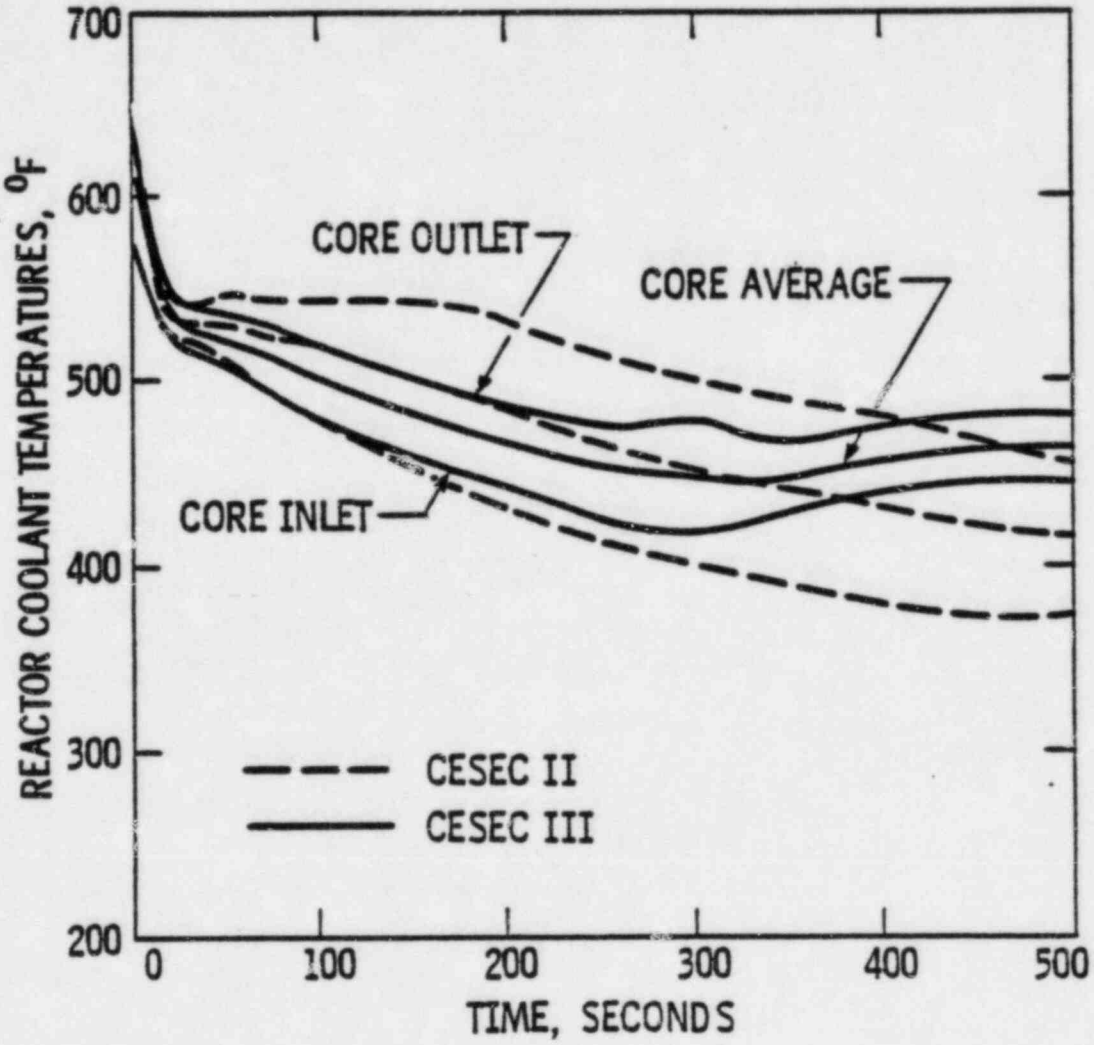

Figure 440.149.A-9
FULL POWER LARGE STEAM LINE BREAK WITH
CONCURRENT LOSS OF OFFSITE POWER
CORE POWER vs TIME

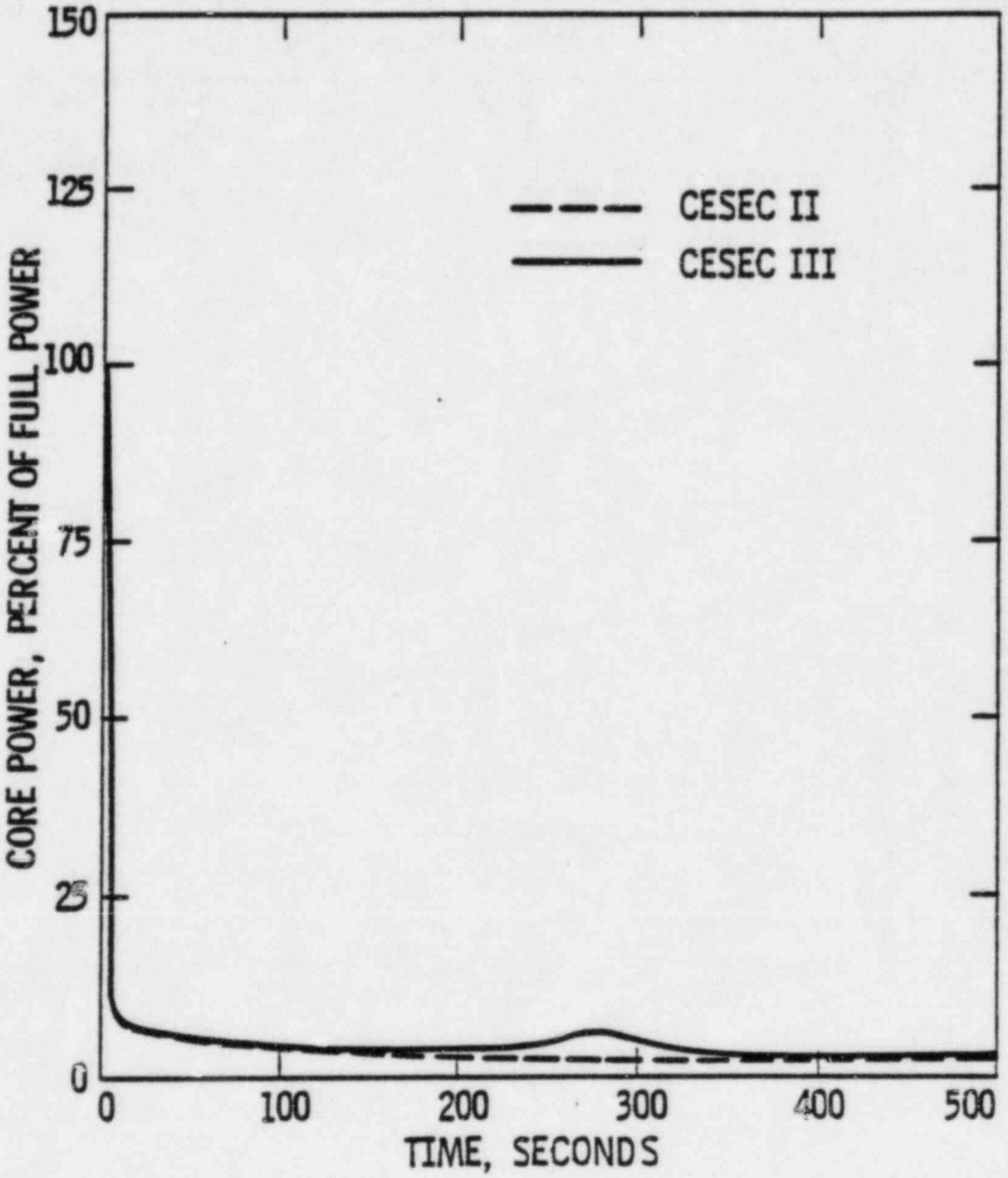

Figure 440.149.A-10
FULL POWER LARGE STEAM LINE BREAK WITH
CONCURRENT LOSS OF OFFSITE POWER
RCS PRESSURE vs TIME

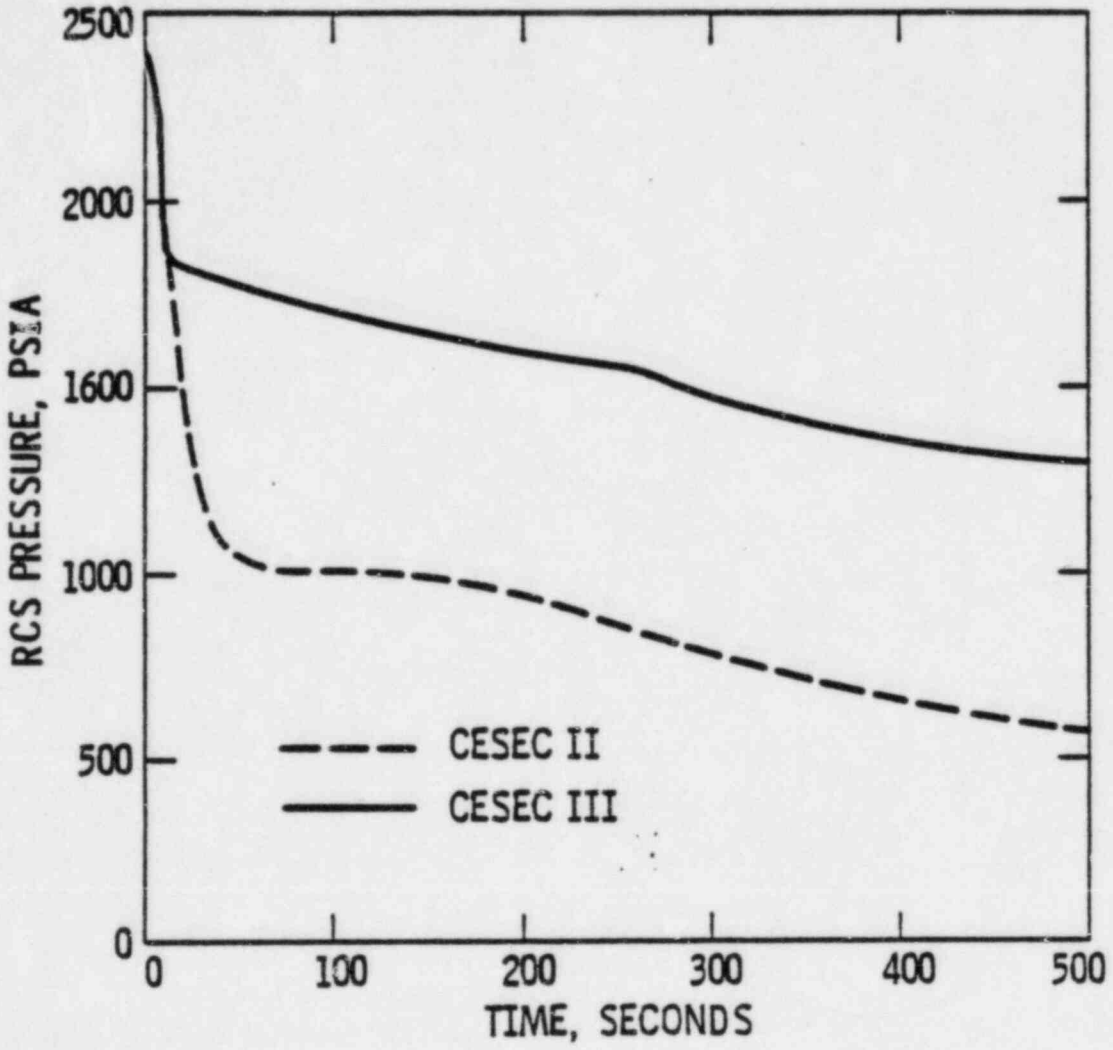

Figure 440.149.A-11
FULL POWER LARGE STEAM LINE BREAK WITH
CONCURRENT LOSS OF OFFSITE POWER
FLOW RATE vs TIME

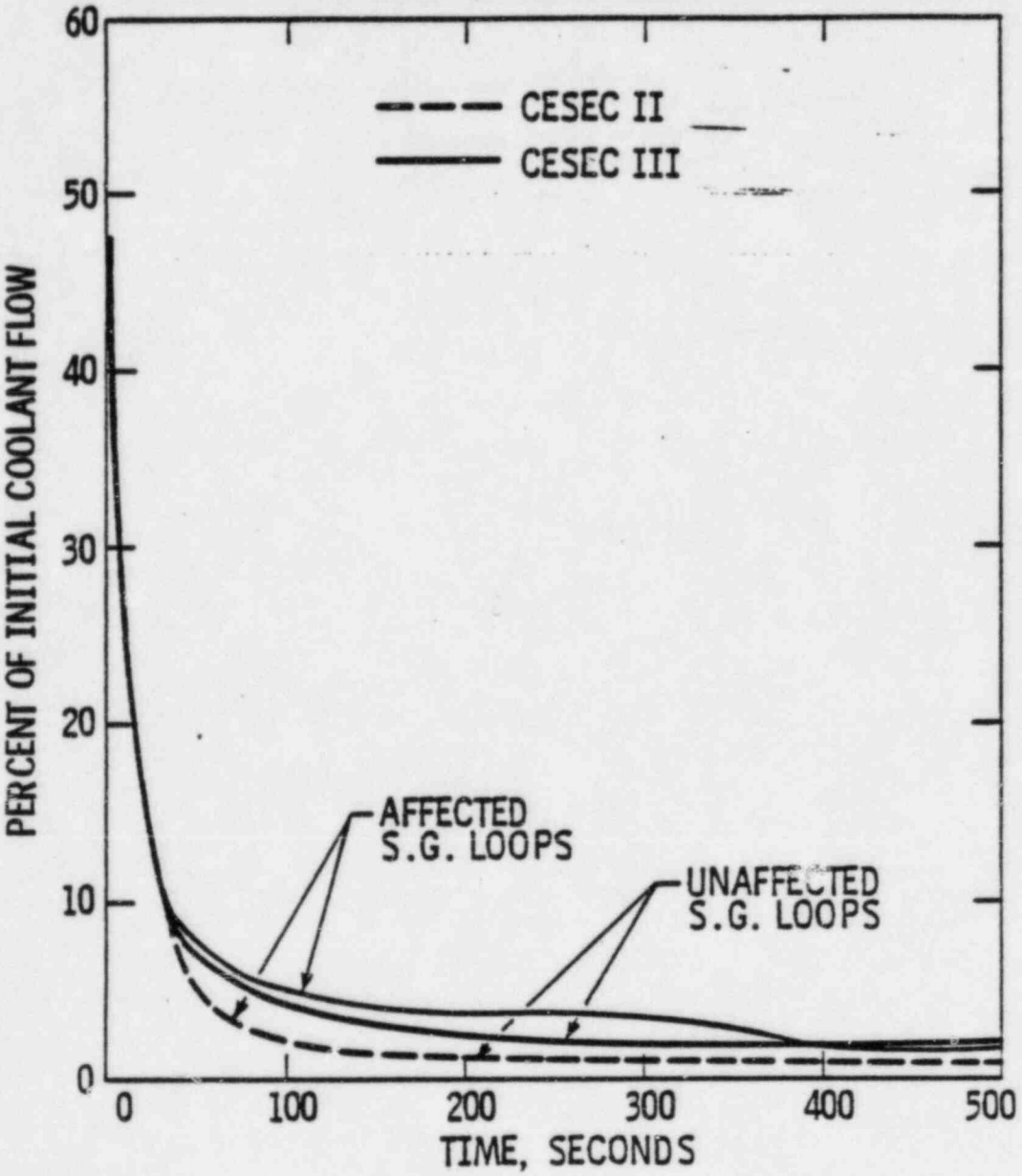

Figure 440.149.A-12

FULL POWER LARGE STEAM LINE BREAK WITH
CONCURRENT LOSS OF OFFSITE POWER
MINIMUM POST-TRIP DNBR vs TIME

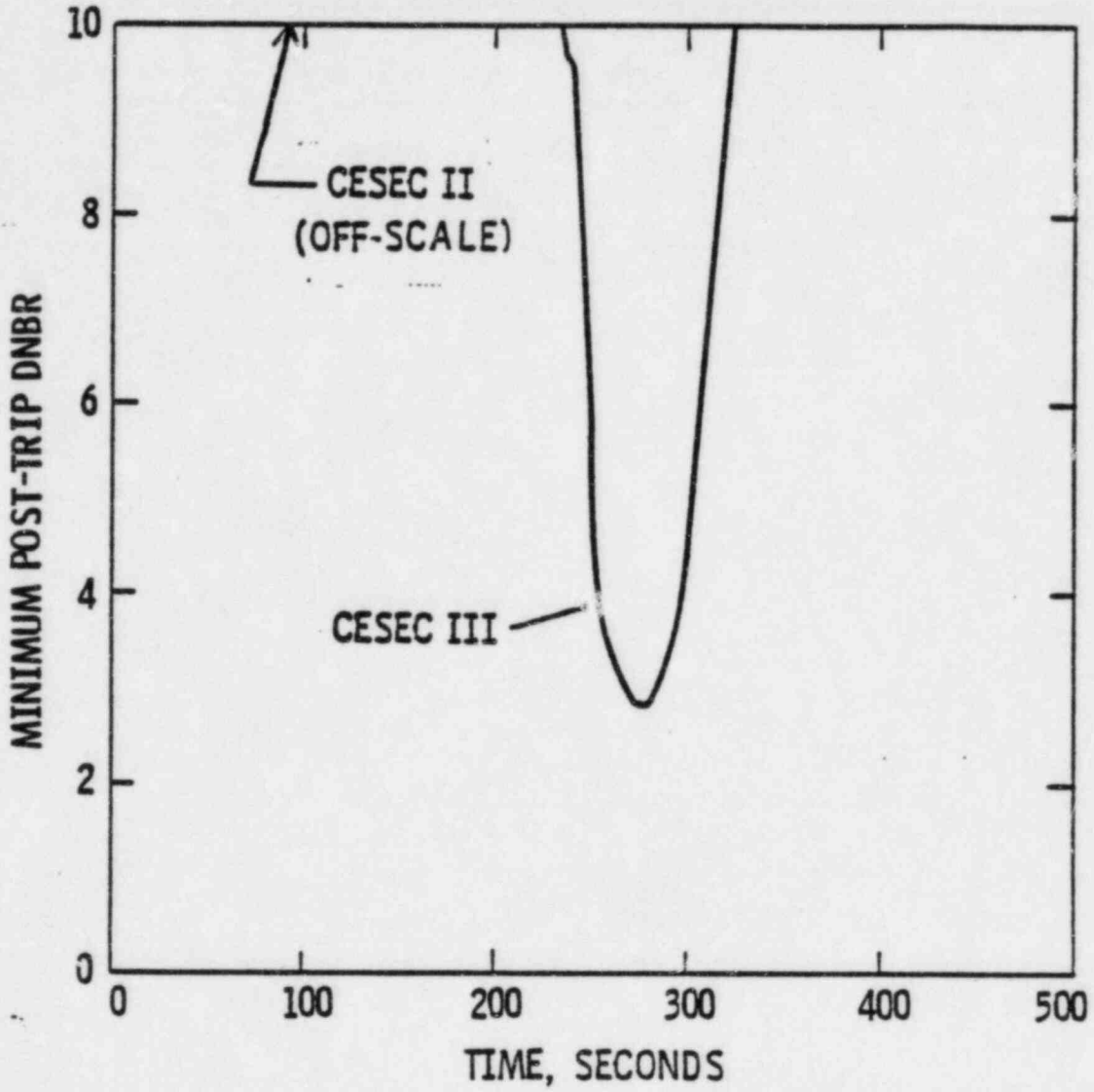

Table 440.149.b-1

Initial Conditions For the Limiting Case

Loss of Feedwater Inventory Event

Parameter	Value
Initial Core Power, mwt	3876
Initial Core Inlet Temperature, F	560
Initial Reactor Vessel Flow, gpm	446,000
Initial Pressurizer Pressure, psia	1920
Fuel Gas Gap Heat Transfer Coefficient, BTU/hr-ft^2 - F	540
Doppler Coefficient Multiplier	1.0
Pressurizer Safety Valves Rated Flow, lbm/hr/valve	460,000
Initial Pressurizer Liquid Volume, ft^3	1120
Initial Steam Generator Inventory, lbm	173,000
Initial Feedwater Enthalpy, BTU/lbm	376
Steam Bypass Control System Mode	Manual
Normal On-Site or Off-Site Electrical Power After Turbine Trip	Unavailable
Feedwater Pipe Break Area, ft^2	0.2
CEA Worth at Trip, 10^{-2}	-10.0

TABLE 440.149.b-2

Comparison of the
Sequence of Events for the Limiting Case Loss
of Feedwater Inventory Event

Time (Sec)			Setpoint or Value	
CESEC II	CESEC III	Event	CESEC II	CESEC III
0.0	0.0	Break in the Main Feedwater Line	0.2 ft^2	0.2 ft^2
0.0	0.0	Instantaneous Loss of All Feedwater Flow to Both Steam Generators		
0.0	0.0	Instantaneous Development of Critical Flow from the Ruptured Steam Generator to the Break		
33.8	33.3	Instantaneous Loss of All Heat Transfer to the Ruptured Steam Generator		
34.4	34.1	High Pressurizer Pressure Trip signal	2475 psia	2475 psia
34.6	33.9	Pressurizer Safety Valves Open	2525 psia	2525 psia
38.2	38.3	Maximum Reactor Coolant Pressure	2843 psia	2850 psia
40.5	38.9	Main Steam Safety Valves Open	1282 psia	1282 psia
44.8	42.4	Maximum Steam Generator Pressure	1318 psia	1319 psia
45.4	43.5	Pressurizer Safety Valves Close	2525 psia	2460 psia
73.8	60.6	Main Steam Safety Valves Close	1218 psia	1218 psia

Figure 440.149.B-1
LOSS OF FEEDWATER INVENTORY
SYSTEM 80
RCS PRESSURE vs TIME

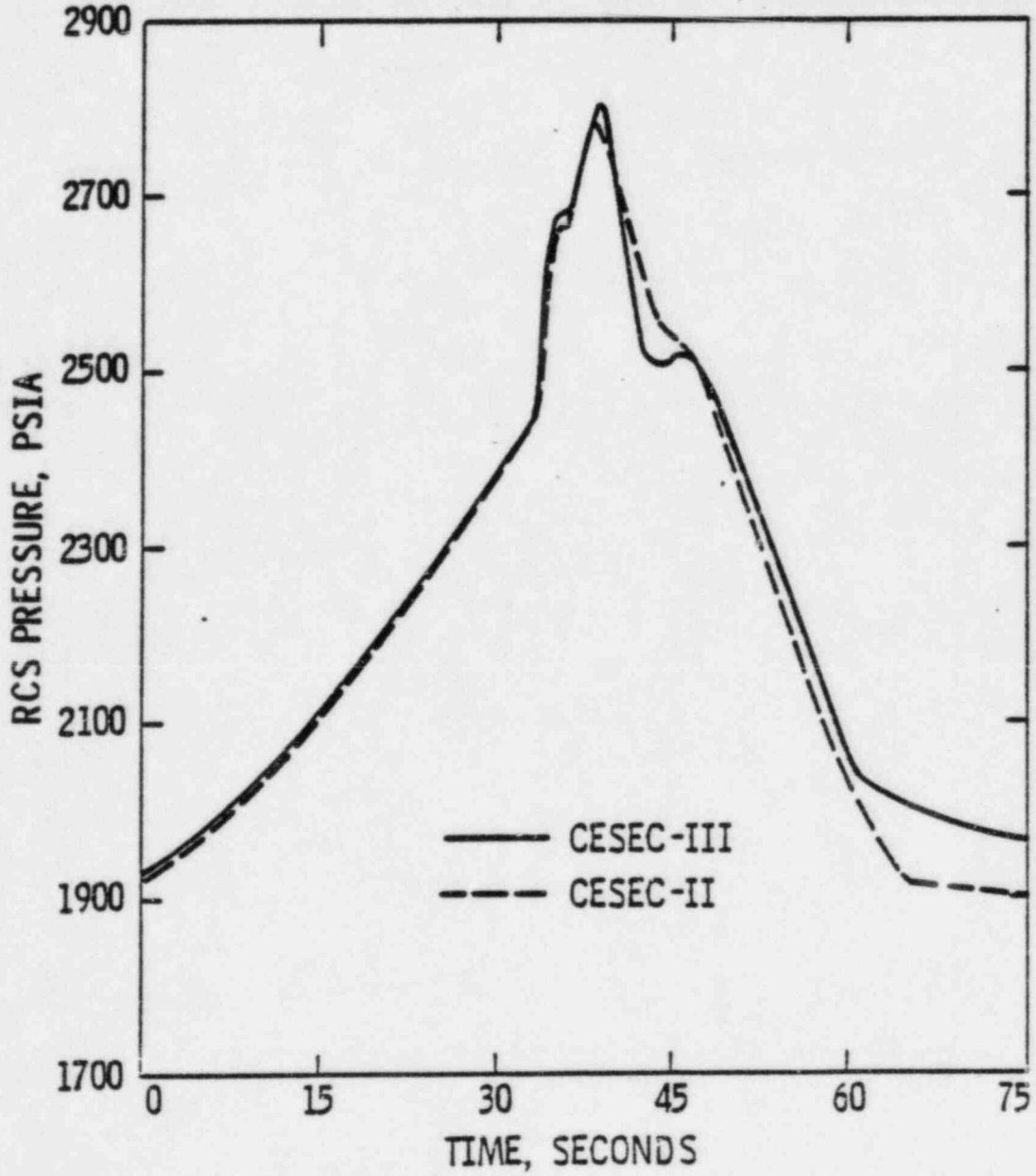

Figure 440.149.B-2
LOSS OF FEEDWATER INVENTORY
SYSTEM 80
CORE POWER vs TIME

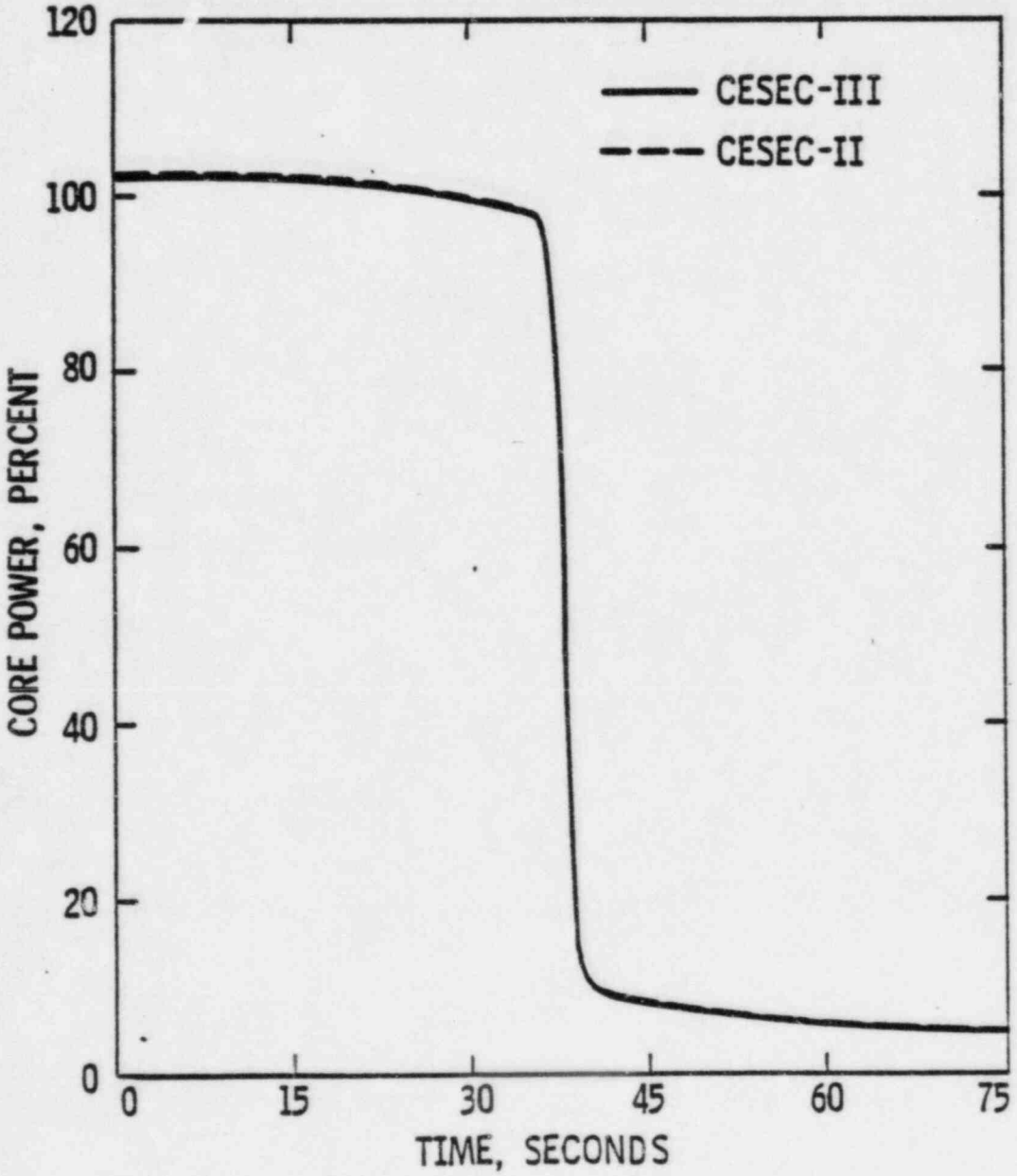

Figure 440.149.B-3
LOSS OF FEEDWATER INVENTORY
SYSTEM 80
RCS TEMPERATURES vs TIME

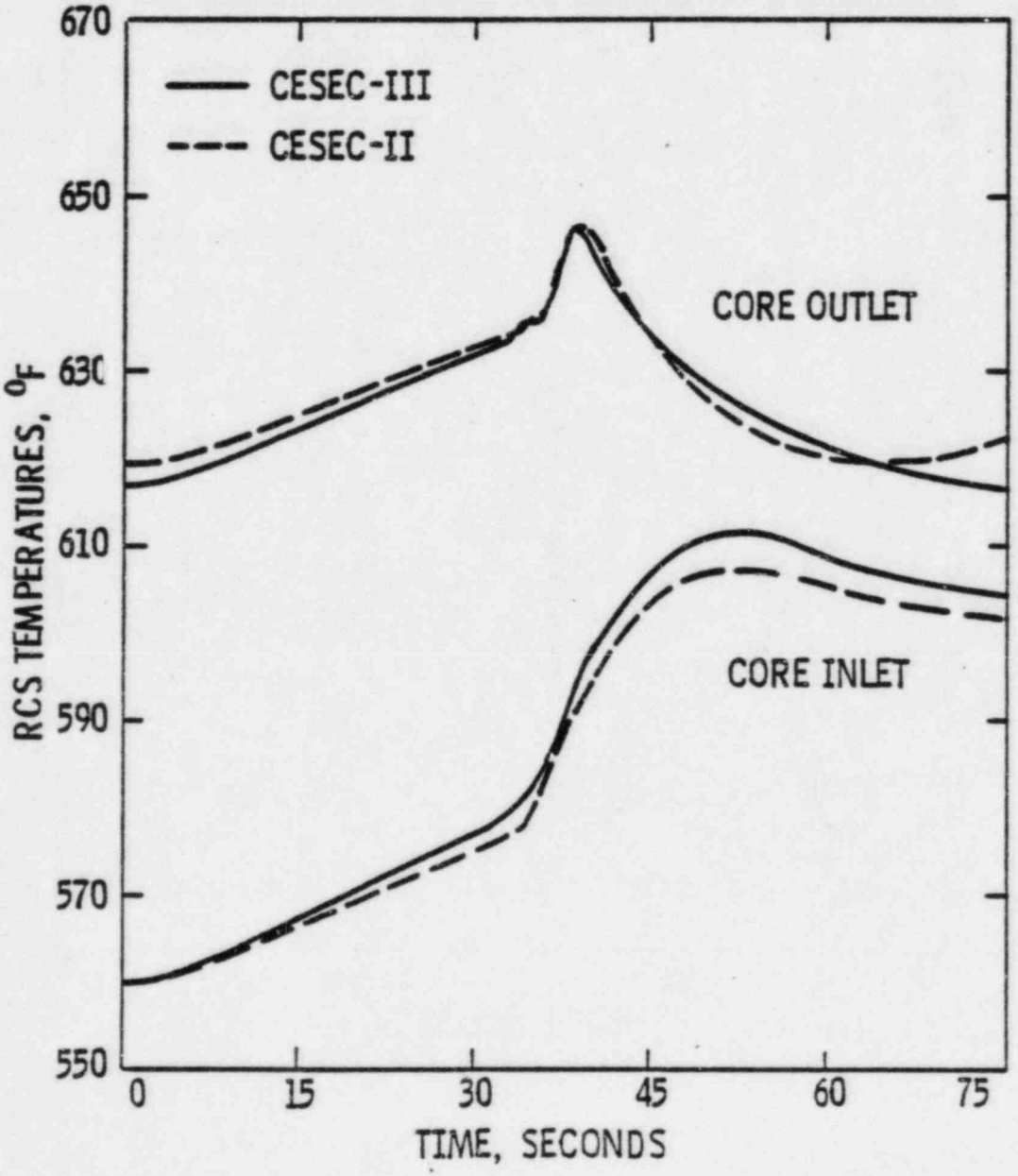

Figure 440.149.B-4
LOSS OF FEEDWATER INVENTORY
SYSTEM 80
RUPTURED STEAM GENERATOR FEED FLOW vs TIME

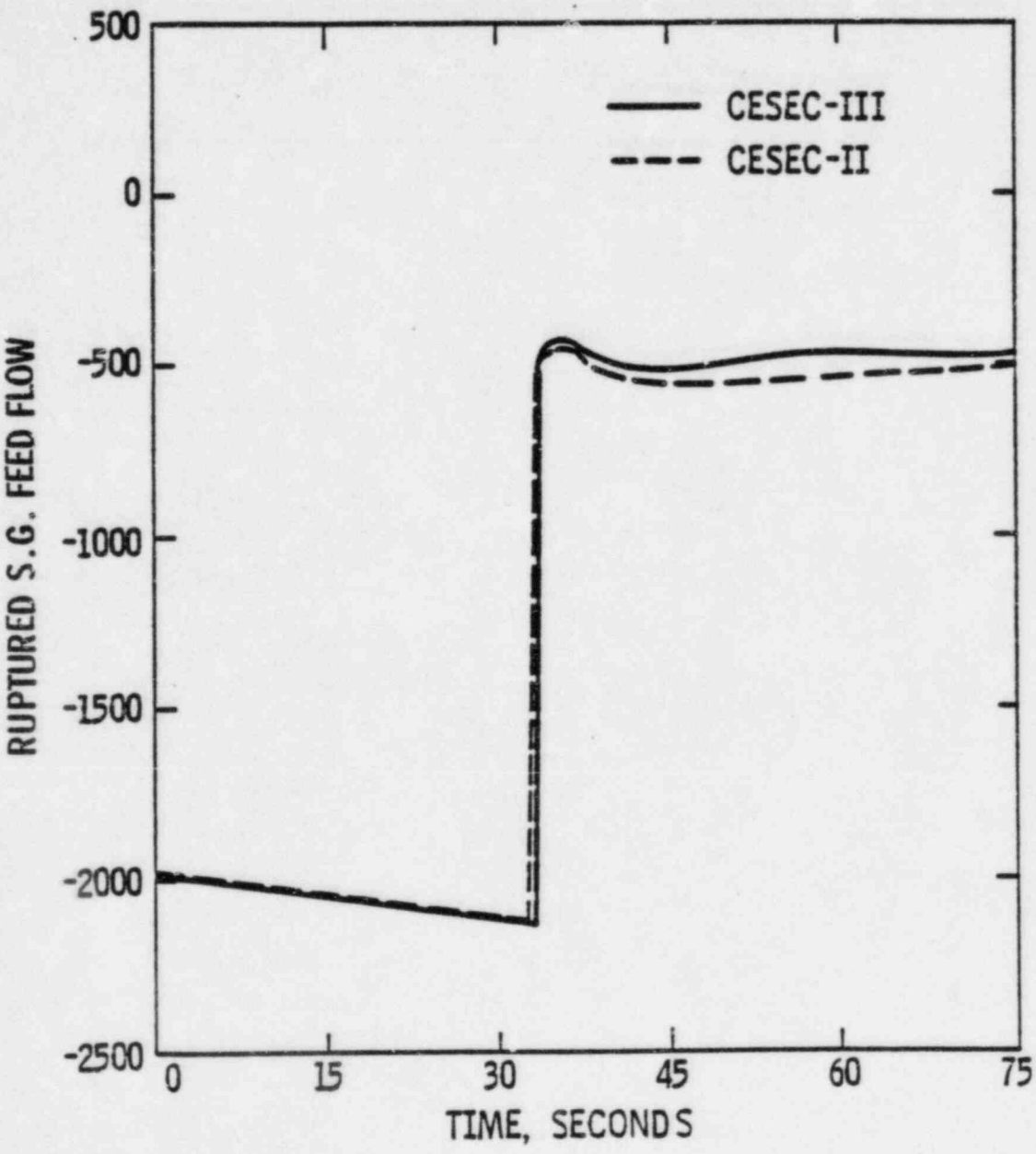

Figure 440.149.B-5
LOSS OF FEEDWATER INVENTORY
SYSTEM 80
RUPTURED S.G. LIQUID MASS vs TIME

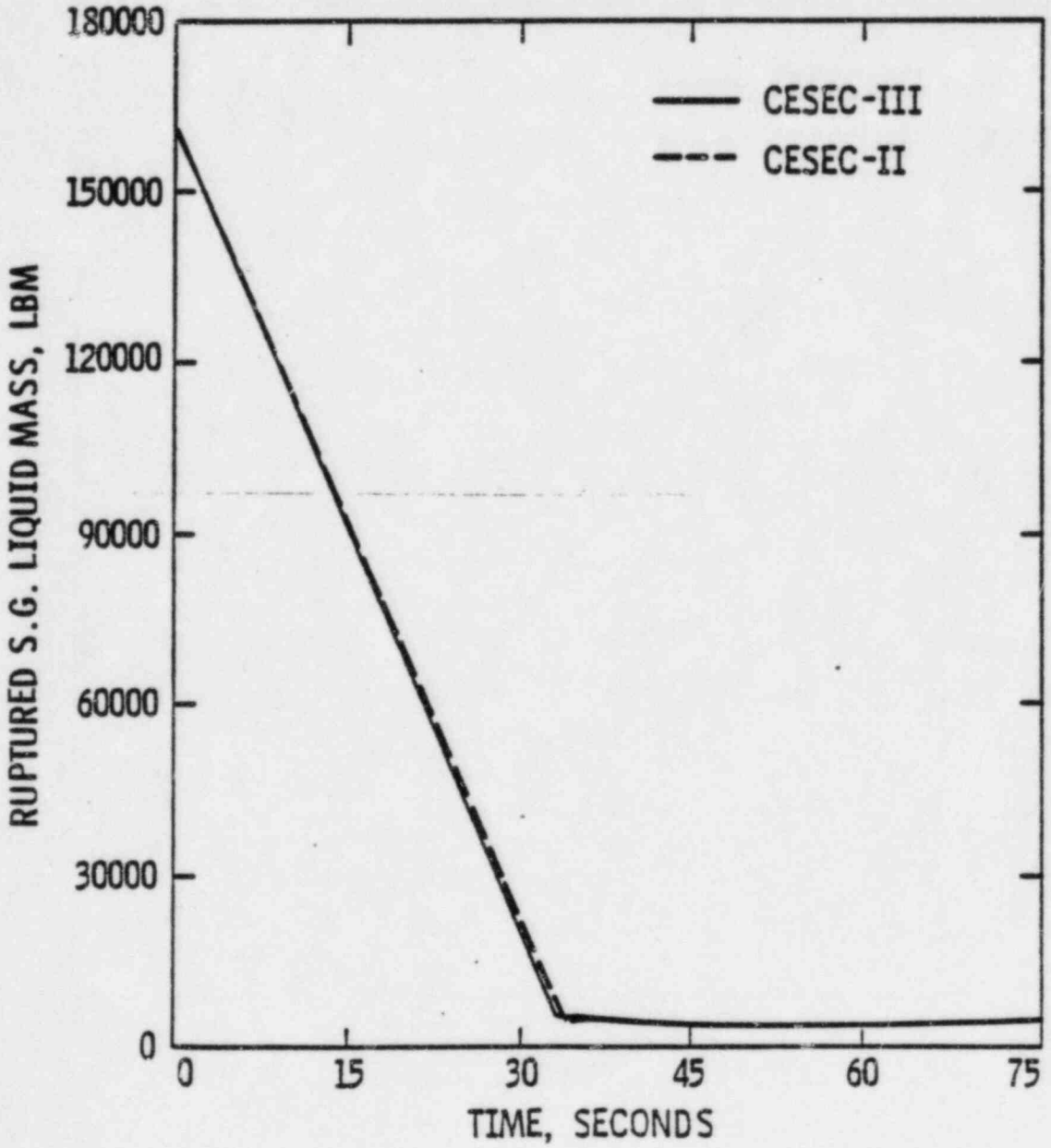

Figure 440.149.B-6
LOSS OF FEEDWATER INVENTORY
SYSTEM 80
INTACT S.G. LIQUID MASS vs TIME

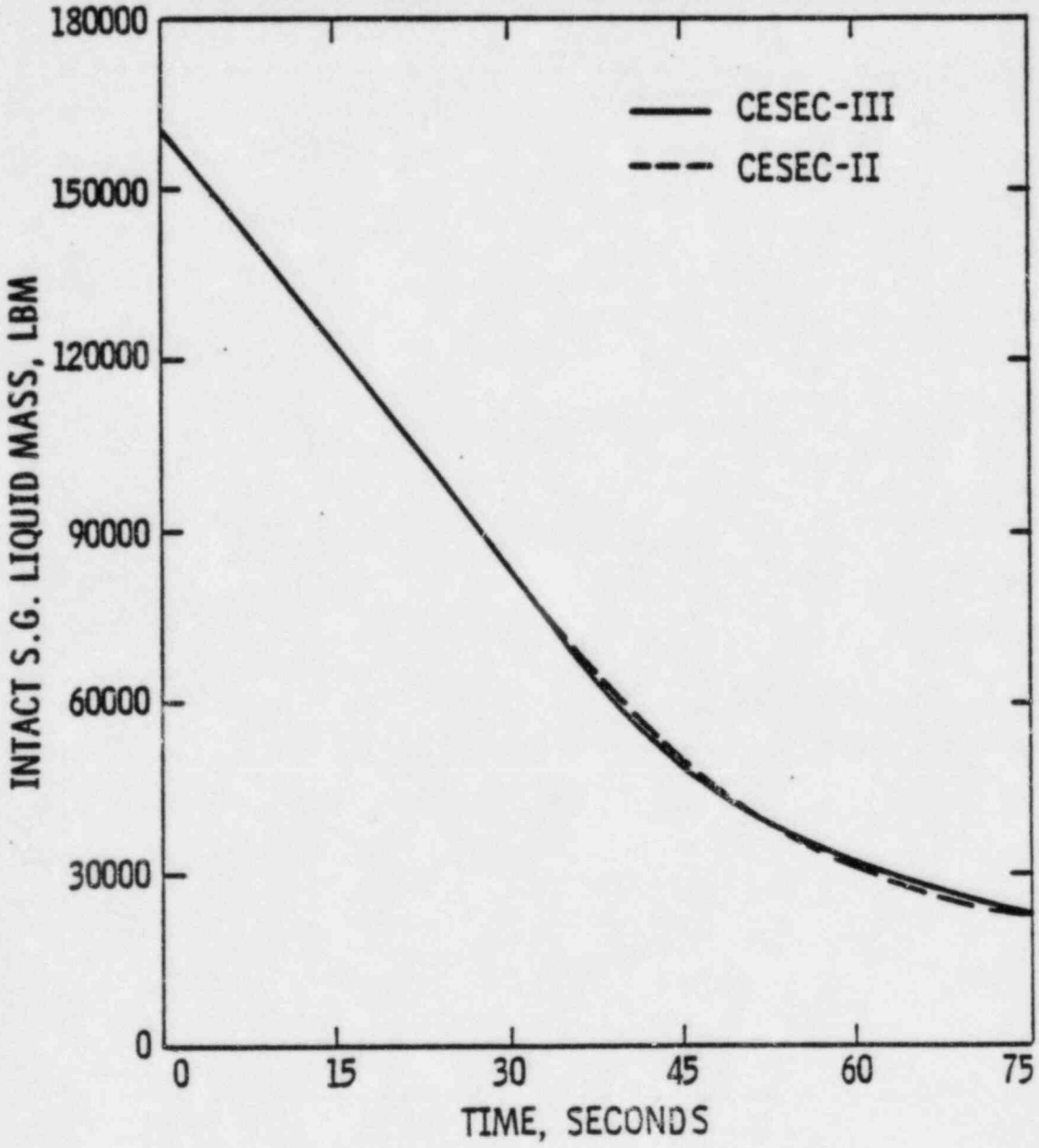

Figure 440.149.B-7
LOSS OF FEEDWATER INVENTORY
SYSTEM 80
RUPTURED S.G. PRESSURE vs TIME

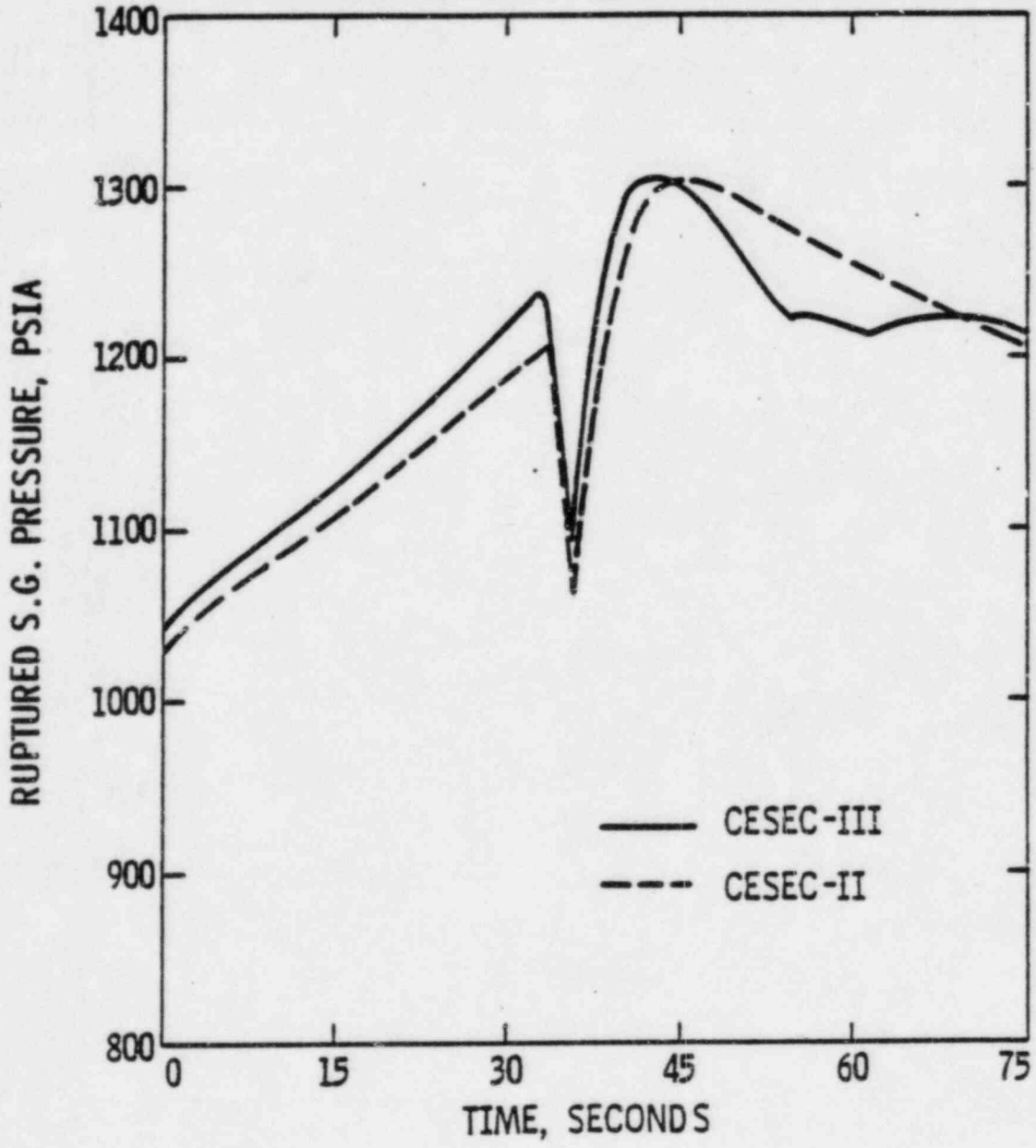

Figure 440.149.B-8
LOSS OF FEEDWATER INVENTORY
SYSTEM 80
INTACT S.G. PRESSURE vs TIME

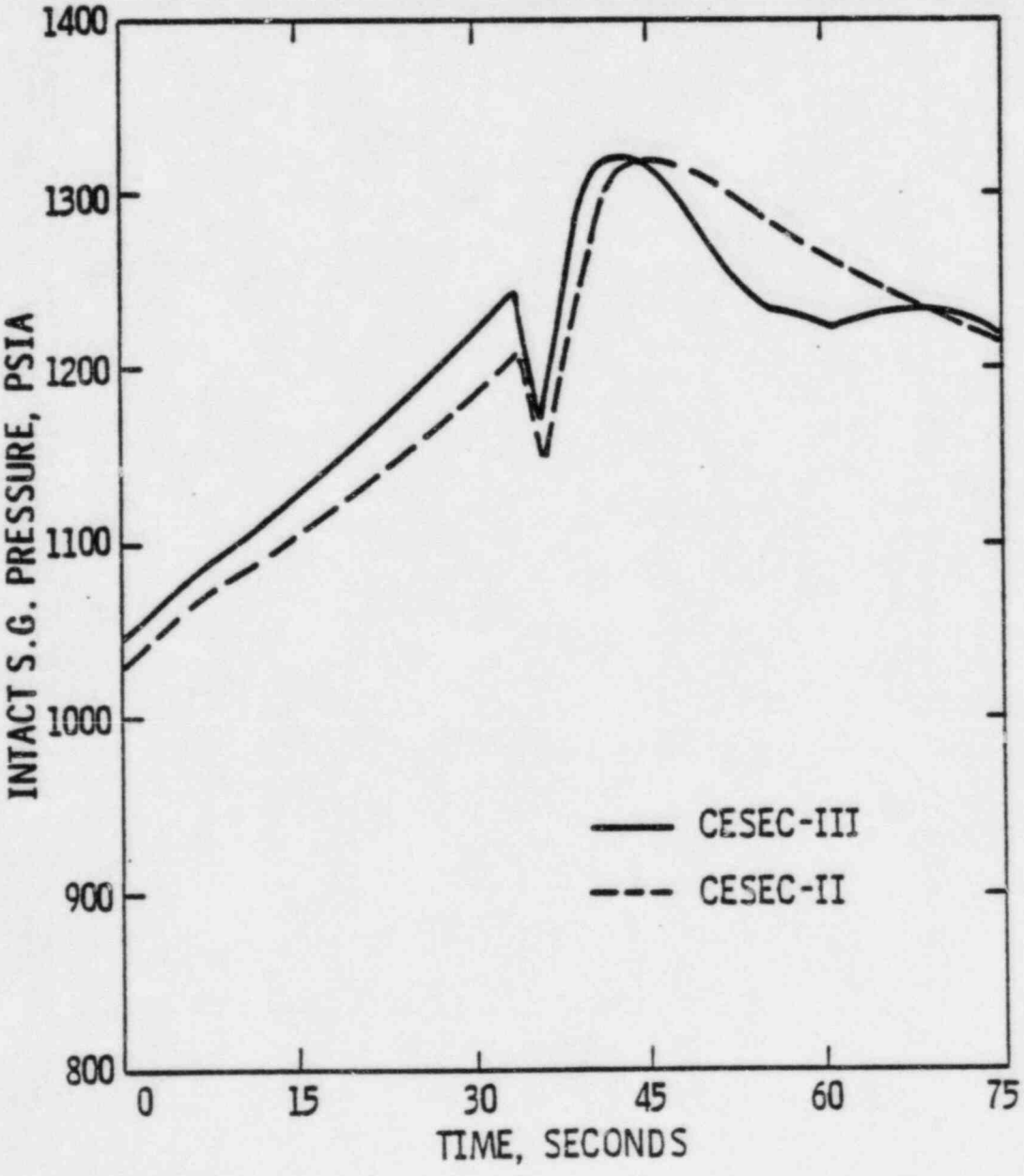

TABLE 440.149-d-1

COMPARISON OF RESULTS

STEAM GENERATOR TUBE RUPTURE WITH

LOSS OF OFFSITE POWER

WATERFORD

	CESEC-I	CESEC-III
Primary-Secondary Integrated Leak (LBM) At 1800 secs.	60,739	65,300
Integrated MSSV Steam Release (LBM) At 1800 secs.	78,300	85,100
Trip Time (Sec)	843	940

Table 440.149.d-2

COMPARISON OF RESULTS

STEAM GENERATOR TUBE RUPTURE WITH

LOSS OF OFFSITE POWER

SYSTEM 80

	CESEC-II	CESEC-III
Primary-Secondary Integrated Leak (LBM) At 1800 secs.	75,400	80,300
Integrated MSSV Steam Release (LBM) At 1800 secs.	95,800	110,000
Trip Time (sec)	1125	1188

Figure 440.149.D-1
STEAM GENERATOR TUBE RUPTURE WITH LOSS OF OFFSITE POWER
WATERFORD
RCS PRESSURE vs TIME

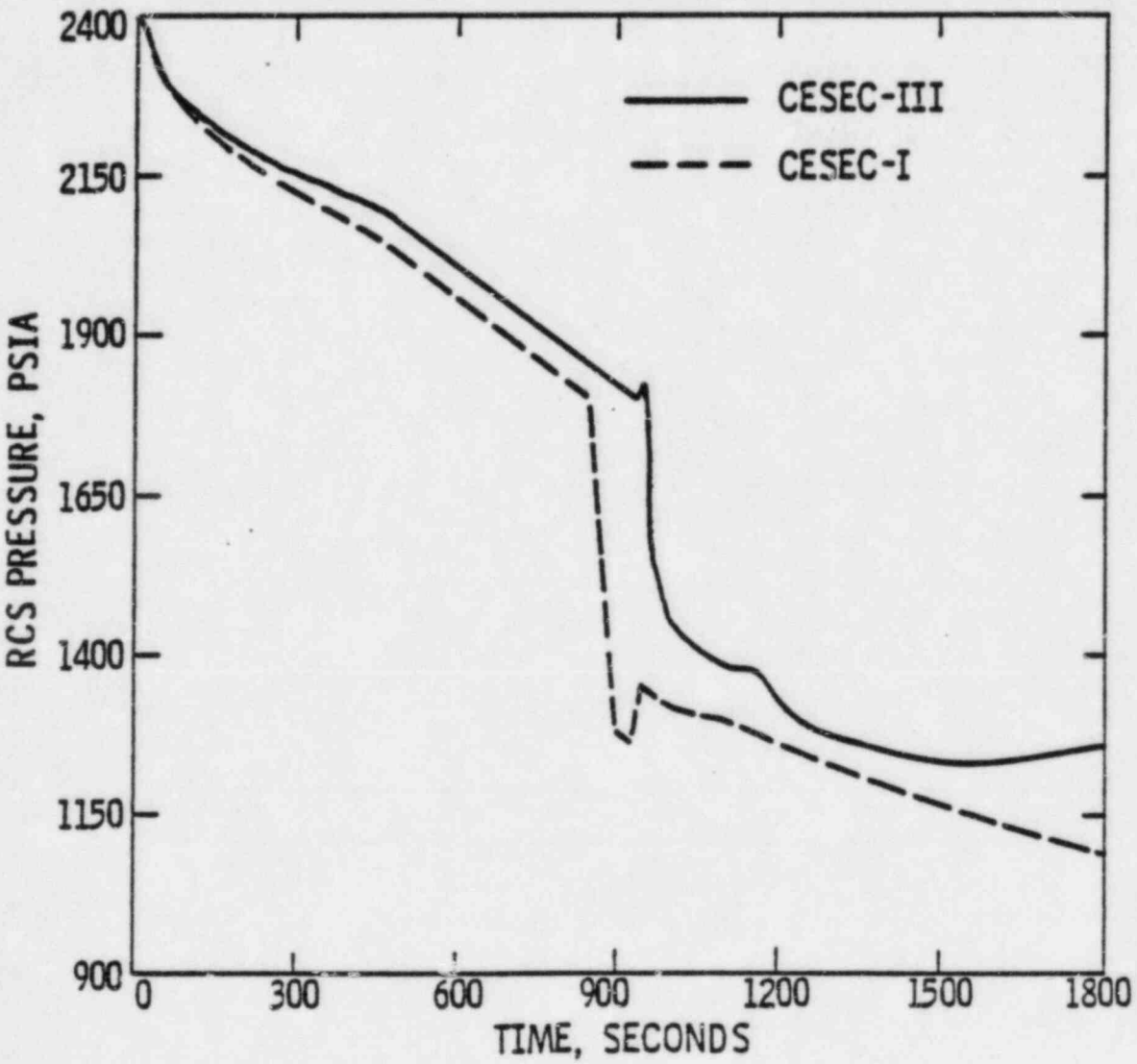

Figure 440.149.D-2
STEAM GENERATOR TUBE RUPTURE WITH LOSS OF OFFSITE POWER
WATERFORD
REACTOR VESSEL LIQUID VOLUME vs TIME

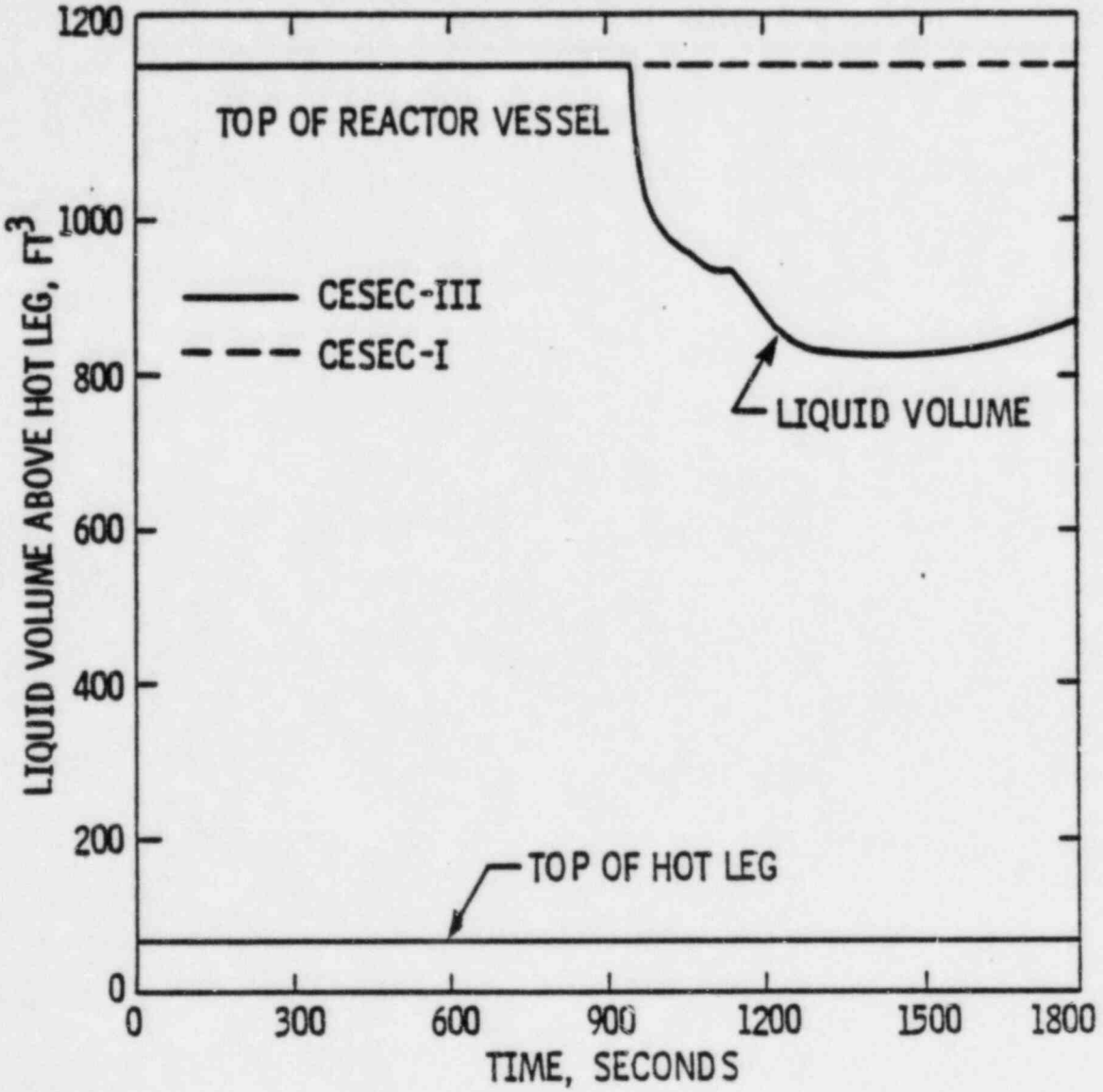

Figure 440.149.D-3
STEAM GENERATOR TUBE RUPTURE WITH LOSS OF OFFSITE POWER
SYSTEM 80
RCS PRESSURE vs TIME

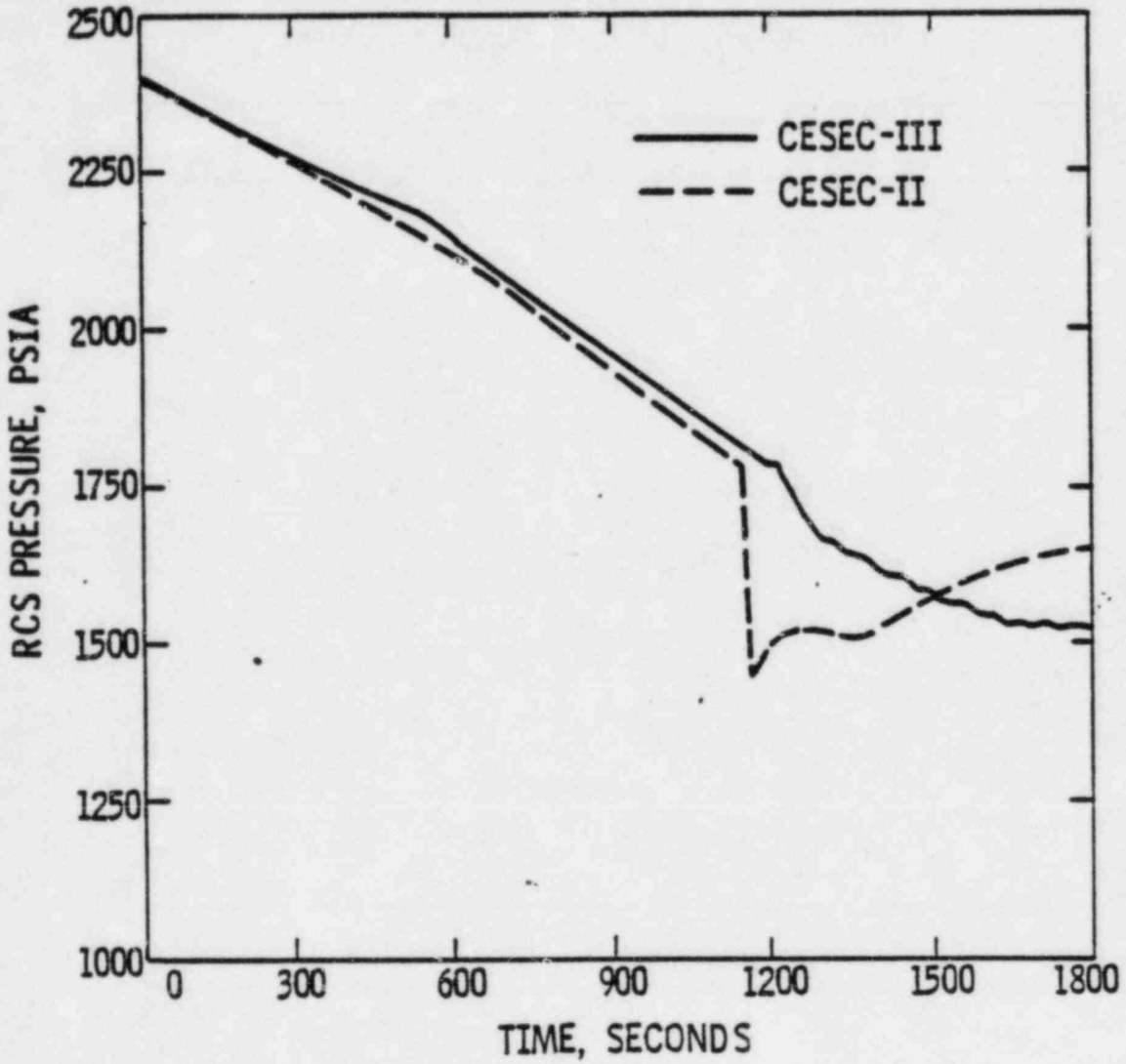

Figure 440.149.D-4
STEAM GENERATOR TUBE RUPTURE WITH LOSS OF OFFSITE POWER
SYSTEM 80
REACTOR VESSEL LIQUID VOLUME vs TIME

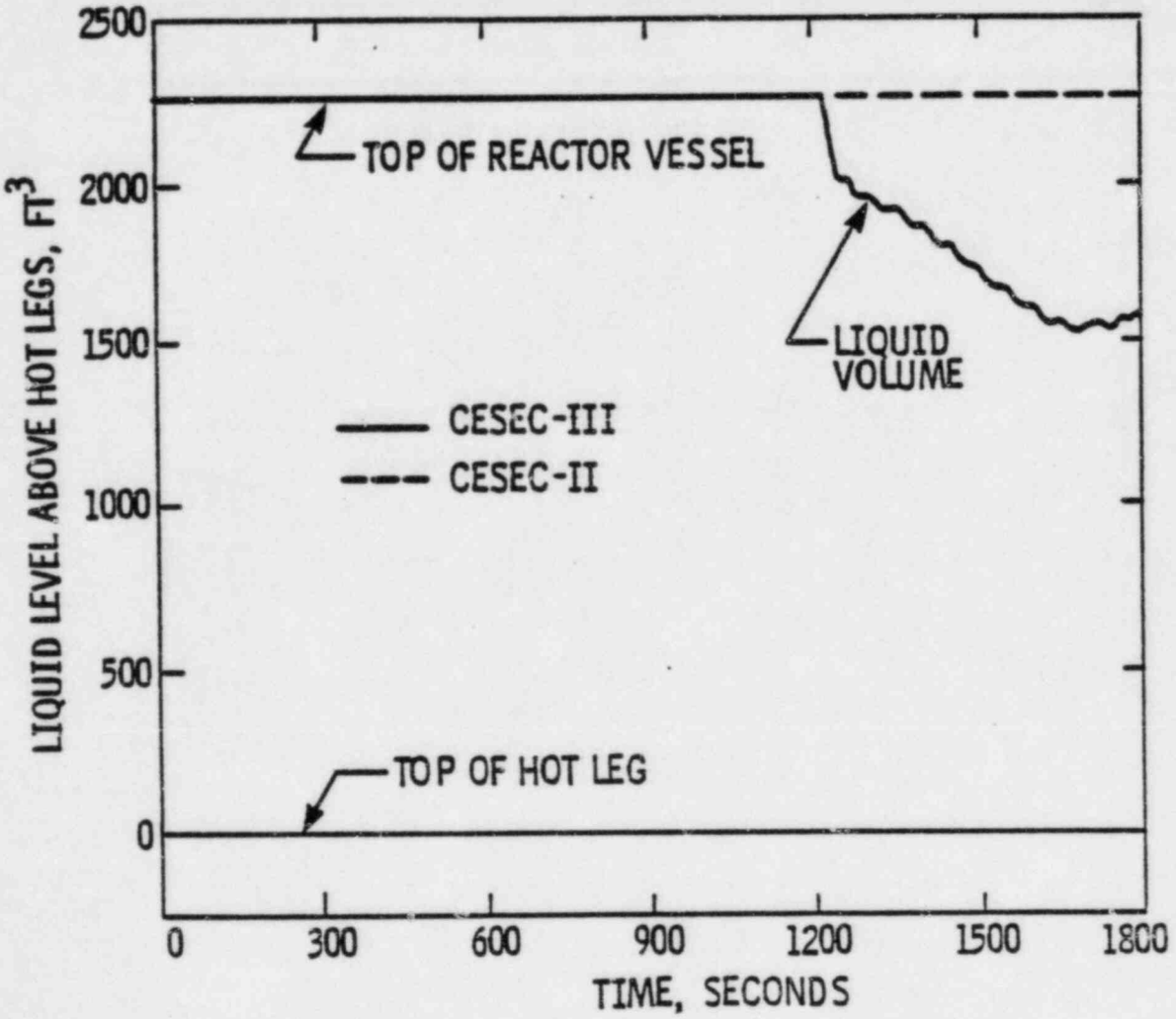

440.150 (440.68) In general, it is our impression that the data[1] presented by FP&L is sufficient to support a general mixing model since only one flow condition was measured. Furthermore, the particular flow condition chosen has a Reynolds number nearly one full order of magnitude below operating conditions.

The experiment represented each core assembly by a single flow tube and used air as its simultant fluid. SO_2 was injected into the air flow of one (of four) reactor vessel inlet nozzles on a roughly 1/4 scale model. The SO_2 concentration was reassured at the exit of each of the "core tubes" and in each of the two reactor vessel outlet nozzles. Although the method appears reasonable for obtaining information on reactor vessel outlet flow, unfortunately, data is presented for only one operating condition. Furthermore, we are concerned about the impact of constraining the core flow in tubes when substantial cross flow is to be expected.

Thus it is our general opinion that this single data point is not an adequate basis upon which to build a computer code model intended to model a wide range of flow conditions. The following speecific questions should be addressed by the applicant.

(a) This data is only for one Re number, representing only one operating condition. Upon what grounds does C-E utilize this data for other flow conditions such as pump coastdown or loss of one pump.

(b) How was this data implemented in the CESEC computer codes, justify and explain in depth.

(c) Discuss the impact of having done these experiments in a geometry which prohibits cross flow between assemblies. How is the cross flow expected to impact the flow split in the exit nozzles. Furthermore, how does this lack of cross flow impact the accuracy of simulation of core moderator temperature during a return to power?

(d) Discuss accuracy of the experiments - what are the fractional errors in the % of flow through the various "core tubes"? The total % of flow going into the two outlet nozzles is (38% 14% = 52% - why is it not 50%? What were the experimental errors?

(1) "Test Report on Fluid Mixing in a Scaled Reactor Vessel Flow Model," CEN-169(L)-P, July, 1981, Combustion Engineering.

Response:

The purpose of Reference 11 is to use mixing data obtained at an appropriate Reynold's number and in a scaled geometry typical of C-E NSSSs to determing mixing factors which can be used to simulate the amount of mixing in the reactor vessel downcomer/lower region and in the outlet plenum region in C-E NSSSs. It is not the intention of this reference to support a general mixing model with data from only one set of flow conditions, but rather to quantify mixing in a very particular geometry. The specific items, asked as sub-sections of question are responded to by item as follows:

(a) For Reynolds numbers greater than about 10^4, momentum transfer for mixing phenomena is substantially independent of the Reynolds number (e.g., Reference 12). This is due to the fact that in highly turbulent flows mixing is mainly due to vortex mixing, rather than diffusion type mixing. The vortex decay is largely independent of the Reynolds number. The test reported in Reference 11 was conducted at a Reynolds number of appproximately 6×10^5, therefore the results of this test should be very nearly independent of the Reynolds number, since it is much greater than 10^4. Typical Reynolds numbers in C-E reactor vessels at 100% flow are of the order of 5×10^7. A Reynolds number of 10^4 would occur at less than 0.1% flow.

The mixing factors used in CESEC are cross flow terms normalized with the mass flow in that branch of the flow net from which the cross flow leaves. For a wide variety of geometries and flow

conditions, see Table 4 of Ref. 32, mixing correlations are cited typically showing a Reynolds number dependency of approximately Re^1. If these mixing terms are expressed as non-dimensional ratios of mass flow (mass flow varies approximately as Re^1) one finds that this normalized mixing factor is only weakly dependent on the Reynolds number as shown in Figure 8 of Ref. 32 or Figures 11 and 12 of Ref. 33. The weak dependencies of mixing on the Reynolds number is evident from Figure 9 of Ref. 32, which covers a range of geometries, sizes, and flow conditions.

Further substantiation for the weak dependence of the mixing factor on the Reynolds number is shown in Ref. 34 in terms of the mixing length vs. the Reynolds number. The geometry involved is one where dye is injected into a pipe flow. A geometric effect is noted in that reference, stating that injection through only one nozzle exhibits a more pronounced Reynolds number dependency, whereas in the case of multiple injection paths (more symmetrical situation than with only one nozzle) only a weak dependence of the mixing length on the Reynolds number exists.

It is therefore appropriate to use the mixing factors obtained at a Reynolds number corresponding to approximately one percent flow for flows up to 100% flow with the understanding that they may underpredict the amount of mixing to a small degree due to the lack of mixing in the reactor core of the scale model test and due to the (weak) increase in the mixing factors which could be expected to occur with increasing flow. For small asymmetries in the flow pattern small increases or decreases in the mixing factors could be

expected. For marked asymmetries the values of the mixing factors obtained from the symmetric scale model tests reported in Ref. 11 could be expected to be inappropriate.

(b) The data of Reference 11 is used to calculate the factors F_I and F_0 (see page 2-2 of Reference 3). The fraction f_1, of the flow from loops 2A annd 2B which reaches loop 1 is (refer to Figure 4-1 of Reference 11).

$$f_1 = \frac{\text{fraction of flow from loop 2A reaching loop 1}}{\text{total fraction of flow in loops 1 and 2 which comes from loop 2A}}$$

The fraction, f_2, of the flow from loops 2A and 2B which reaches the opposite half of the core is determined from the average of the fractions of flow in the core tubes on the half of the opposite loop 2, which are supplied from the traced inlet (loop 2A). F_I and F_C are related to f_1 and f_2 by

$$F_I = \frac{f_2}{1 - f_2}$$

$$F_0 = \frac{f_1 - f_2}{1 - (f_2 + f_1)}$$

Figure 440.150-1 illustrates the flow paths in the CESEC model for the reactor vessel region. This figure is the same as the reactor vessel region of Figure 2-1 of the CESEC Report (Reference 13). The following discussion will focus on the "cross flows," $W_{14,2}$ and $W_{19,7}$ (or "density driven terms") and on the "mixing flows," $W_{2,15}$, $W_{14,3}$ $W_{6,19}$, and $W_{18,7}$ (or "hardwired terms"). The "cross flows," $W_{14,2}$ and $W_{19,7}$, are determined by direct solution of the thermal hydraulic equations (Eqns. 2-1 and 2-2) of Ref. 13). The "mixing flows" are calculated as described on p. 2-2 of Ref. 13 using experimentally determined mixing factors, F_I and F_O:

$$W_{2,15} = F_I W_{2,3}$$

$$W_{14,3} = F_I W_{14,15}$$

$$W_{6,19} = F_O W_{6,7}$$

and

$$W_{18,7} = F_O W_{18,19},$$

where $W_{2,3}$, $W_{14,15}$, $W_{6,7}$, and $W_{18,19}$ are found from the solution of Eqns. 2-1 and 2-2 of Ref. 13.

This model represents the flow paths internal to the reactor vessel in much more detail than did previous models. CESEC-II, for example, represented the reactor vessel by only three nodes: one

equivalent to nodes 2, 3, 14, and 15 of CESEC-III, a second equivalent to nodes 5 and 17, and a third equivalent to nodes 6, 7, 18, 19, and 25. In CESEC-II the flow from all four cold legs was mixed completely in the first reactor vessel node.

(c) CESEC does not model cross flow in the core. The effect of cross flow is included in the 3D reactivity feedback only as described in the response to Question 440.101. Moderator reactivity feedback, other than the 3D feedback, conservatively factors out the effect of mixing to use the density on the cold edge of the core, as described in the response to Question 440.145

The transient which producted the greatest asymmetry in loop flows and which is at the same time affected by these asymmetries is the main steam line break (SLB) with concurrent loss of offsite power. The algorithm for h_{edge} (see the response to Question 440.145) factors out the effect of the mixing between the reactor vessel inlet nozzle and the core inlet plane flows to yield a conservatively low enthalpy for the moderator reactivity calculation, thus eliminating the direct effect of mixing on moderator reactivity. However this calculation is based on current values of core enthalpies and does not factor out the indirect effect of mixing which may have occured during previous loop cycles: An increase in mixing in the reactor vessel will cause an increase in the enthalpy of the fluid entering the hot leg of the loop with the ruptured steam generator. This in turn will cause an increase in the enthalpy of the fluid reaching the core from this loop after sufficient time has elapsed for this fluid to be transported around the loop and back into the reactor vessel. An examination of the results of steam line break transients and of the sensitivity of their consequences to the mixing shows that this indirect effect does not have a significant effect on these consequences.

Figures 440.150-2A through E present the flow distributions in the reactor vessel region at important times during the most limiting full power main steam line break with concurrent loss of offsite power event analyzed for System 80. Flow distributions are shown for times after event initiation of 1, 60, 120, 140, and 270 seconds. The first of these times is chosen to illustrate the flow distributions at the very beginning of the event. At one minute into the transient the asymmetry of the loop flows is approximately 7%. By two minutes this asymmetry is 13%. The maximum post-trip reactivity occurs at approximately 260 seconds; the maximum post-trip power occurs shortly after 270 seconds into the transient, with minimum post-trip DNBR at 277 seconds. At the flow rates present during these parts of the transient, fluid reaching the reactor core at the time of the maximum post-trip reactivity cannot have left the reactor vessel later than approximately two minutes into the transient. The fluid present in the core at the time of minimum DNBR had to have left the reactor vessel prior to 140 seconds into the transient. At 140 seconds the vessel flow asymmetry is 15%, by 270 seconds it is still only 25%. In all of this period the total vessel flow is well above the 1% value at which the mixing factors were measured.

The cross flows serve to balance the difference in contractions of the fluids in the two steam generator loops and to redistribute the unequal loop flows into nearly equal flows through the two halves of the core. For example, at 1 second the net cross flow is from the loop with the pressurizer to the other loop, since pressurizer outsurge is compensating for contraction in both loops. At 60

seconds net cross flow is to the loop with the ruptured steam generator. By 270 seconds a small net cross flow to the loop with the unaffected steam generator exists: the ruptured steam generator has dried out, while the intact steam generator is being cooled by auxiliary feedwater.

If it is assumed that an increasing asymmetry decreases mixing and that this decrease is of the order of the asymmetry, then it could be estimated that over the period of the transient between one and two minutes an approximately 10% reduction in mixing might be expected. Since during the first minute of the transient, when the cooldown rate and its effect upon reactivity is greatest, there is much less asymmetry, the overall effect should be much less than or the order of 10%. It is possible that this is less than the amount by which the mixing factors used are too low due to the experimental configuration.

Figures 440.150-3 and 4 show the sensitivity of the results of this SLB to variations in the assumed mixing factors. Figure 440.150-3 shows the sensitivity of maximum post-trip fission power to mixing. The sensivitity of minimum post-trip DNBR is presented in Figure 440.150-4. The abscissa for both of these figures is a mixing factor multiplier. This multiplier was used to reduce or increase both F_I and F_O by a fixed factor for an entire transient. Thus a mixing factor multiplier of 1.2 corresponds to a 20% increase in both F_I and F_O over the values normally used.

A reduction in mixing of the order of 10% for this transient would

yield an increase in maximum post-trip fission power of less than 10 MW out of a total of 100 MW and a reduction in minimum post-trip DNBR of less than 0.2 out of a total of 2.7. Since actual mixing may be higher, rather than lower, than the values used, the consequences of this event could be less adverse by similar small amounts.

(d) The accuracy of the mixing data reported in Reference 1 is $\pm$ 3%.

In summary, the mixing factors obtained from Ref. 11 used together with the CESEC-III model of the flow paths in the reactor vessel yield transient results which are much more realistic than those available from earlier models. The results obtained from Ref. 11 are applicable for use in the transient analyses for which CESEC is used. The effect of possible uncertainties, or flow asymmetry dependencies, in the mixing factors is not of sufficient magnitude to alter the conclusions of any FSAR analysis. This is demonstrated by a sensivitity study using the main steam line break with concurrent loss of offsite power, which is the event that is most sensitive to uncertainties in the dependency of the mixing on flow asymmetry.

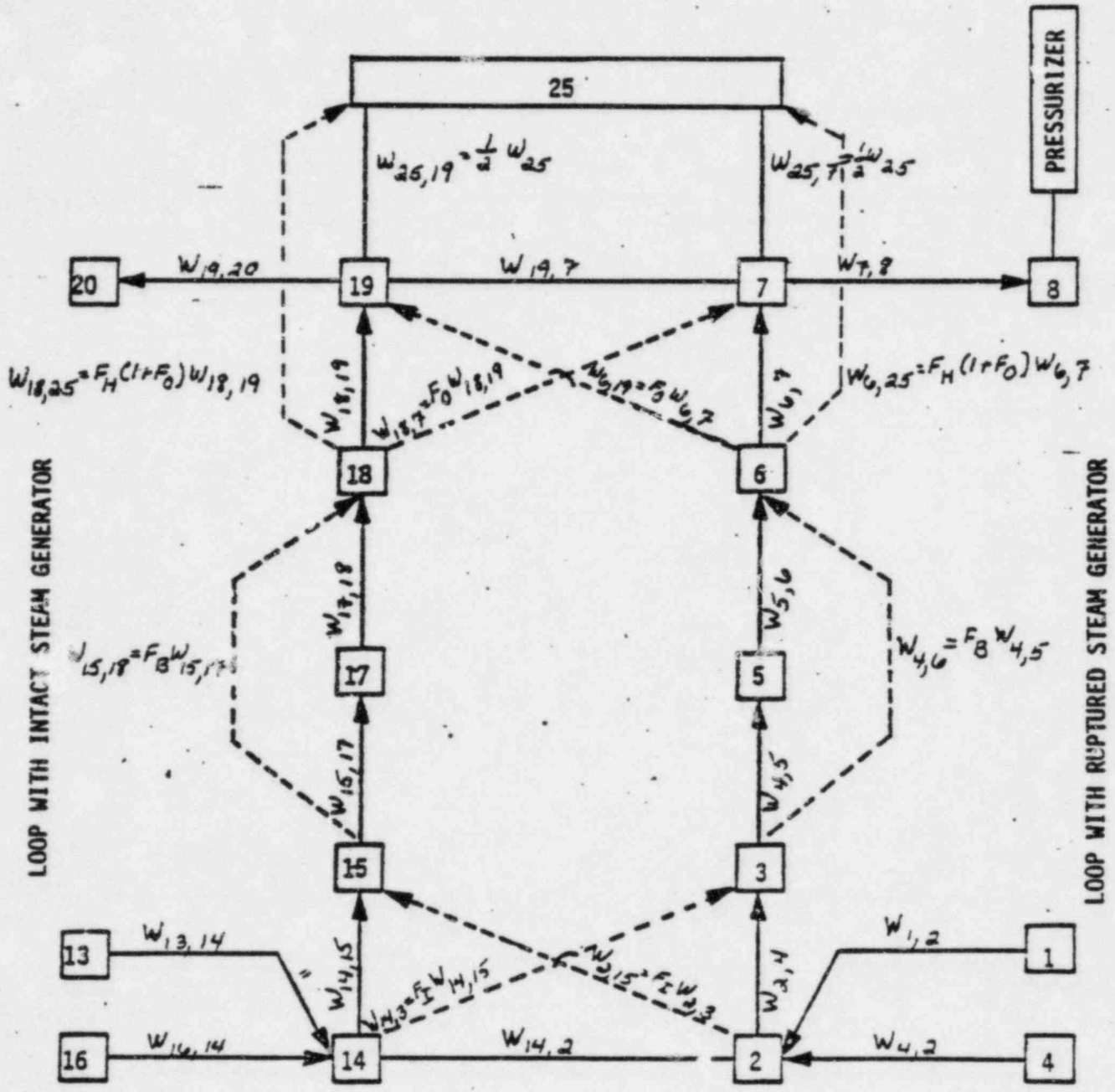

(NOTE: F_H SET EQUAL ZERO AT BEGINNING OF SLB TRANSIENT TO MAXIMIZE RCS PRESSURE THUS MINIMIZING SI REACTIVITY)

FIGURE 440.150-1

CESEC FLOW PATHS FOR REACTOR VESSEL REGION

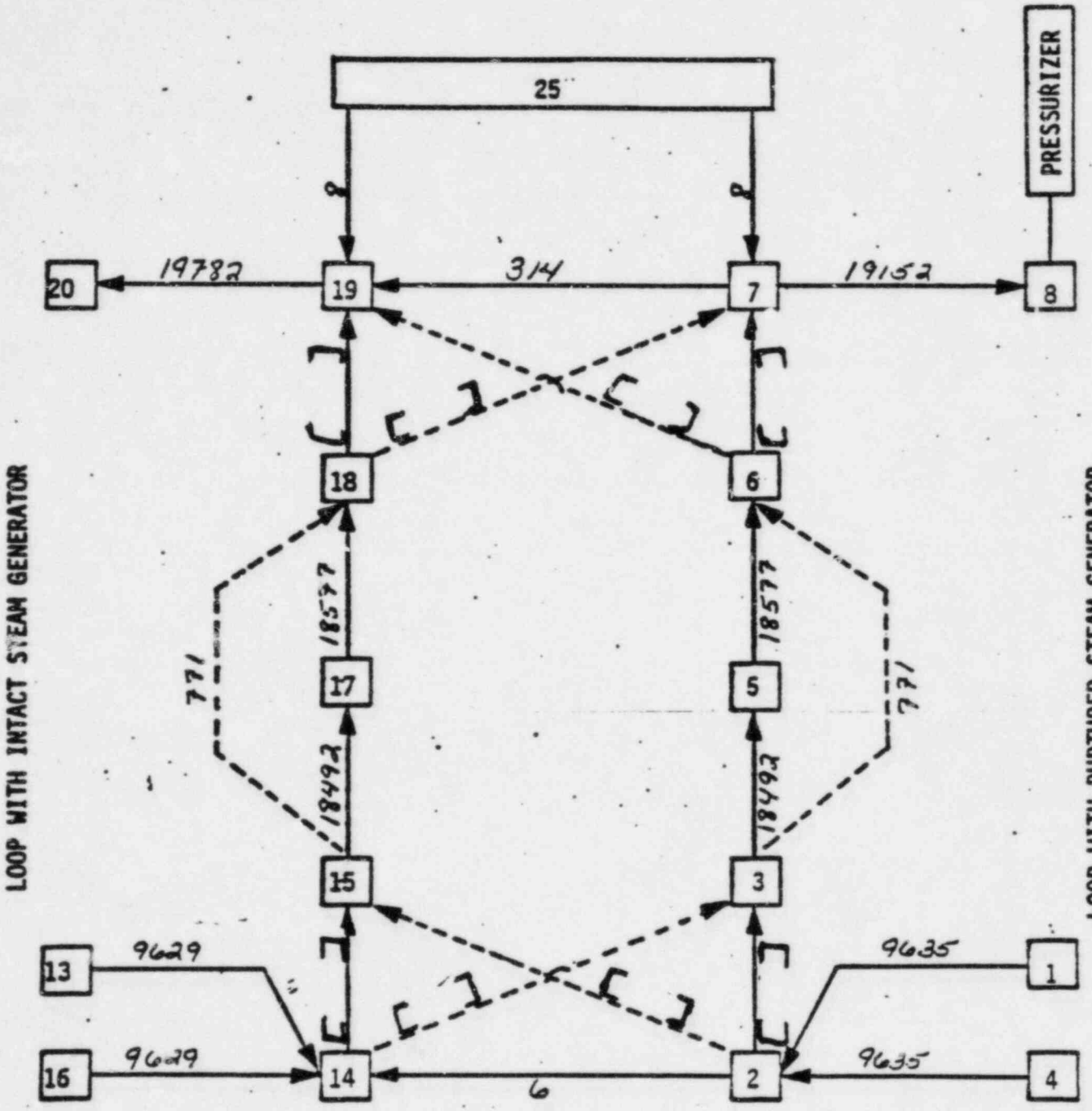

FIGURE 440.150-2 A

FLOW DISTRIBUTION IN REACTOR VESSEL REGION AT 1 SECOND AFTER INITIATION OF A FULL POWER LARGE STEAM LINE BREAK WITH CONCURRENT LOSS OF OFFSITE POWER FOR SYSTEM 80 (FLOWS IN LBM/SEC)

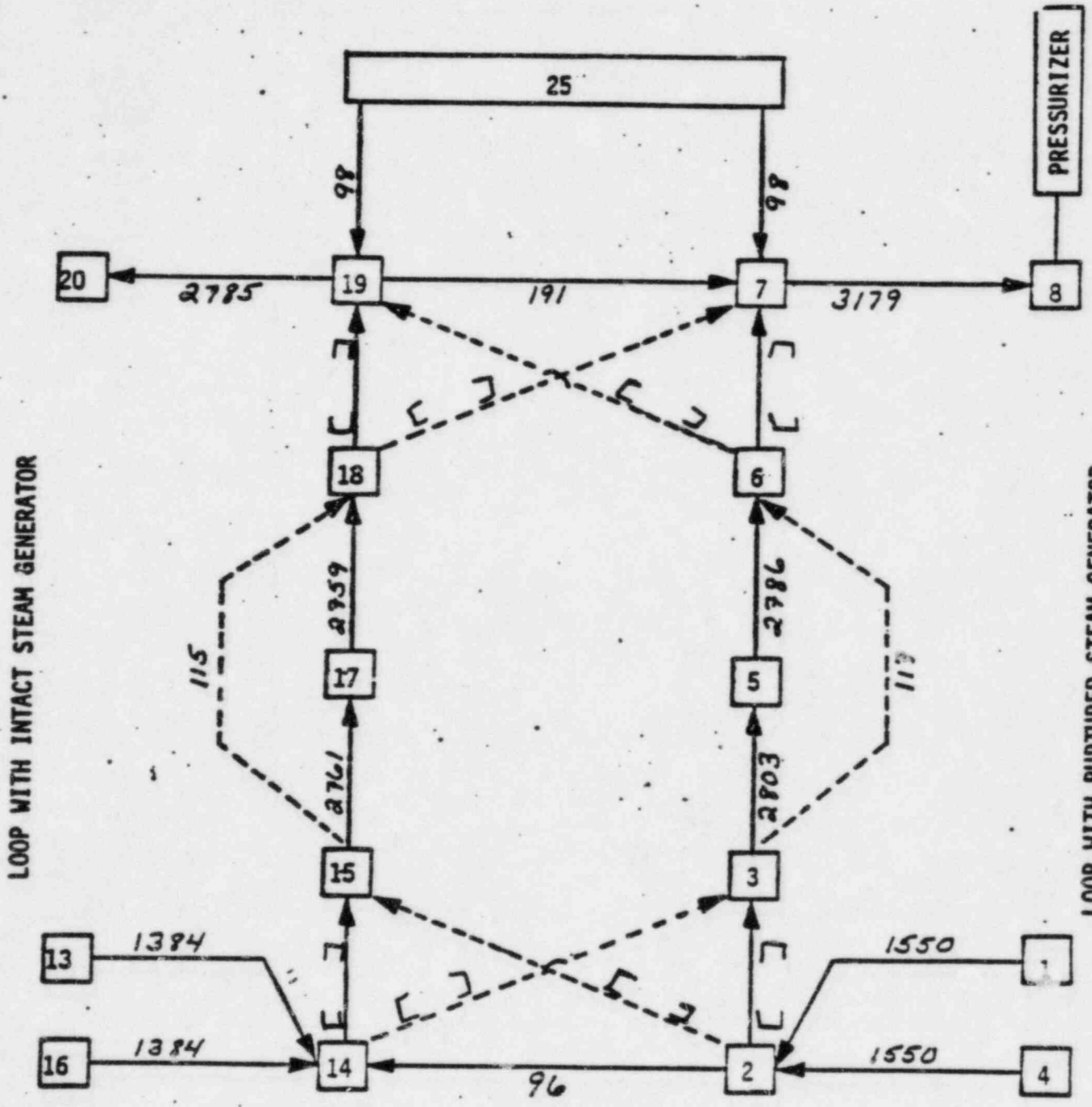

FIGURE 440.150-2 B

FLOW DISTRIBUTION IN REACTOR VESSEL REGION AT 60 SECONDS AFTER INITIATION OF A FULL POWER LARGE STEAM LINE BREAK WITH CONCURRENT LOSS OF OFFSITE POWER FOR SYSTEM 80 (FLOWS IN LBM/SEC)

147

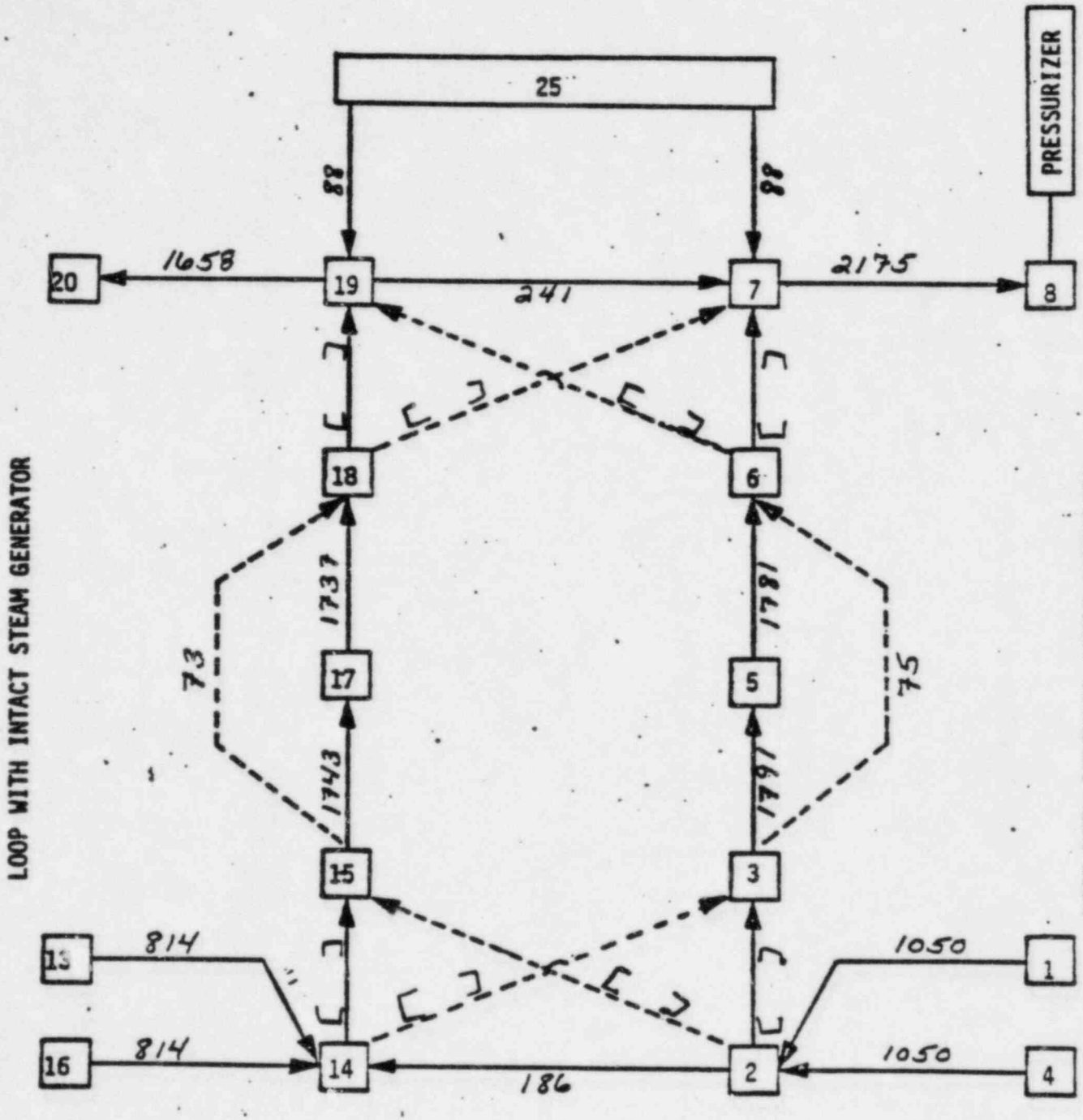

FIGURE 440.150-2 C

FLOW DISTRIBUTION IN REACTOR VESSEL REGION AT 120 SECONDS AFTER INITIATION OF A FULL POWER LARGE STEAM LINE BREAK WITH CONCURRENT LOSS OF OFFSITE POWER FOR SYSTEM 80 (FLOWS IN LBM/SEC)

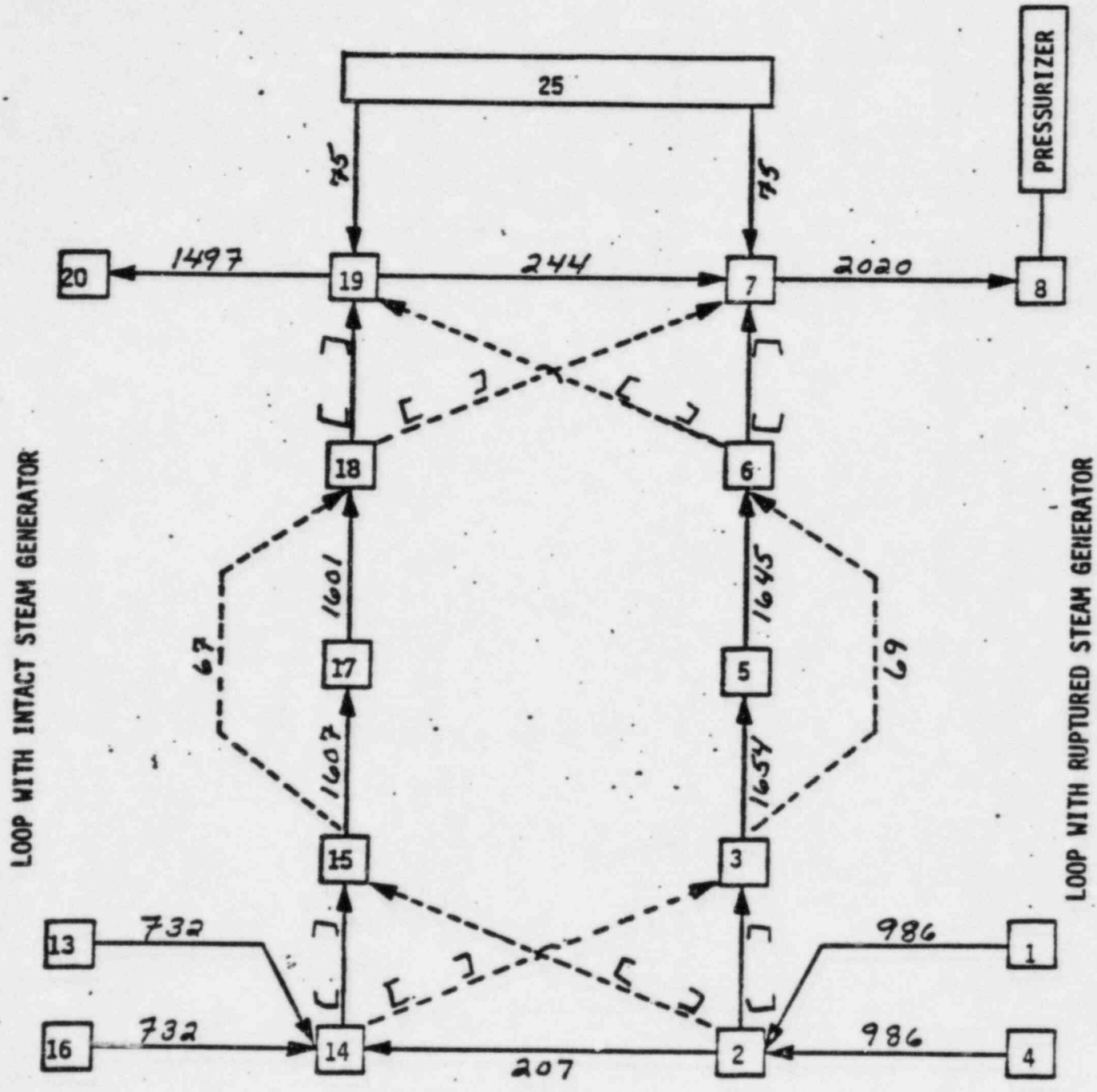

FIGURE 440.150-2D

FLOW DISTRIBUTION IN REACTOR VESSEL REGION AT 140 SECONDS AFTER INITIATION OF A FULL POWER LARGE STEAM LINE BREAK WITH CONCURRENT LOSS OF OFFSITE POWER FOR SYSTEM 80

(FLOWS IN LBM/SEC)

63

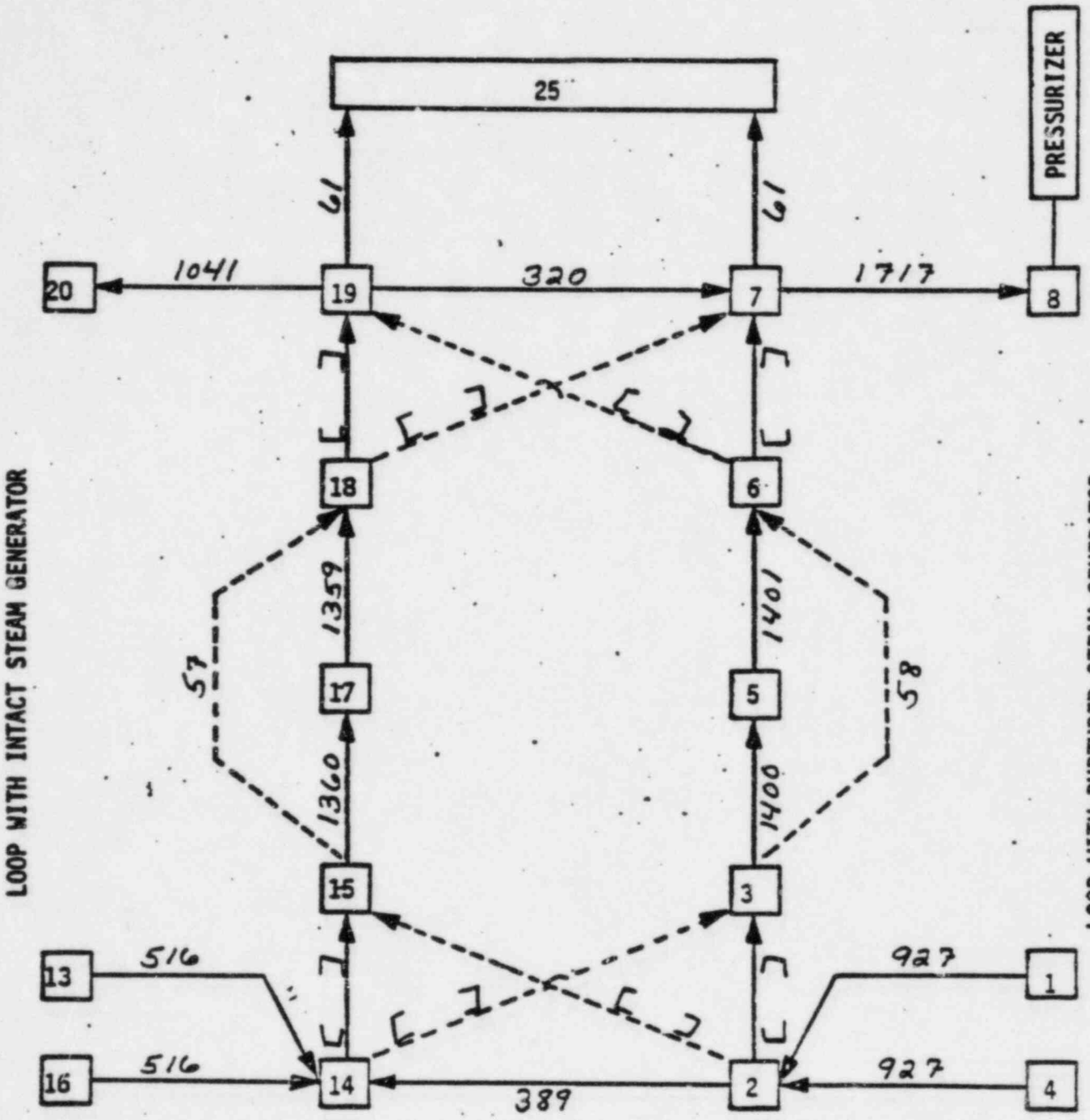

FIGURE 440.150-2E

FLOW DISTRIBUTION IN REACTOR VESSEL REGION AT 270 SECONDS AFTER INITIATION OF A FULL POWER LARGE STEAM LINE BREAK WITH CONCURRENT LOSS OF OFFSITE POWER FOR SYSTEM 80 (FLOWS IN LBM/SEC)

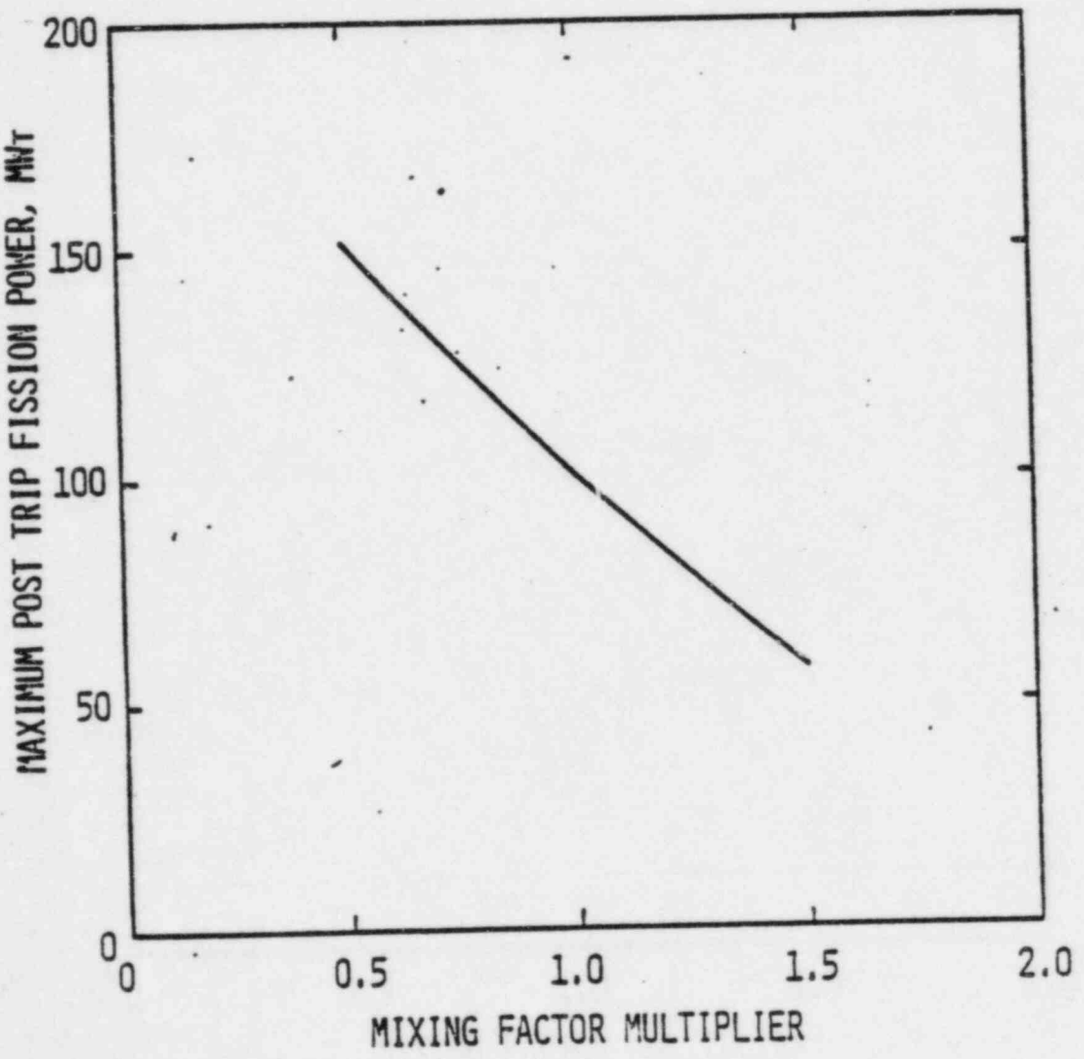

FIGURE 440.150-3
SENSITIVITY OF MAXIMUM POST-TRIP FISSION POWER
TO MIXING IN REACTOR VESSEL

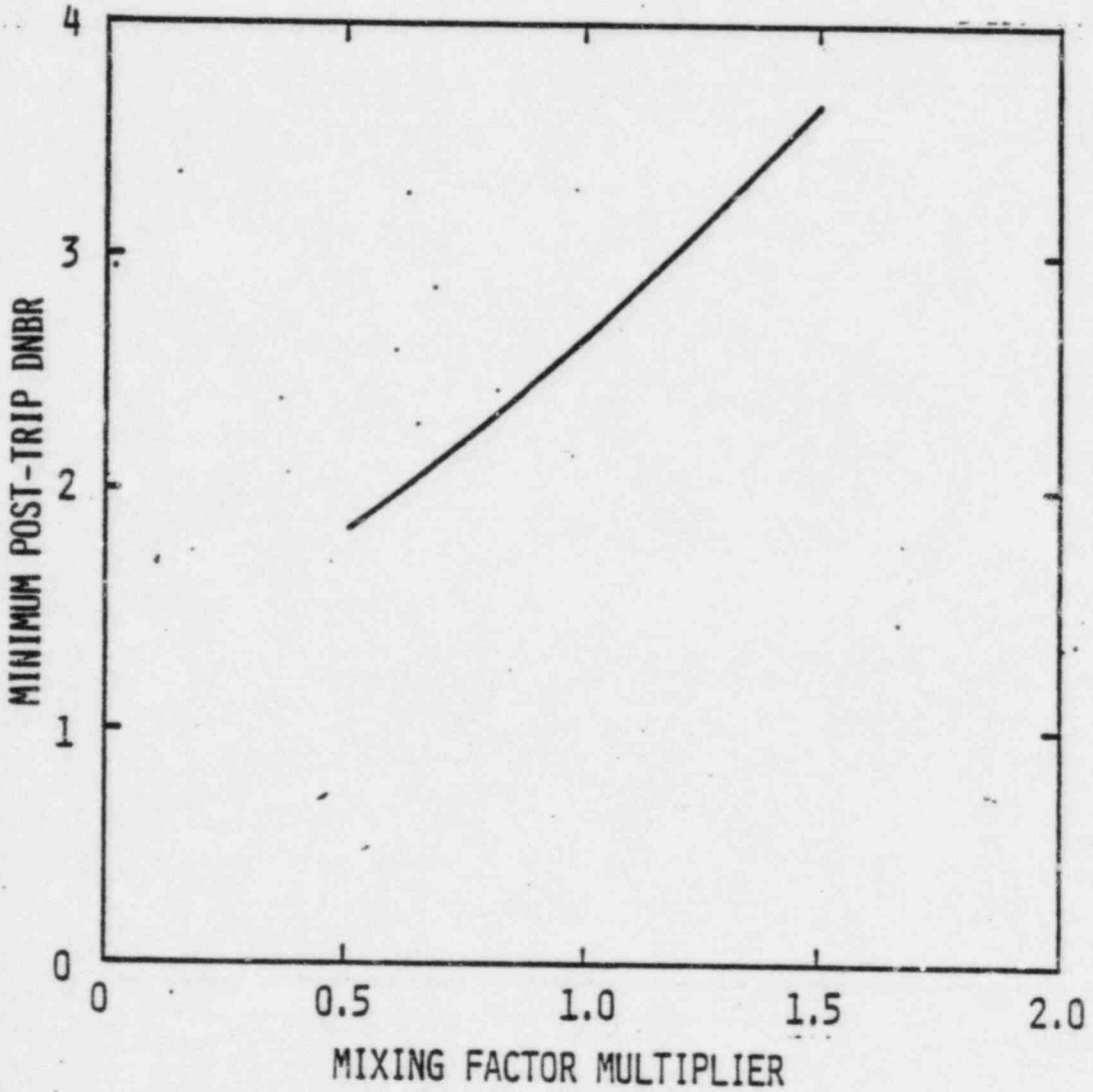

FIGURE 440.150-4
SENSITIVITY OF MINIMUM POST-TRIP DNBR
TO MIXING IN REACTOR VESSEL.

References

1. CENPD-107 "CESEC-Digital Simulation of a Combustion Engineering Nuclear Steam Supply System" C-E Proprietary Report (April, 1974).

2. CENPD-107, Supplement 1 "ATWS Model Modifications to CESEC" C-E Proprietary Report (September, 1974).

3. CENPD-107, Supplement 1, Amendment 1-P "ATWS Model Modifications to CESEC" C-E Proprietary Report (November, 1975).

4. CENPD-107 Supplement 2 "ATWS Models for Reactivity Feedback and Effect of Pressure on Fuel" C-E Proprietary Report (September, 1974).

5. CENPD-107 Supplement 3 "ATWS Model Modifications to CESEC" C-E Proprietary Report (August, 1975).

6. CENPD-107 Supplement 4 "ATWS Model Modifications to CESEC" C-E Proprietary Report (December, 1975).

7. CENPD-107 Supplement 5 "ATWS Model Modifications to CESEC" C-E Proprietry Report (June, 1976).

8. CENPD-188-A "HERMITE: A Multi-Dimensional Space-Time Kinetics Code for PWR Transients," C-E Proprietary Report (July, 1976).

9. CENPD-161-P, "TORC: A Computer Code for Determining the Thermal Margin of a Reactor Core," C-E Proprietary Report (July, 1975).

10. CENPD-266-P, "The ROCS and DIT Computer Codes for Nuclear Design, C-E Proprietary Report (December, 1981).

11. CEN-169(L)-P, "Test Report on Fluid Mixing in a Scaled Reactor Vessel Flow Model," Combustion Enginering, Inc., Proprietary Report (July, 1981).

12. Johnstone, R. E., and Thring, M. W., Pilot Plants, Models, and Scale-Up, Methods in Chemical Engineering, McGraw-Hill Book Co., New York (1957), pp. 115-116.

13. Enclosure 1-P to LD-82-001, January 6, 1982, "CESEC Digital Simulation of a Combustion Engineering Nuclear Steam Supply System" Combustion Engineering, Inc., Proprietary Report (Dec., 1981).

14. CENPD-206-P, "TORC Code Verification and Simplified Modeling Methods," C-E Proprietary Report (January, 1977).

15. CENPD-132, "Calculative Methods for the C-E Large Break LOCA Evaluation Model," (Vol. 1, August, 1974).

16. CENPD-133, "CEFLASH-4A, A Fortran IV Digital Computer Program for Reactor Blowdown Analysis," (August, 1974).

17. Dittus, F. W., and Boelter, L. M. K., "Heat Transfer in Automobile Radiators of the Tubular Type," Pub. in Eng., Vol. 2, n. 13, Univ. of California, pp. 443-461, 1930.

18. CEN-199, "Effects of Vessel Head Voiding during Transients and Accidents in C-E NSSS's, March, 1982.

19. Intentionally Blank.

20. Intentionally Blank.

21. Intentionally Blank.

22. "Flow of Fluids," Tech. Paper No. 41, Crane Co., 1957.

23. Nahavandi, A. N., and M. Rashevsky, "Computer Program for Critical Flow Discharge of Two Phase Steam-Water Mixtures," CVNA-128, Feb. 1962.

24. An Analytical representation of convection-boiling function by S. Edelstein, A. Perez, J. C. Chen, Dept. of Chemical Engineering, Lehigh University.

25. A Theoretical Model for the calculation of Large Transients in Nuclear Natural Circulation U-Tube Steam Generator, A. Hoeld Nuclear Engineering and Design 47 (1978).

26. CENPD-137 P, "Calculative Methods for the C-E Small Break LOCA Evaluation Model," August, 1974.

27. CENPD-137, Supplement 1-P, "Calculative Methods for the C-E Small Break LOCA Evaluation Model, January, 1977.

28. CENPD-133 P, Supplement 1, "CEFLASH-4AS, A Computer Program for the Reactor Blowdown Analysis of the Small Break Loss-of-Coolant Accident," August, 1974.

29. CENPD-133, P, Supplement 3, "CEFLASH-4AS, A Computer Program for the Reactor Blowdown Analysis of the Small Break Loss-of-Coolant Accident," January, 1977.

30. CEN-114-P, Amendment 1-P, "Review of Small Break Transients in Combustion Engineering Nuclear Steam Supply Systems," July, 1979.

31. McClintock, R. S., and Silvestri, G. J., "Formulations and Interactive Procedures for the Calculation of Properties of Steam," ASME Publication H-17, 1967.

32. Galbraith, K. P., and Knudsen, J. G., "Turbulent Mixing Between Adjacent Channels for Single Phase Flow in a Simulated Rod Bundle", AICHE SYMPOS. SERIES 68 (118), 1972, pp. 20-100.

33. Rowe, D. S., and Angle, C. W., "Crossflow Mixing Between Parallel Flow Channels During Boiling," Part III, EFFECT OF SPACERS ON MIXING BETWEEN TWO CHANNELS, BNWL-371, PT 3, UC-80 Reactor Technology.

34. Clayton, C. G., Ball, A. M., and Spackman, R., "Dispersion and Mixing During Turbulent Flow of Water in a Circular Pipe," UKAEA, Ma., 1968, AERE-R-5569.

35. Lance, G. N., "Numerical Methods for High Speed Computers, ILIFFE & Sons, Ltd, London (1960) pp. 54-57.

36. M. M. El-Wakil, Nuclear Heat Transport, (Table E-1), International Text Book Company, 1971.

37. Chen, John C., "A Correlation for Boiling Heat Transfer to Saturated Fluids in Convection Flow," ASME Paper 63-HT-34, 1963.

COMBUSTION ENGINEERING, INC.